

# **Neutral dendrimer approach towards protein binding**



**Ibrahim Althobaiti**

**Department of Chemistry  
The University of Sheffield**

**Submitted to the University of Sheffield  
In fulfilment of the requirements for the  
degree of  
Doctor of Philosophy**

**April 2020**

## ACKNOWLEDGEMENTS

I am offering up my success to my beloved mother, who is the source of joy in my life, as well as to my sisters and brothers, without whom I would not have reached this stage in my career.

I wish to thank my supervisor, Dr. Lance Twyman, for his encouragement and unstinting support, and for giving me the opportunity to take part in this project. He was an invaluable source of advice and help during the entire research period. Secondly, I owe a debt of thanks to Dr. Azrah Abdul Aziz, who worked with me throughout the project. She always generously shared her knowledge with me and offered valuable practical suggestions. In addition, I would like to thank Ms. Heather Grievson, Mr. Simon Thorpe and Mr. Nick Smith for their technical assistance, and to extend my thanks to everyone in the department of chemistry, in particular the staff of the teaching lab, NMR, mass spectrum and the IT services for their unfailing help.

Dr. Meshari Alsharif suggested the right university and the best supervisor for my project, for which I thank him.

I am grateful to Dr. Hamza Qasim, who welcomed me to the department on arrival, and encouraged me from the very beginning. Fahad Alotibi, the best friend anyone can hope for, accompanied me during my studies in the US and Britain, and showed me the value and blessing of a lifelong friendship.

I wish to thank Mr. Abdullah Alotaibi for his recent assistance in the lab, his ongoing encouragement, and his contribution to the happiness I felt in Sheffield, where he and Mr. Mohamad Alassaf enriched my everyday life.

Many thanks to the Twyman's group, Mr. Bonaian, Mr. Talal, Mr. Abdulfatah and Mr. Reyad and Mr. Abdullatif.

Particular thanks are due to the secret which originally showed me this path and supported me throughout my studies.

Finally, I wish to thank Jouf University for providing me with the financial assistance which enabled me to undertake these PhD studies.

## ABSTRACT

This study explored the factors that would maximally facilitate the binding of encapsulated neutral dendrimers to protein. The study had two aims. Firstly, to identify the factors that would achieve best encapsulation of the linear chain; factors included hydrophobicity and varying the length number of hydrogen bonds in the linear chain e.g. one H-bond (1HB-LC), two H-bonds (2HB-LC) and three H-bonds (3HB-LC). Secondly, the study aimed to establish how binding was moderated by functionalising the linear chains with various amino acids.

Due to its water-soluble quality, PAMAM neutral dendrimer was chosen as the scaffold to create a functionalised linear chain. This was important as it meant the ligand and protein were in the same phase. Even more importantly, the terminal groups on the dendrimers were neutral and inert, thus ensuring that in the absence of any encapsulated functionality, there was no prospect of the dendrimers binding or interacting with binding surface of the protein. In this situation, only those dendrimers that had been functionalised with linear chains were able to bind. Using different numbers of hydrogen bonds, each hydrophobic linear chain had a terminal amino acid that used H-bonds and hydrophobic interactions to bind to the inside of the dendrimer. To create a surface functionalised system, multiple diverse linear chains were synthesised and incorporated into dendrimers. The encapsulation of 2HB-LC-Tyr or 2HB-LC-Val in the dendrimer resulted in a 10-nm bathochromic shift in  $\lambda_{max}$ ; for 3HB-LC-Tyr and 3HB-LC-Val the bathochromic shift was 5 nm. This finding is expected, because the water that solvates the linear chains is being replaced by the interior groups of the dendrimer. The extent of encapsulation is influenced by the number of hydrogen bonding sites present on the chain; those sites capable of forming three H-bonds, resulted in superior encapsulation than those with two H-bonds. The postulated mechanism for complexes to form is a collaborative relationship between  $n$  H-bonds and hydrophobic interactions. 3HB-LC-Tyr demonstrated the highest binding affinity, exhibiting an inhibition constant ( $K_i$ ) of 1.23  $\mu\text{M}$ ; in contrast, the  $K_i$  of 2HB-LC-Tyr, was 1.51  $\mu\text{M}$ . 3HB-LC-Tyr bound most strongly of the different amino acids that were used to functionalise the non-binding dendrimer (G3.5-OH). The mechanism for this is attributed to polyvalent interactions occurring between the surface of the Chy and the amino acids. Apart from the valine-functionalised dendrimer, which failed to bind, all of the compounds were competitive inhibitors,

The study's attention was turned next to cytochrome-c. To explore this, the non-covalent methodology that had been applied to  $\alpha$ -chymotrypsin binding was used. Encapsulated tetrahydroxyphenyl porphyrin (THPP) was applied as an internal quench, facilitating direct measurement of binding. Zinc was added to THPP, enabling the dendrimer's internal amines to coordinate to THPP. The results reveal that no binding took place for valine and non-functionalised dendrimers, and the dissociation constant ( $K_d$ ) of 3HB-LC-Tyr was 5.55 nm. These findings indicate that this method can be used to prepare libraries of dendrimer scaffolds, binding groups and sensing units, enabling immeasurable combinations that can be applied to diverse proteins.

## ABBREVIATIONS

**PAMAM** Poly(amido amine)  
**PAMAM-OH** Neutral Hydroxyl Terminated PAMAM  
**PAMAM-COOH** Acid Terminated PAMAM  
**DCC** Dynamic combinatorial chemistry  
**DCLs** Dynamic combinatorial libraries  
**DCM** Dichloromethane  
**DCCI** Dicyclohexyl carbodiimide  
**DCU** Dicyclohexyl urea  
**DMSO** Dimethylsulphoxide  
**EDA** Ethylenediamine  
**EDC** 1-Ethyl-3-(3-dimethylaminopropyl)carbodiimide  
**DMAP** 4-Dimethylaminopyridine  
**MA** Methyl Acrylate  
**BTNA** N-benzoyltyrosine-p-nitroanilide  
**<sup>1</sup>H NMR** Proton Nuclear Magnetic Resonance Spectrometry  
**<sup>13</sup>C NMR** Carbon-13 Nuclear Magnetic Resonance Spectrometry  
**IR/FTIR** Infra Red/Fourier Transfer Infra Red Spectrometry  
**ES-TOF MS** Electron Spray Time-Of-Flight Mass Spectrometry  
**MALDI-TOF MS** Matrix Assisted Laser Desorption Ionisation Time of Flight  
**Chy**  $\alpha$ -chymotrypsin  
**Cyt-c** cytochrome-c  
**NaOH** Sodium Hydroxide  
**K<sub>2</sub>CO<sub>3</sub>** Potassium Carbonate  
**TRIS** Tris(hydroxymethyl)aminomethane  
**UV/Vis Spectrometry** Ultra Violet/Visible Spectrometry  
 **$\epsilon$**  Extinction coefficient  
**nm** Nanometre.  
**DLS** Dynamic light scattering  
**TRIS** Tris(hydroxymethyl)aminomethane.  
**THPP** Tetra-4-hydroxyphenyl porphyrin.  
**ZnTHPP** Zinc-tetra-4-hydroxyphenyl porphyrin.  
**1HB-LC-Boc-Tyr** One hydrogen bonding of linear chain with Boc Tyrosine  
**1HB-LC-Tyr** One hydrogen bonding of linear chain with Tyrosine  
**2HB-LC-Boc-Tyr** Two hydrogen bonding of linear chain with Boc Tyrosine  
**2HB-LC-Tyr** Two hydrogen bonding of linear chain with Tyrosine  
**2HB-LC-Boc-Val** Two hydrogen bonding of linear chain with Boc Valine  
**2HB-LC-Val** Two hydrogen bonding of linear chain with Valine  
**3HB-LC-Boc-Tyr** Three hydrogen bonding of linear chain with Boc Tyrosine  
**3HB-LC-Tyr** Three hydrogen bonding of linear chain with Tyrosine  
**3HB-LC-Boc-Val** Three hydrogen bonding of linear chain with Boc Valine  
**3HB-LC-Val** Three hydrogen bonding of linear chain with Valine

# Contents

<b>ACKNOWLEDGEMENTS</b> .....	ii
<i>CHAPTER 1</i> .....	7
<i>INTRODUCTION</i> .....	7
1.0 Introduction to Protein-Protein Interactions .....	8
1.1 Protein-Protein Binding Interface .....	9
1.2 Inhibiting Protein-Protein Interactions .....	13
1.3 Protein-Protein Inhibition With Low Molecular Weight Synthetic Agents .....	14
1.3.1 Small Molecule Inhibitors.....	14
1.3.2 $\alpha$ -Helix Mimetics .....	19
1.3.2 Porphyrin and Calixarene Based Receptors.....	23
1.3.3 Supramolecular Protein Scaffold .....	30
1.4 Dendritic Polymer Synthesis.....	32
1.4.1 Dendrimer Synthesis .....	32
1.4.2 Divergent Approach.....	33
1.4.3 Convergent Approach .....	35
1.5 Concerns Surrounding Synthetic Inhibitors.....	36
1.6 Dynamic Combinatorial Libraries .....	41
<i>CHAPTER 2</i> .....	43
2.0 Aims and Objectives .....	44
<i>CHAPTER 3</i> .....	49
<i>Preparation of functionalized dendrimer</i> .....	49
3.1 INTRODUCTION AND AIMS.....	50
3.2 Results and Discussion .....	54
3.3 Synthesis of PAMAM dendrimers.....	54
3.4 Synthesis of dendrimers with hydroxy terminal groups.....	60
3.5 Synthesis of linear chain .....	65
3.5.1 Synthesis of the one amide H-bonding linear chain .....	67
3.5.2 Synthesis of the two amide H-bonding linear chains.....	69
3.5.3 Synthesis of two linear chains with tyrosine and valine .....	73
3.5.2 Synthesis of the three amide H-bonding linear chains.....	75
3.6 Encapsulation of functionalized linear chain .....	79
3.7 Conclusions.....	84
<i>CHAPTER 4</i> .....	85
<i>Non-covalent functionalized dendrimers to inhibit <math>\alpha</math>-chymotrypsin</i> .....	85
4.0 Introduction and Aim.....	86
4.1 Assessment of Protein Binding Using an Enzyme Inhibition Assay.....	87
4.2 Inhibition using 2 hydrogen bonding chain .....	94
4.3 Inhibition using 3 hydrogen bonding chain .....	102
4.4 Comparison of the 1, 2 and 3 hydrogen bonding linear chains .....	105
4.5 Conclusions.....	107
4.6 Future works .....	108
4.7 References.....	109
<i>CHAPTER 5</i> .....	116
<i>An orthogonal supramolecular approach towards protein binding and protein sensing using dendrimers as scaffolds for the non-covalent assembly of binding and sensing groups.</i> .....	116
5.0 Abstract.....	117
5.1 Introduction and Aim.....	118

5.2	Results and Discussion .....	121
5.2.1	Design and synthesis of materials.....	121
5.2.3	Encapsulation and self-assembly of protein binding units. ....	124
5.2.4	Protein interaction and quantification of binding affinities for the 2-H bonding system. ....	127
5.2.5	Protein interaction and quantification of binding affinities for the 3-H bonding system. ....	127
5.2.6	Control experiments.....	131
5.3	Conclusions.....	133
5.4	Experimental.....	135
5.5	Synthesis of Functionalised PAMAM .....	138
5.5.1	Synthesis of two hydrogen bonding linear chain.....	139
5.5.2	Synthesis of three hydrogen bonding.....	142
5.6	References.....	147

***CHAPTER 1***  
***INTRODUCTION***

## **1.0 Introduction to Protein-Protein Interactions**

When proteins interact with other proteins, protein-protein complexes are formed. These complexes can be categorised into the following groups: firstly, homocomplexes, which are characterised by their stability and durability; and secondly, heterocomplexes, which – despite potentially being durable – can be strongly affected by external factors.<sup>1</sup> Hence, the existence of heterocomplexes depends on the presence of a protein that is not dependent on something else for its own existence. Protein-protein complexation plays a fundamental role in almost all biological processes. Examples include signal transduction, cytoskeletal remodelling, cell regulation, and others.<sup>2</sup> In view of this, the interaction of a pair of proteins occurs systematically and non-randomly. The protein-protein association is organised and regulated in a detailed manner, the purpose being to achieve a specific objective.<sup>3</sup>

As noted previously, protein-protein interactions are critically important to for the biological functions that sustain life. These biological processes include protease-inhibitor complexes, antibody-antigen complexes, and hormone-receptor complexes. In these particular cases, the complexes have been extensively studied and comprehended, but there are a great many complexes that have yet to yield to modern scientific inquiry. At the same time, irregular protein-protein interactions have been identified, which are implicated in the pathogenesis and pathophysiology of a range of diseases. For example, sickle cell anaemia results from the oligomerisation of mutant haemoglobin, which emphasises the potentially negative effects of unwanted protein-protein interactions.<sup>4</sup> Additionally, protein-protein interactions with a lower level of specificity have been identified in the literature, which occur when proteins give rise to aggregates. A range of diseases, including Alzheimer's and various types of rheumatoid arthritis, are associated with amyloid fibrils and misfolded protein aggregates.

## 1.1 Protein-Protein Binding Interface

Given the prominence of protein-protein interactions in various types of biological process, researchers have naturally developed an interest in understanding them and, moreover, controlling them. To produce molecules that interfere with protein-protein interactions, however, it is necessary to understand protein-protein binding interfaces.<sup>6</sup> It is possible to consider the protein-protein interface a specific surface that is available on each of the proteins in the pair, which are no longer accessible upon interaction, and which are principally hydrophobic.<sup>7</sup>

Protein-protein complexation is marked by conformational alterations, and researchers have devised a range of models to account for the mechanism of action. Fischer's "lock and key" model, proposed in 1894, supposed that shape selectivity was the operating principle, which does not depend on conformational change. Nevertheless, this model fails to account for interactions of proteins with substances that do not have a uniform shape. In 1958, Koshland devised the "induced fit" model to account for this limitation. The model posits that the active site is slightly elastic, thus facilitating its accommodation of the ligand and, in turn, resulting in a conformational change. The final idea proposed regarding the protein-protein binding interface is that of a "pre-existing equilibrium". The model suggests that the protein's native site presents a collection of conformations at the active site, thereby creating a situation in which the ligand is drawn to an active conformation.<sup>8</sup>

Due to cooperative binding that affords stability to molecule-molecule interactions, a strength obtains to the forces in combination that was not available when they were independent.<sup>5</sup> A range of biological and biochemical functions can take place based on cooperative binding.

When apparent affinity increases, this reflects positive cooperation, which increases the likelihood that a second molecule is bound. It is reasonable to view this phenomenon as a substantial increase in the relative concentration of the ligand for the second binding.<sup>9</sup> The results of cooperative binding are given in Figure 1. The first bond is established between the original binding site and the ligand at the rate of  $K_1$ . Once this bond has been formed, the next interaction takes place at a faster pace and, alongside this, is stronger. This is because the second ligand's relative concentration is greater than those of the other molecules. Additionally,  $K_1$  is significantly smaller than  $K_2$ , meaning that the impact is non-additive. Noteworthy, cooperative binding is associated with a greater additive effect.<sup>10</sup>

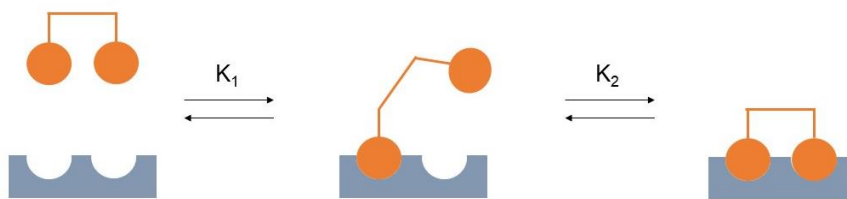


Figure 1: Impact of cooperative binding, where  $K_2$  is significantly greater than  $K_1$

The complexity of the mechanism that underpins protein-protein interactions stems from the expansive surface area involved. Additionally, hydrophobicity and electrostatics perform a critical function. Ultimately, viable interactions are the result of the collaborative impacts of countless parameters.<sup>11-12</sup> The specificity of the mechanism is significant, where proteins select other proteins with a similarly sized interfacial area, which has a three-dimensional shape. Additionally, intermolecular forces are taken into account, as well as the locations of the amino acids. Figure 2 provides a simplified overview of the mechanism involved in protein-protein interaction, demonstrating how specific the protein selection process is.<sup>13</sup>

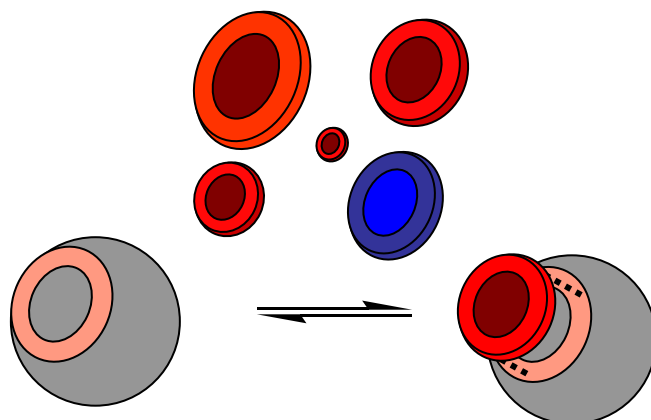


Figure 2: Partner selection mechanism in protein-protein interaction

The processes and details that underlie protein-protein interactions have yet to be clarified in the literature. In the studies conducted by Bogan and Thorn, the researchers drew on alanine screening and kinetic and thermodynamic measurements to illuminate the issue.<sup>12</sup> In particular, the researchers sought to identify the contribution of specific residues to the key binding region (i.e., the “hot spot”, an idea proposed by Clackson and Wells, which itself stemmed from the observation of free energy of binding consisting of a restricted region of amino acid residues).<sup>13</sup> As Bogan and Thorn recognised, the residues within the key binding region perform a critical function in the degree to which the protein complex is stable.<sup>12</sup> Hence, the key binding region plays a key role in the protein-protein interface.

Further, Bogan and Thorn indicated that the key binding regions of binding energy are situated proximal to the interface’s centre, while the residues situated at the interface do not play a role in binding.<sup>12</sup> Additionally, findings indicated that residues in the area surrounding the key binding area probably operate by ensuring that bulk solvent does not contact the interacting residues. The literature indicates that the separation between bulk solvent and interacting residues is a prerequisite for successful protein-protein interactions. Additionally, Bogan and Thorn explored amino acid preferences within the key binding region, noting that these regions

are enriched with the following types of amino acid, each of which has a proportion of greater than 10%: firstly, tryptophan (21%), tyrosine (12.3%), and arginine (13.3%). Given the non-random nature of the amino acid composition in key binding regions, preference towards specific amino acids was discerned in terms of the high-energy interactions between two particular proteins in a heterodimer.<sup>12</sup>

The density of certain amino acids within the binding interface is greater than the density associated with other regions of the protein molecule. Compared to the exterior of the molecule, amino acids of this kind are associated with a greater level of hydrophobicity. As a consequence, it is possible to improve the binding interactions that occur between the proteins by capitalising on hydrophobic interactions. Additionally, large aromatic amino acids are typically preferred at the binding interfaces, while the binding surface is the protein region associated with the greatest likelihood of containing amino acids such as tyrosine.<sup>7-8</sup> Table 1 presents possible target proteins for evaluating the binding capability of polymers, as well as the capacity to differentiate between protein surfaces in a specific enzyme family. When interactions between synthetic inhibitors and proteins are disrupted, this relies on the emergence of robust affiliated synthetic subunit molecule and protein complexes, which undermine the initiation of interactions between protein subunits.

<b>Mechanism</b>	<b>Protein</b>	<b>Amino acid residue</b>	<b>Inhibitor</b>	<b>Cleavage site</b>
Serine protease	Elastase	240	$\alpha$ -anititrypsin	Ala, Gly
	$\alpha$ -chymotrypsin	241	Aprotinin	Phe, Tyr, Trp
	Trypsin	233	<i>p</i> -amino-benzamidine	Arg, Lys
	Kallikrein	619	Aprotinin	Arg
	Thrombin	308	Argatroban	Arg
Zinc protease	Carboxypeptidase A	307	Benzomercapto-propanoic acid	Phe, Trp, Leu
Aspartate protease	Cathepsin D	346	Pepstatin A	Phe-Phe

**Table 1:** Enzymes based on their cleavage site and standard inhibitor

Investigating protein structures in this way offers insights into the manner in which protein-protein interactions operate. Equipped with this understanding, it is possible to begin investigating the design and delivery of novel synthetic agents that could disrupt undesirable, disease-causing interactions.

## 1.2 Inhibiting Protein-Protein Interactions

Owing to the critical part they play in biological processes and systems, protein-protein interactions, when interfered and disrupted, can point the way towards novel therapeutic agents. Developments have occurred in recent years in the studies that have examined synthetic agent design for disrupting protein-protein interactions. Moreover, substantial amounts of research have been directed towards the issue of designing molecules with varying molecular weights that can inhibit protein-protein binding.<sup>14</sup>

Non-covalent interactions, including hydrophobic effects, electrostatic interactions, Van der Waals forces, and hydrogen bonding, succeed when protein-protein complexes are formed.<sup>15</sup>

The following are the strategic approaches that can be used to facilitate the inhibition of

protein-protein binding: targeting the protein's interior active site, which is not exposed to the bulk solvent; and targeting the protein's exterior surface, which is not isolated from the bulk solvent.<sup>16</sup>

## **1.3 Protein-Protein Inhibition With Low Molecular Weight Synthetic Agents**

### **1.3.1 Small Molecule Inhibitors**

Most pharmaceutical studies in this field have sought to design small molecules for the inhibition of protein-protein interactions.<sup>17</sup> In many research projects, the aim has been to design small molecules that can interact with a specific site in the enzyme or the enzyme's active site. The predominant interactions within a protein's active site are electrostatic interactions, hydrogen bonding, and salt bridges. Resultantly, small "drug-like" molecules, which display hydrogen bond donor groups and hydrophilic features, have been associated with potential efficacy.<sup>18</sup> Nevertheless, a range of obstacles must be overcome when designing therapeutic agents that address a protein-protein interactions. For example, the region needed for recognition is substantial in size (i.e., from 700-1500Å<sup>2</sup> per protein),<sup>19</sup> which is problematic for small molecule inhibitors. Additionally, interacting surfaces have been identified as cavities with a high level of shallowness, and which do not have specific features. As such, selective targeting is a complex affair.<sup>20</sup>

Yet another challenge relates to the nature of the binding region of the two proteins involved in the protein-protein interaction. Often, the binding site is considered non-contiguous, the implication being that mimicry with simple synthetic peptides would not achieve the goal.<sup>21</sup> Additionally, dissimilar to enzyme-ligand interactions, the surfaces involved in protein-protein interactions are marked by significantly greater complexity. Rather than one of the partners

having a “pocket” that its counterpart occupies, each of the proteins can have protruding areas and “sub-pockets”, which poses substantial challenges for inhibitor design.<sup>22</sup> Moreover, regarding the use of small molecules as possible drug molecules, they must have efficacy *in vivo*. Aside from needing to display sufficient effectiveness in relation to the target protein, it is necessary for them to satisfy toxicity and bioavailability demands. Generally speaking, molecules with these “drug-like” features tend to have molecular weights that are not higher than 500.<sup>23</sup>

In the 1990s, the design of small molecule inhibitors experienced noteworthy strides forward. Quershi et al., in 1999, established a non-peptide antagonist (Figure 3), which was identified based on screening a chemical library of inhibitors of human erythropoietin, binding to the erythropoietin receptor’s extracellular region. This resulted in the identification of a derivative of biphenyl indole, which was associated with considerable efficacy as an inhibitor. The derivative was shown to have a maximal inhibitory concentration of 60 $\mu$ L.<sup>24 26</sup>

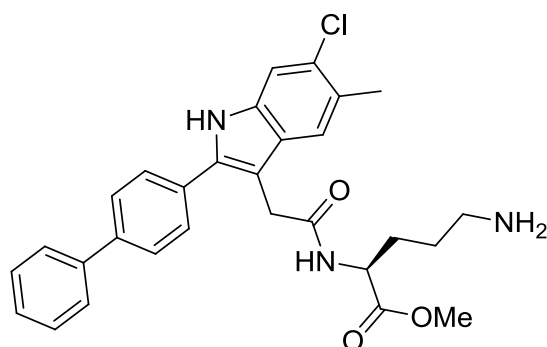


Figure 3: Chemical structure of non-peptide erythropoietin antagonist

In the study conducted by Tilley et al.,<sup>27</sup> the researchers found small molecules that could serve as inhibitors of cytokine receptor signalling. As a cytokine, interleukin-2 (IL-2) performs an

important function in growth activation and T cell differentiation.<sup>28</sup> At the outset, the small molecule (see Figure 4a) was established to imitate arginine and phenylalanine side chains of IL-2, which is implicated in binding to the  $\alpha$  subunit of the IL-2 receptor (IL-2R $\alpha$ ). Although the molecule's value as a mimic was non-existent, further investigation revealed that it was a strong IL-2 inhibitor, binding to its receptor.<sup>29-31</sup> As such, this discovery was the first case in which a small molecule had been identified that could inhibit protein-protein interactions, in which the inhibitor bound to the protein partner rather than the receptor. In Braisted et al.'s study,<sup>32</sup> the scholars developed this research project to establish an analogue with even greater potency (Figure 4b). The IC<sub>50</sub> of this compound was 60 nM, and it bound to IL-2 with a 1:1 stoichiometry and a K<sub>d</sub> amounting to 100 nM. Building on this work, Waal et al. established a nonpeptidic, potent inhibitor (Figure 4c).<sup>33</sup> These researchers drew on a chemical alteration of the previous analogues to promote the capacity of the inhibitor. Experimental evidence revealed that the furanoic acid incorporation led to an enhancement in the inhibitor's activity by 23 times.

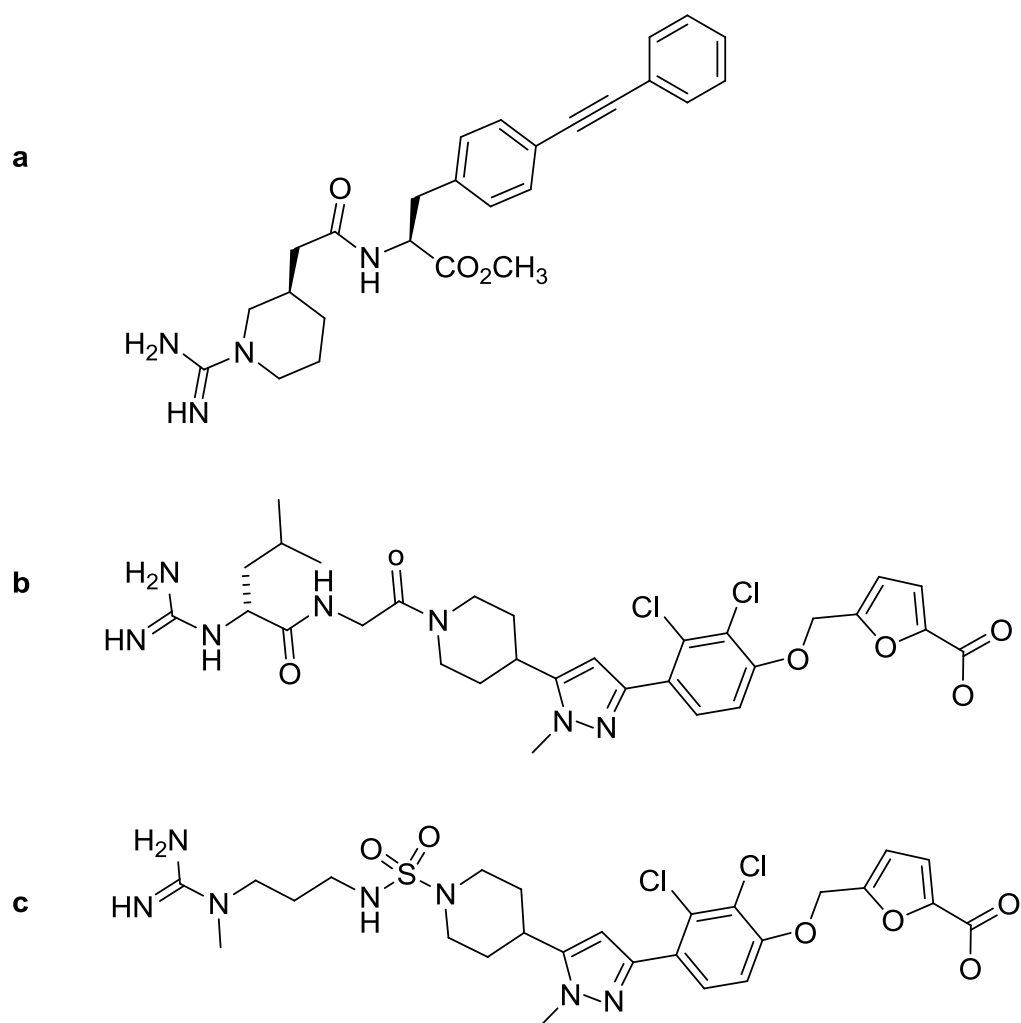


Figure 4: Small molecule inhibitors of IL-2 and IL-2R $\alpha$  interaction. (a) acylphenylalanine-based compound<sup>83</sup> (b-c) chemically-altered derivatives of compound a.

A notable protein target is inducible nitric oxide synthase (iNOS). As a molecule that plays a critical function in signal transduction, and which is produced by the dimeric enzyme nitric oxide synthase, nitric oxide's inducible isoform, iNOS, is implicated in tissue damage in various autoimmune diseases. An inhibitor designed to address iNOS, therefore, is associated with considerable clinical value. In view of this, McMillan et al. sought to establish an iNOS inhibitor by leveraging combinatorial chemistry ( Figure 5). Perturbation of the dimerization interface and substrate binding site was verified using X-ray crystallography. Additionally, it

was noted that the inhibitor operates by interrupting dimer formation, where these operation is dependent on an allosteric mechanism. Drawing on a rat model, the *in vivo* studies indicated that the inhibitor showed activity with ED<sub>50</sub> values of less than 2 mg/kg. The results indicate the therapeutic value associated with inhibitors of this kind.<sup>34</sup>

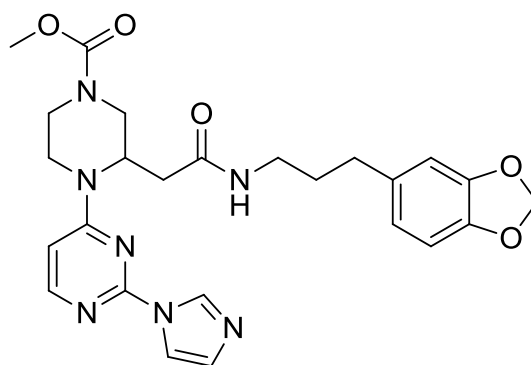


Figure 5: Chemical structure of iNOS

Tumour necrosis factor alpha (TNF- $\alpha$ ), a member of the cytokine family that is implicated in inflammatory conditions, is another prominent target. Research into the direct inhibition of TNF- $\alpha$  has identified a range of inhibitory antibodies, including Enbrel, Humira, and Remicade, several of which have been identified as efficacious for rheumatoid arthritis treatment.<sup>80</sup> Nevertheless, small molecule inhibitors are preferable as a result of their cost-effectiveness and the advantageous method of delivery. In the study conducted by He et al.,<sup>87</sup> the researchers developed a strong TNF- $\alpha$  inhibitor, the chemical structure of which is illustrated in Figure 6. This inhibitor leads to the displacement of a subunit of the biologically active trimer, thereby creating the inactive dimer.

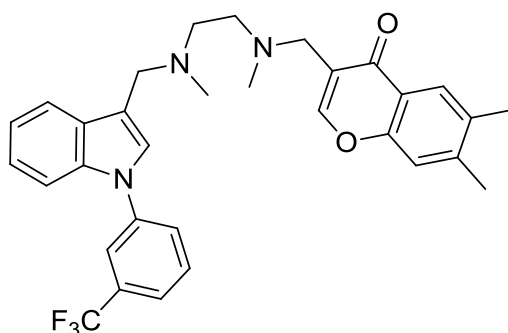


Figure 6: Chemical structure of TNF- $\alpha$  small molecule inhibitor

### 1.3.2 $\alpha$ -Helix Mimetics

A notable development took place in this area of study when researchers identified the critical function played by helical segments in various protein-protein interactions. In view of this, helical mimics synthesis was identified as a way to develop new treatments for a range of conditions.<sup>88</sup> The literature indicates that around 15% of the protein data bank, as of August 2009, comprised protein-protein complexes. Additionally, 62% of these complexes contained a helix at the interface. With this in mind, it is clear that  $\alpha$ -helices are highly-consequential for protein-protein interactions.<sup>89</sup> In Restorp and Rebek's study, the researchers provided an account of the synthesis of a series of heterocyclic piperazine-based scaffolds (Figure 7). These scaffolds could mimic the  $i$ ,  $i+4$ ,  $i+8$ , and  $i+11$  side chains of an  $\alpha$ -helix. It is possible to use the general synthetic process identified to synthesise  $\alpha$ -helix mimetics, and to tailor these to a particular interaction. The design of the compounds was intended to mimic the amphiphilic nature of  $\alpha$ -helices, and this was achieved by drawing on a hydrophilic surface for hydrogen bonding, paired with a hydrophobic surface for protein interaction.<sup>90</sup>

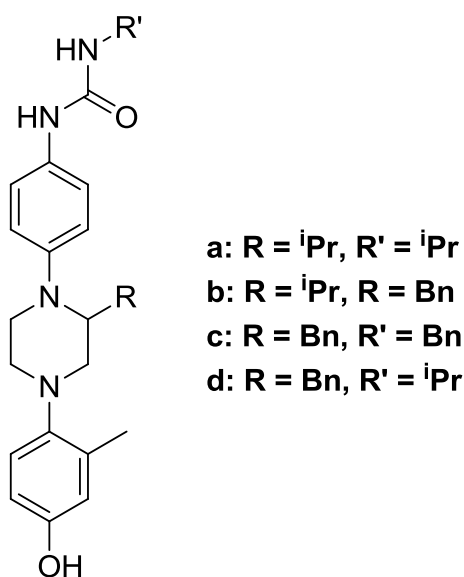


Figure 7: Chemical structure for the skeleton of several heterocyclic piperazine-based scaffolds

Therapeutic interventions for cancer patients also rely on protein-protein interaction inhibitors. P53, the tumour suppressor protein, has been identified as a notable transcription factor that safeguards cells from adverse transformations. Additionally, *h*DM2 regulates the activity and level of P53, the overexpression of which will undermine protein function.<sup>31</sup> The interaction between P53 and *h*DM2 incorporates the following hydrophobic residues from the tumour suppressor protein, thereby coordinating a helical conformation to a hydrophobic cleft that is a feature of *h*DM2: namely, Phe19, Trp23 and Leu26.<sup>32-34</sup> In view of this, a *h*DM2-P53 interaction can lead to protein stabilisation, thereby pointing the way towards a novel intervention for cancerous conditions. In the study conducted by Vassilev et al.,<sup>35</sup> the researchers devised a small molecule inhibitor which coordinates *h*DM2 inside the binding pocket of P53, thereby resulting in the activation of its pathway in cancer cells. Nude mice studies indicated that the outcomes included apoptosis, cell arrest, and inhibition of the growth of human tumour xenografts. X-ray crystallography research indicated that *h*DM2 is marked by a deep cavity, which contains side chains from the peptide's helical region. The small molecule antagonists were identified as a group of cis-imadazoline analogues, which are called

Nutlins. Following chemical optimisation, Nutlin-3 was established (see Figure 8), and it was identified as an inhibitor of *hDM2*-P53 complexes. In particular, it was associated with  $IC_{50}$  and 90 nM, and the small molecule antagonist showed activity in relation to xenografts *in vivo*.

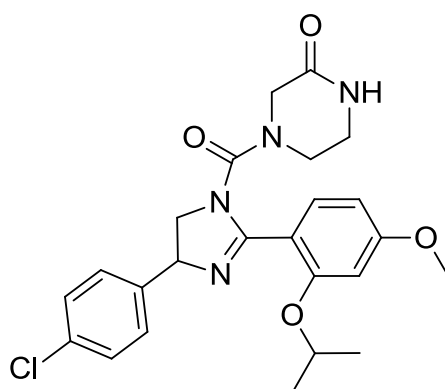


Figure 8: Chemical structure of Nutlin-3

Due to the finding that protein-protein interaction inhibitors are associated with potential clinical value in cancer treatment and management, many studies were conducted that focused on disrupting this specific interaction. For example, Plante et al.'s research was concerned with identifying oligobenzamide proteomimetic inhibitors. As mentioned above, Phe19, Trp23, and Leu26 are the main residues that are identified at the *hDM2*-P53 complex interface. A critical strategic approach in scaffold design for a helical mimic is that the scaffold must have the capacity to imitate the residues at the P53 helix's *i*, *i*+4, and *i*+7 side chains. Oligobenzamide, which is illustrated in Figure 9, was one of the compounds that came from this research initiative, and it was placed on top of the face of the P53 helix. Clearly, O-alkyl substituents of the amino terminated tri-benzamide are lying on a single face and, moreover, mimic the spatial orientation of the  $\alpha$ -helix's *i*, *i*+4, and *i*+7 residues. On the basis of these findings, it is clear that it is possible to design an efficacious mimic.

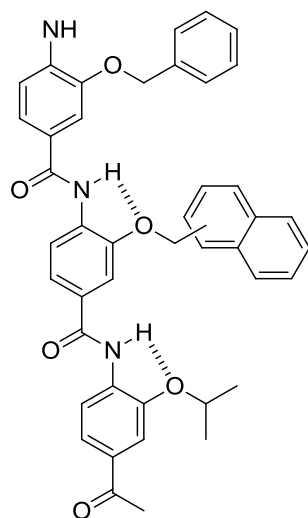


Figure 9: Chemical structure of oligobenzamide proteomimetic inhibitor

As previously noted, the synthesis of a nonpeptidic small molecule  $\alpha$ -helical mimic, which can serve as an inhibitor of protein-protein interactions, has long been an active area of research in the literature. Lee et al. sought to synthesise a novel pyrrolopyrimidine-based receptor, which is illustrated in Figure 10. The capacity of this scaffold for interrupting the P53-MDMX interaction was examined by the researchers, thereby informing its potential efficacy as an  $\alpha$ -helical mimic. At the outset, the researchers screened the scaffold using a 900-compound library, and primary amines containing hydrophobic groups were chosen. Noteworthy, the hydrophobic groups played a critical role in facilitating the mimicry of the side chains of the amino acids identified in P53. The features of this scaffold include conformational rigidity, cell permeability, and positive aqueous stability. Additionally, the synthetic route is straightforward, as a consequence of which the synthetic process complies with the establishment of expansive libraries and elevated throughput screening. Resultantly, the scaffold is associated with considerable promise as a way in which to discover comparable inhibitors in the future.

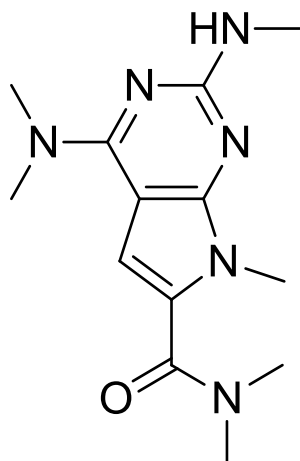


Figure 10: Chemical structure of pyrrolopyrimidine-based receptor

The reader should note that the information presented throughout this section is by no means comprehensive. Other, more exhaustive, articles have been published on protein-protein interactions with nonpeptidic small molecule  $\alpha$ -helix mimetics.<sup>36</sup>

### 1.3.2 Porphyrin and Calixarene Based Receptors

Since designing small molecule inhibitors is a complex affair, scholars have also sought to examine the efficacy of large scaffold molecules as protein binding agents. As noted earlier, designing synthetic agents to bind an active site is a highly-active area of research. Nevertheless, a different approach for disrupting protein-protein association involves binding to the surface of a protein that is near to the active site but not within it directly.<sup>36</sup> The peripheral surface is unique for every protein, and it contains hydrophilic, hydrophobic, and charged areas. Additionally, the interface between a pair of connecting proteins involves hydrogen bonding, electrostatic interactions, and  $\pi$ - $\pi$  stacking interactions.<sup>37</sup>

Most of the molecules that have been examined in the literature achieve the disruption of interactions by binding within active cavities on proteins. As a result, relatively few studies have sought to investigate synthetic molecules that intervene in the functioning of a protein through binding to the external surface. Studies in this area could promote the design of novel agents and, at the same time, aid in understanding the periphery of proteins and the mechanisms associated with surface recognition.<sup>35</sup>

Fischer et al.'s 1985 study reported on evidence that a tetracarboxyphenyl porphyrin, which is illustrated in Figure 11, was a corresponding topological mimic for cytochrome-c, and that it would bind with a  $K_d$  of 5  $\mu\text{M}$ .<sup>36</sup> As an electron transport protein that has been identified in horse heart, cytochrome-c is a protein that has been studied more extensively than most others in the literature. It is regarded as a viable target, and it performs a crucial function not only in apoptosis but also in electron transfer. The haem edge's surface contains a collection of arrangements of cationic lysine residues and hydrophobic domains, thereby indicating a high level of dependence, particularly in terms of electrostatic interactions.<sup>37</sup>

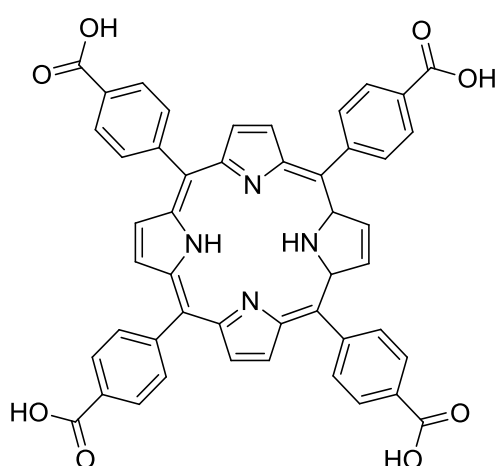


Figure 11: Chemical structure of tetracarboxyphenyl porphyrin

Hamilton et al. extended this body of research by examining tetraphenyl porphyrin scaffolds and calyx[4]arene scaffolds, drawing on several techniques (e.g., fluorescence spectroscopy).<sup>38</sup> The researchers' strategy involved leveraging a macrocyclic scaffold, on which the peptide loops could be attached using covalent bonds. Following this, a mimic of an antibody, grounded on calix[4]arene connected to four constrained peptide loops, was synthesised (Figure 12).<sup>39</sup> The rationale for selecting calix[4]arene stemmed from its accessibility and its ability to be set in a cone configuration, thereby meaning that para substituents would be propelled onto a single edge of the ring (and, in this way, creating a binding domain).<sup>40</sup>

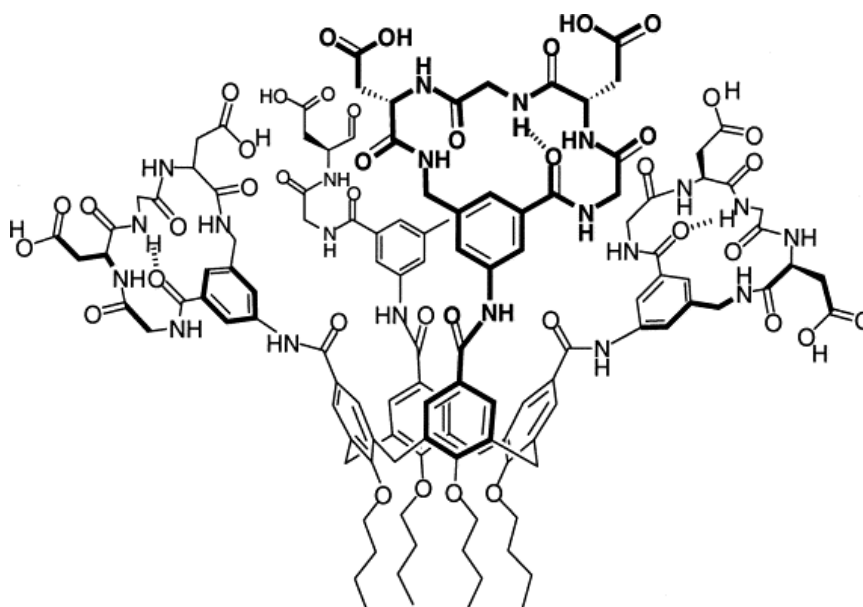


Figure 12: Chemical structure for an antibody mimic based on calix[4]arene scaffold and covalently attached to four peptide loops of the sequence (Gly-Asp-Gly-Asp)

The first target protein employed in the study was cytochrome-c, which has been extensively investigated, well characterised, and identified as having a surface that is positively charged. The peptide loops consist of a sequence that is negatively charged (namely, Gly-Asp-Gly-Asp), the opposite charge being important for complementing cytochrome-c's positively charged surface. X-ray investigation indicated that four peptide loops had the capacity to interact with

four lysine residues, the implication being that the coverage of the synthetic receptor extended to a significant surface of the protein. The results indicated that the receptor disrupted the formation of cytochrome c/cytochrome c peroxidase complex, confirming the X-ray findings.<sup>41</sup> In a subsequent study conducted by the same researchers, it was found that a comparable antibody mimic could interact with chymotrypsin surface, thereby facilitating the disruption of protease-proteinaceous inhibitor interactions.<sup>42</sup> Calixarene receptors were identified as undesirable due to the complex synthetic procedures needed, as well as the negligible yields that resulted. Several studies have been conducted on other supramolecular scaffold-based receptors.<sup>43-44</sup>

The same researchers, in 2000, published a study in which it was shown that cytochrome-c's surface had the capacity to be recognised by a tetraphenyl porphyrin scaffold with a variety of amino acid and peptide derivatives around the outside edge (Figure 13).<sup>45</sup> The results were indicative of the fact that the a receptor's relative affinity to the protein surface was informed by the number of anionic and hydrophobic groups. The affinity of these receptors in terms of binding was elevated in an aqueous medium, and receptor 19 (see Figure 13) was associated with the greatest affinity with respect to the surface of cytochrome-c ( $K_d = 20$  nM). Additionally, the study's outcomes pointed the way towards the possible clinical value of receptor 19. Studies conducted prior to this one demonstrated that cytochrome-c has the capacity to interact with an apoptotic protease activating factor, namely APAF1.<sup>46</sup> This particular interaction could trigger apoptosis. Hence, receptors of this kind were identified as potentially viable ways to facilitate the disruption of this protein-protein interaction.<sup>47</sup>

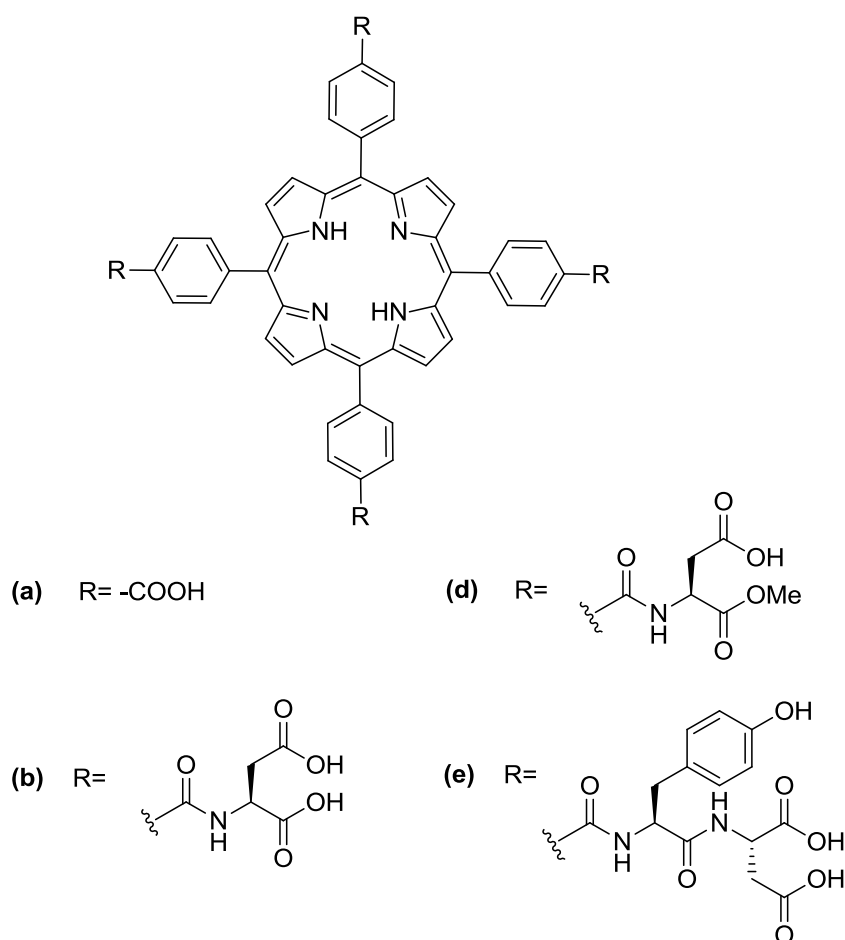


Figure 13: Chemical structures for tetraphenyl porphyrin scaffolds for recognition of peripheral surface of cytochrome-c

A protein's peripheral surface plays a fundamental role in the mediation of protein-protein binding in various biological procedures, including cell growth and cell proliferation. In view of this, synthetic molecules that serve as complements to the structural characteristics of the protein periphery are anticipated to bind, thus disrupting the surface, rather than the active site of the enzyme. Hamilton et al.'s 2003 study found that a group of tetrabiphenyl porphyrin-based receptors, particularly receptor 20 (see Figure 14), were associated with a heightened affinity with respect to the surface of cytochrome-c, exhibiting a  $K_d$  value of 0.6 nM. The researchers leveraged circular dichroism to examine the impact of coordination of this receptor in relation to the protein. Without the receptor, cytochrome-c's melting temperature was 85 °C, whereas when the porphyrin receptor was present, this temperature fell to 35 °C. On the basis

of these results, other studies were conducted to examine the potential of porphyrin-based receptors for protein denaturation and protein surface recognition. Additionally, as an outgrowth of this study, Hamilton's research group devised a sequence of metalloporphyrin dimers for the acceleration of proteolysis in cytochrome-c.<sup>46-47</sup>

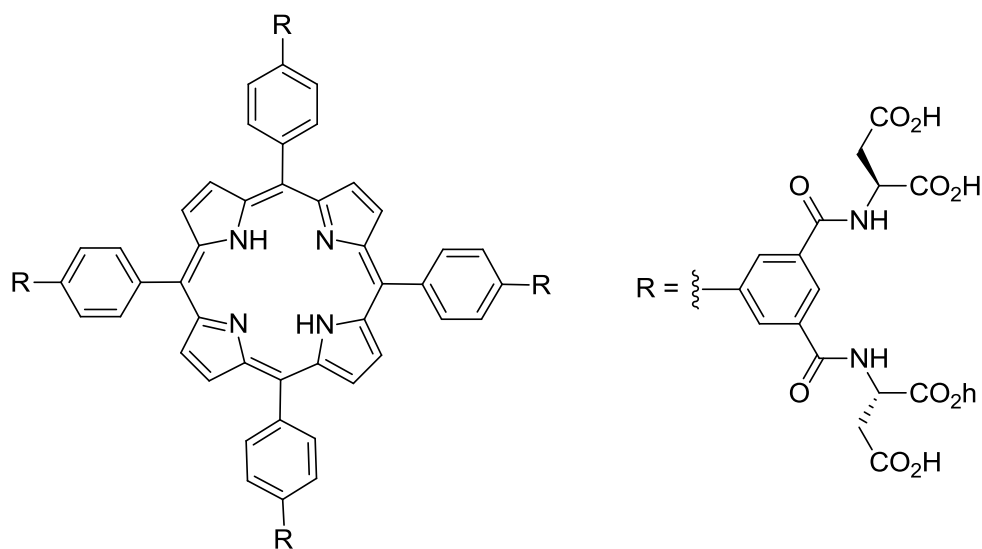


Figure 14: Chemical structure of tetrabiphenyl porphyrin-based receptor for surface recognition and improved unfolding of cytochrome-c

Trauner et al.'s study, published in 2003, resulted in the development of a set of porphyrin-based ligands associated with value for potassium channel surface recognition.<sup>48</sup> The researchers revealed that the four-fold symmetrical molecules served as peptide toxin mimics, thereby binding to the channel's four subunits. The result of the ligands binding to the potassium channels' K<sub>v</sub>1x class was the partial obstruction of conductance. Noteworthy, potassium channels facilitate the regulation of membrane potential and, furthermore, they are implicated in numerous cellular procedures. Hence, they are an attractive target for new drug development. The formulation of synthetic inhibitors could offer clinical solutions for a range of disease processes, including those associated with cardiac or autoimmune disorders.<sup>49</sup> The

set of porphyrin ligands were employed for competitive binding assays with <sup>50</sup>I-hongo-toxin<sub>1</sub>-A19Y/Y37Ff. One of the functions of this toxin is to coordinate to the external vestibule of K<sub>v</sub>1.3 channels. In the activation of human T-lymphocyte, this potassium channel, which is voltage-gated, plays a fundamental role. Studies indicate that the cationic ligands in Figure 15 were associated with the most potent interactions with respect to the K<sub>v</sub>1.3 channel. The cationic side chains were identified as having the ability to establish salt bridges to aspartate residues, which accounted for the high level of affinity. Additionally, in terms of their geometric features, ligands (a-c)-were viable for sufficient binding. As this research project attests to, developing a class of compounds of this kind has significant value for new drug development in various areas.<sup>49</sup>

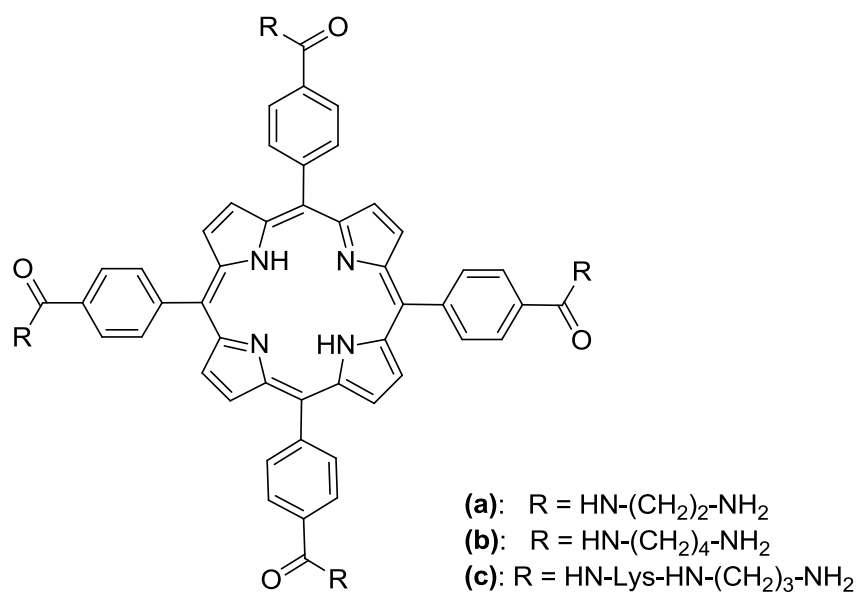


Figure 15: Chemical structures of several cationic porphyrin-based ligands for the potassium channel surface recognition

If the abovementioned obstacles are set aside for one moment, the reader may be motivated to reflect on the countless developments that have taken place in this field. In particular, it is noteworthy that there are many cases of synthetic ligands with a low molecular weight that have the capacity to facilitate the inhibition of protein-protein interactions.

### **1.3.3 Supramolecular Protein Scaffold**

Determining what impact nanomaterials have on protein function and biophysical characteristics is crucial for bio-nanotechnological research. As protein molecules that are ubiquitous in all of the biological processes that underpin life, the function of enzymes is dependent on their structural integrity (at both the secondary and tertiary levels). It is unfortunate to note that enzymes can experience conformational change as a result of the disruption of the non-covalent interactions that promote their stabilisation (e.g., electrostatic interactions, Van der Waals forces, and hydrogen bonds). Additionally, protein molecules' structural dynamics play a substantial role in regulating effective catalytic function, which has only been taken into consideration recently in research projects addressing the impact of nanomaterials on proteins. To give an example, protein dynamics are impacted in the event that the enzyme is attached in a covalent way to graphene oxide (GO) nanosheets. Recognition of substrate depends on the flexibility of the protein in view of the fact that it underpins conformational modifications at the substrate-binding region.<sup>45</sup> Therefore, fluctuant protein dynamics, which come about due to the nanomaterial, can have an impact on the protein's catalytic activity.

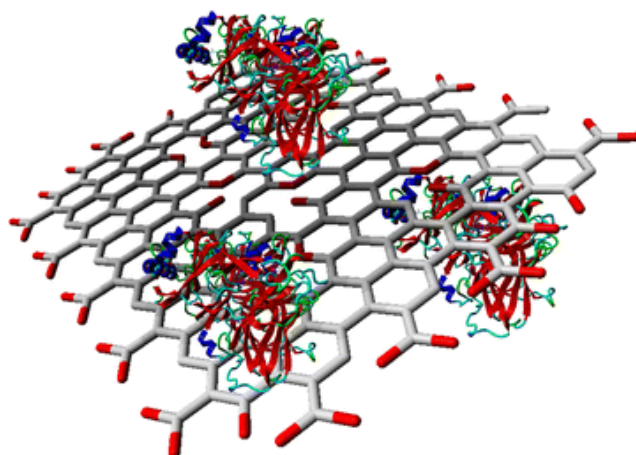
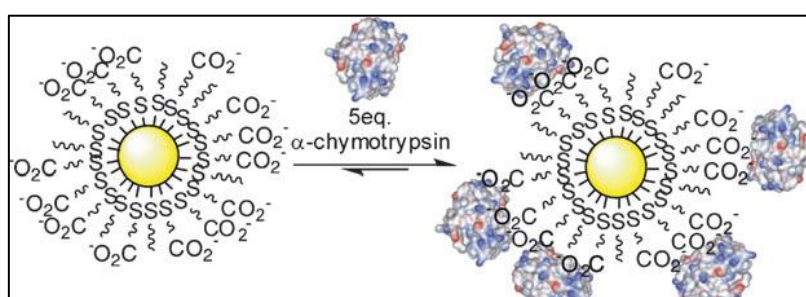


Figure 16: Glycosylated bilirubin oxidase (BOD) immobilised onto GO nanosheets

To facilitate surface recognition, Rotello drew on self-assembled systems as part of an approach that incorporated mixed-monolayer protected gold clusters (MMPCs), functionalized using terminal anionic groups. These anionic groups were made to bind to a positively charged  $\alpha$ -chymotrypsin surface, the purpose being to restrict enzymatic activity by means of a two-stage mechanism (i.e., rapid reversible suppression followed by a less rapid, gradual, and irreversible enzyme breakdown procedure) (*see Scheme 1*).



Scheme 1: MMPC use in surface recognition

The researchers found that the electrostatic interactions were efficacious because the process revealed selectivity when compared to elastase. The confirmation of the elevated efficiency of

the interaction between  $\alpha$ -chymotrypsin and the gold nanoparticle took place based on circular dichroism spectroscopy. In this process, 10 nM  $K_i(\text{app})$  and stoichiometry were used, consisting of five protein molecules for a single MMPC. Noteworthy, the selectivity of the mechanism of inhibition was higher for  $\alpha$ -chymotrypsin than it was for  $\beta$ -galactosidase.

Synthetic receptor and inhibitor of  $\alpha$ -chymotrypsin activity were the functions of the surface carboxylate group. In particular, the level of  $\alpha$ -chymotrypsin suppression was greater based on dose response (i.e., by weight) when compared to the other synthetic inhibitors.<sup>31</sup> Wang et al. offered data to suggest that a nanocomposite material could be devised to facilitate new drug development to intervene in conditions such as Alzheimer's, where this material would be based on GO and iron oxide (IO) integration.<sup>32</sup>

Other possible protein inhibitors that are worth paying attention to are dendrimers, which are associated with terminal groups that enhance their interaction with the hot spot residue. Owing to the comparable sizes and contours of critical proteins, dendritic polymers are regularly referred to as artificial globular proteins.<sup>33</sup>

## **1.4 Dendritic Polymer Synthesis**

### **1.4.1 Dendrimer Synthesis**

Flory's 1952 paper initiated a new era in dendritic polymer chemistry.<sup>25</sup> The researcher's theory centres on a condensation between  $AB_x$  (where  $x \geq 2$ ) monomer molecules. Vögtle et al.,<sup>3</sup> building on this theory, proposed the initial iterative synthetic process for dendrimer synthesis, which was based on aliphatic amine  $AB_2$  type monomer molecules. Condensation engendered the synthesis of so-called "cascade" polymers.<sup>3</sup> As monodisperse symmetrical macromolecules, dendrimer synthesis depends on close synthetic control, which can be

achieved by a layered approach to dendrimer construction. As a complex synthesis process, a range of deprotection, protection, and purification phases are involved at every step of the process. The first synthesis processes were devised in 1978, and – at present – there are two broad categories: firstly, the divergent approach; and secondly, the convergent approach.

### **1.4.2 Divergent Approach**

Divergent dendrimer synthesis, devised based on the branched model of Tomalia et al., begins with an initiator core, after which layers are added via sequences of coupling and activation stages to build outwards in the direction of the molecule's periphery.<sup>26</sup> The growth of a dendrimer using the divergent approach is illustrated in Figure 17. The terminal groups of every generation are reacted with the complementary reactive group on the monomer unit.<sup>27</sup> Hence, branch points are created at every site, thereby leading to a growth in the amount of terminal functionalized groups. This is known as the coupling step. When the initial coupling stage has been completed, this is followed by an activation step, in which dormant functional groups are activated. This enables the monomer to react, thereby increasing generation.<sup>26</sup> Noteworthy, the availability of active hydrogen available determines the number of branches in the macromolecular intermediate. These are linked in sequence to other interior generations.<sup>10</sup>

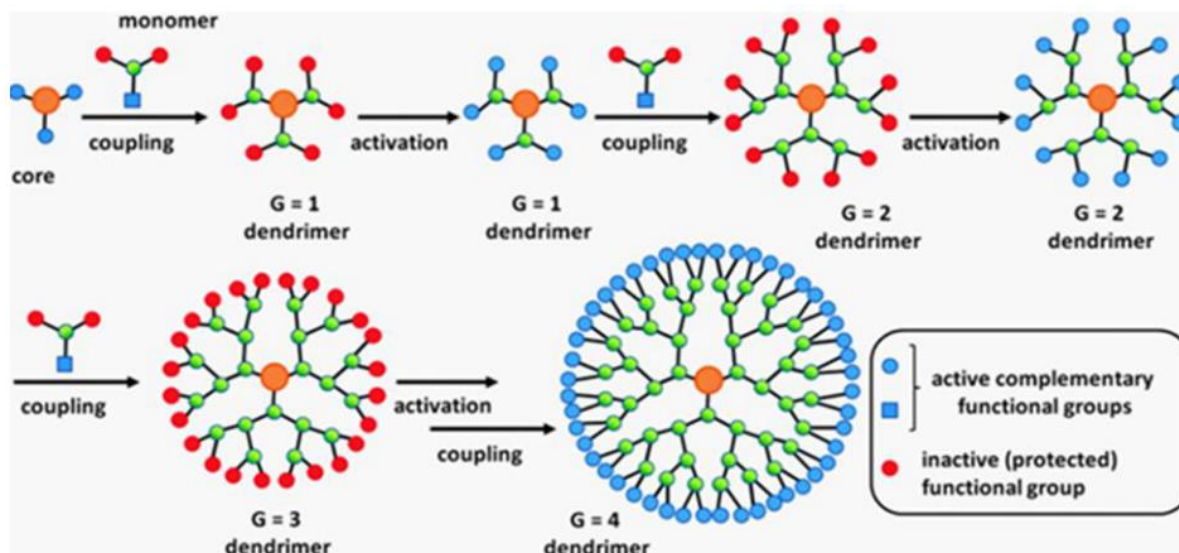


Figure 17: Divergent dendrimer synthesis

Divergent dendrimer synthesis benefits from its straightforward nature, as well as the fact that, when viable reaction conditions can be sustained and fitting reagents are employed, industrial scale synthesis is entirely achievable. Nevertheless, given the sequence of activation and coupling reaction phases required in this approach, the number of reactions required at the perimeter increases exponentially. Hence, to guarantee that each reaction step finishes as expected, a considerable excess of reagents is required. The manner in which the required amount of coupling reactions scales with every generation, as well as the likelihood of undesirable side-effects (and the resulting possibility of incomplete by-products), is another disadvantage. Additionally, the activating reagent must be eliminated completely to safeguard against the formation of unnecessary dendritic structures.<sup>27</sup>

Polyamido amines (or “starburst” dendrimers), which were originally characterised by Tomalia et al. in 1985,<sup>26</sup> were the initial family of dendrimers that were synthesised and, in turn, made commercially available. As an extensively studied family of dendrimers, further information can be found in the literature.<sup>10, 28-30</sup>

### 1.4.3 Convergent Approach

Fréchet and Hawker were the first researchers to document the convergent approach for dendritic polymer synthesis.<sup>6, 26, 31</sup> The approach begins with the periphery of the final dendritic structure and proceeds towards the core, thereby creating a reactive dendron. To produce a globular dendritic architecture, a group of dendrons are reacted with a polyfunctional core molecule.<sup>28</sup> Hence, convergent synthesis differs from divergent synthesis in that the core is included in the macromolecule at the ultimate reaction phase.<sup>32</sup> The convergent approach is illustrated in Figure 18.

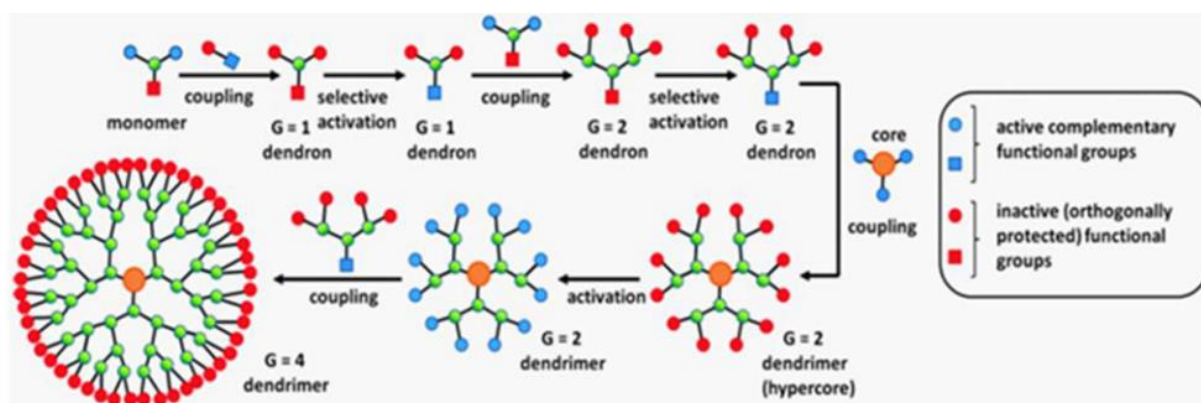


Figure 18: Convergent dendrimer synthesis

Following coupling, it is possible to use an activation process to trigger the dendron's focal point. The architectural control associated with this approach is high because the process moves from the periphery towards the core, thereby meaning that a reduced number of coupling reactions are required at every phase. Hence, slight surplus reagents are needed, which contrasts with the divergent approach, and which assists in purification. Another way in which

the convergent approach is superior to the divergent approach stems from its capacity to distribute functional groups across the architecture selectively. As such, the approaches used to manufacture symmetrical or unsymmetrical dendrimers in this way benefit from accuracy and high levels of definition. In terms of the approach's disadvantages, steric crowding may emerge due to the movement from the periphery to the interior. Large generation dendrimers are complex to produce, and defective structural features are common.<sup>12</sup> Poly (benzyl ethers) are regularly produced using this approach, and they have been manufactured by Grayson and Fréchet.<sup>6, 32</sup>

## **1.5 Concerns Surrounding Synthetic Inhibitors**

As previously noted, gaining insight into protein-protein interactions is vital for the advancement of research into the discovery of novel drug molecules and inhibitors.<sup>116, 117</sup> Owing to the sizeable nature of the interfacial areas that proteins have, identifying small “drug-like” molecules that can serve as effective inhibitors has been a complex task. Nevertheless, significant progress has been made in recent years. As a case in point, studies have demonstrated that small molecules can, in fact, disrupt protein-protein interactions, thereby serving as effective inhibitors.<sup>118</sup> Figure 19 illustrates the distribution of interfacial areas from common protein-protein complexes, as identified in the literature.<sup>77</sup> The amount of complexes characterised by comparable binding areas are grouped into one region, after which they are plotted against the size of the interfacial area.

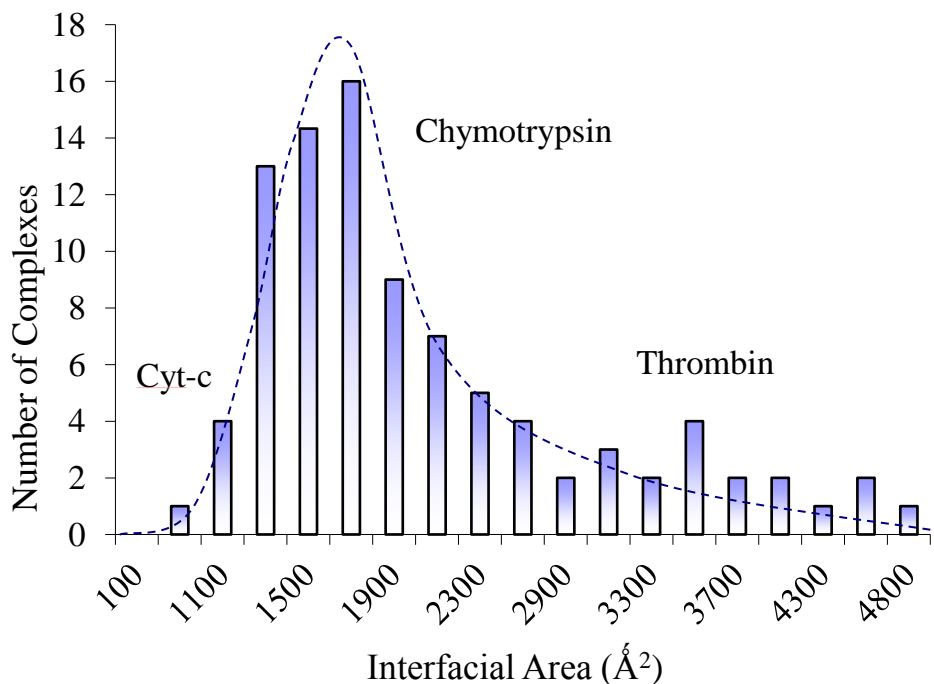


Figure 19: Number of protein complexes found in the literature plotted against the size of the interfacial area

As the figure above indicates, the coverage of protein complexes is broad, and so molecules with high molecular weights have been identified as synthetic protein-protein binding inhibitors that could be efficacious. Given the sizeable nature of a protein’s interfacial area, a critical issue is synthesising a sequence of macromolecular structures that can interact over several areas. Key variables that have strong implications for protein-protein interactions include three-dimensional shape, functionality, and the location of this particular functionality inside the interacting region. In view of this, the purpose of the present research project is to facilitate the synthesis of a sequence of macromolecular structures that satisfy these parameters.

The first of the large molecules that are worthy of consideration are linear polymers, which have been studied in several research projects addressing the interaction between proteins and linear polymers. Bruening et al. published results attesting to the high capacity binding of proteins by poly (acrylic acid) brushes, where thick polymer brushes were devised to facilitate

the immobilisation of several protein monolayers.<sup>119</sup> Drawing on a nitro triacetate/copper complex ((NTA)-Cu<sup>2+</sup>), PAA brushes were derivatised, after which they displayed a capacity to bind to various proteins. The capacity of a protein to interact with a surface is potentially invaluable for protein purification. Additionally, in the study conducted by Wowk et al., the researchers demonstrated that simple linear polymers (in this case, polyglycerol and polyvinyl alcohol) could inhibit bacterial ice nucleation, specifically the ice nucleating activity of *Pseudomonas syringae* proteins. Polyglycerol was associated with higher potency and specificity, but the combined use of polyglycerol with polyvinyl alcohol resulted in more effectiveness than the independent use of each agent.<sup>120</sup>

For the present research project, specificity is a fundamental prerequisite. In view of this, the dynamism and flexibility associated with linear polymers means that they are not suitable (see Figure 20a). Polyvalent effects underpin the interaction between linear polymers and proteins, which means that a directly proportional relationship exists between the number of charges present and the strength of the bond. Hence, size specificity is not a feature, and a linear polymer can dynamically alter its morphological and structural features to improve binding. Resultantly, interactions between linear polymers and proteins are designated as “non-specific”.<sup>121</sup>

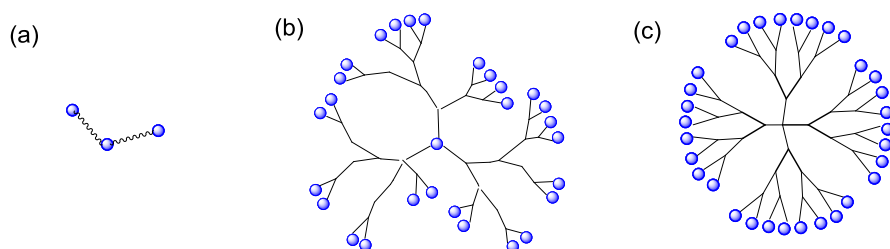


Figure 20: Structure of (a) linear polymer, (b) hyperbranched polymer, and (c) dendrimer

Hyperbranched polymers and dendritic polymers, both of which are presented in Figure 20, were also considered in this research. Dendritic polymers are distinct when compared to conventionally branched polymers, specifically with respect to the branching possibilities at every monomer repeat unit. Hence, vast numbers of functionalized terminal groups exist in this structural arrangement. Owing to the fact that protein surfaces are highly charged in certain places, dendritic polymers were considered a promising possibility.

Hyperbranched polymers are characterised by irregular branching architectures, which is the main feature that differentiates them from dendrimers. As a result of this irregularity, their flexibility is considerable, and – as was determined in the present study – potentially overly flexible. As noted previously, a high level of flexibility typically corresponds to a lower level of specificity, which is relevant because specificity is the principal focal point of this research project. In contrast, dendrimers are marked by the regularity of their branching architectures, their symmetric nature, and their property of being monodisperse. When considered in relation to hyperbranched polymers and linear polymers, dendrimers display a high level of molecular uniformity and an aspect of rigidity. Hence, it is possible to quantify their maximum addressable area as the square of their diameter. The functionalisation of a dendrimer's outer surface is also a straightforward task, which lends itself to the mechanism of protein-protein binding, in which the matching of size, shape, terminal functionality, and the location of this functionality is critical. Hence, dendrimers hold considerable promise as potential large molecule inhibitors for protein-protein binding.

The research group coordinated by Twyman reported on a size effect associated with dendrimers, which can be leveraged to formulate a size-selective binding mechanism for inhibiting protein-protein interactions. In other words, the optimal dendrimer for binding to a specific protein is that which has an addressable area which corresponds most closely in size

to the protein's interfacial area. In the event that a large ligand interacts with an enzyme's active site, it becomes blocked, thus undermining the enzyme's function. Hence, the dendrimer that can bind most effectively is simultaneously the strongest inhibitor.<sup>35</sup> The utilised dendrimers were PAMAM dendrimers, which are presented in Figure 21. The figure also shows the addressable areas of each dendrimer.

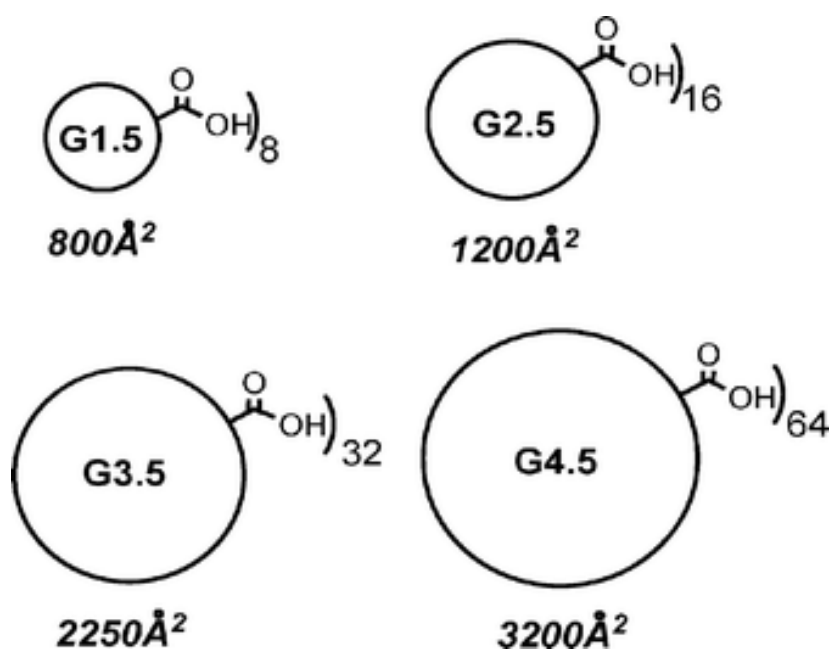


Figure 21: PAMAM dendrimers and addressable areas

Ronald's dendrimer-supported dynamic combinatorial chemistry (DCC), which is marked by high support loadings, homogenous purification, routine intermediate characterisation, and solution phase chemistry, relies on the use of dendrimers in the form of soluble supports. The results indicate that it is possible to generate effective combinatorial libraries using DCC. Therefore, given that they underpin the accessibility of molecular networks, dynamic

combinatorial libraries (DCLs) have significant potential for the advancement and interrogation of chemical complexity.<sup>36</sup>

## 1.6 Dynamic Combinatorial Libraries

Dynamic combinatorial libraries (DCLs) are aggregations of molecules that are in continuous, reversible equilibrium. Through the use of interactions, whether covalent or non-covalent, molecules of this kind can self-assemble into complexes that are thermodynamically controllable.<sup>37</sup> The structural arrangement of the DCL is determined by the relative stability of each constituent, which is itself informed by exposure to external templates or factors (e.g., a protein). An illustration of DCLs is given in Figure 22.

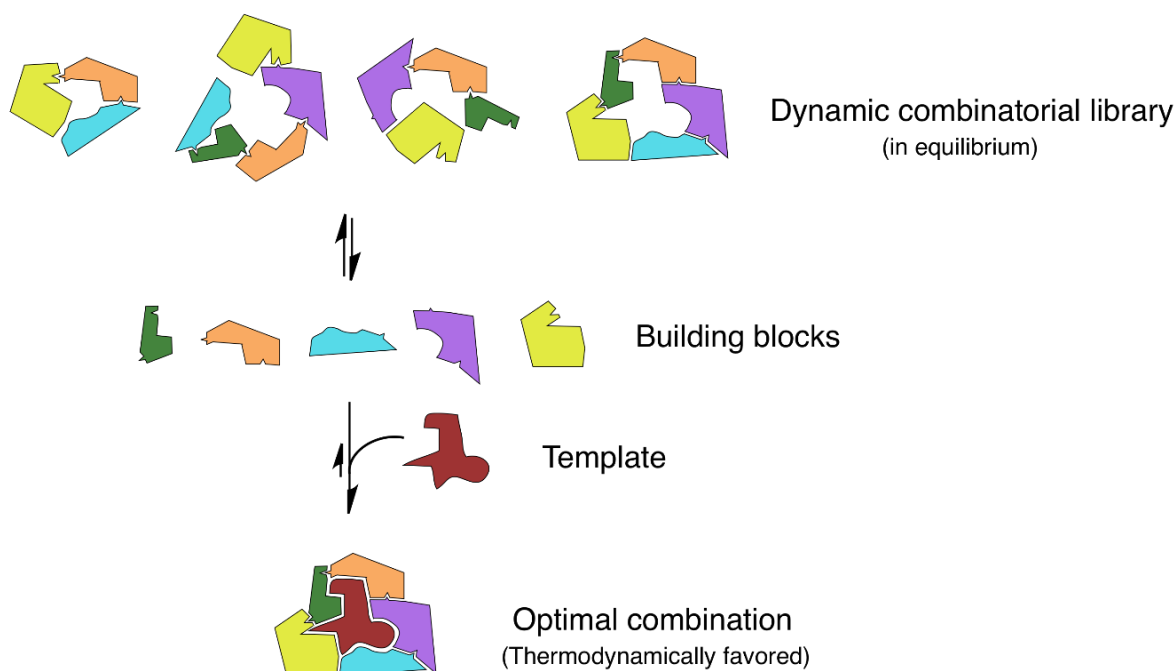


Figure 22: Dynamic combinatorial libraries (DCLs) . Image reprinted with permission from Li, J., Nowak, P. & Otto, S.. *J. Am. Chem. Soc* 135, 9222–9239 (2013)

It is possible to combine a template molecule with the reaction, on the basis of the utilisation of DCLs, thereby driving it to the product that displays the most potent level of affinity for the template (informed by non-covalent effects and size). Consequently, the ideal dendrimer-chain complexes can be targeted for using proteins as template molecules to identify the configuration with the highest binding affinity. In view of this, the process of identifying new drugs, which has historically been time-intensive, can be made more efficient through the development of DCLs.<sup>39</sup> Although the level of control associated with this method is acceptable, it is quite rigid for library generation because every structure must be designed and produced independently. Nevertheless, in the event that dynamic characteristics can be included in the generation procedure, it is possible to imagine a novel aspect of the combinatorial procedure. In such situations, the library becomes flexible and, moreover, can adjust autonomously based on the target macromolecule at a particular time in a particular environment. Furthermore, owing to the reversible processes of supramolecular and molecular interchange, adaptability to the limitations of the system is reasonable.

***CHAPTER 2***  
***AIMS AND OBJECTIVES***

## 2.0 Aims and Objectives

A helpful strategic approach for the inhibition of disease-related protein-protein complexes involves the development of macro-ligands with the capacity to interact with the expansive binding surfaces of proteins. Despite the fact that dendrimers have been successful, they do not bind in a selective manner.

Previous studies have demonstrated that carboxylate dendrimers can bind to proteins with positively charged interfacial areas. The results of these studies indicate that it is possible to achieve selective binding by matching the size (or maximum addressable area) of the dendrimer to the protein's interfacial area.<sup>15</sup> Improved binding can be achieved by adding various amino acids to the dendrimers. Binding studies have also revealed that a tyrosine dendrimer binds most effectively to  $\alpha$ -chymotrypsin, with an affinity that is 30% higher than a non-functionalized dendrimer of compatible size and charge (Figure 23).

Although the studies using mono-functionalized dendrimers exhibited improved binding, the approach was not appropriate for the synthesis of dendrimers with a range of different terminal groups. That is to say, it is not possible to regulate the three-dimensional position of every group in relation to the others. In the present study, the focal point of investigation was the use of dendrimers and functionalized dendrimers as protein binding ligands.

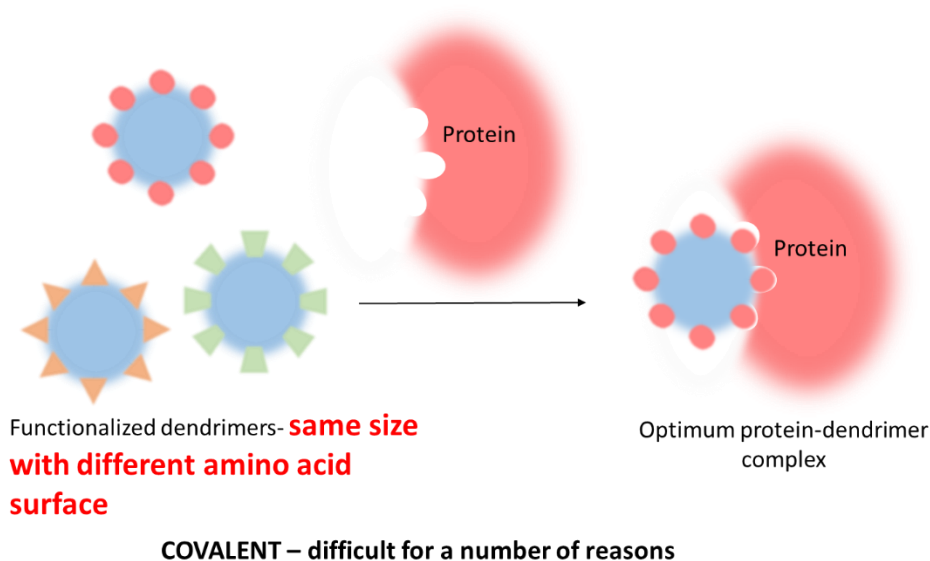
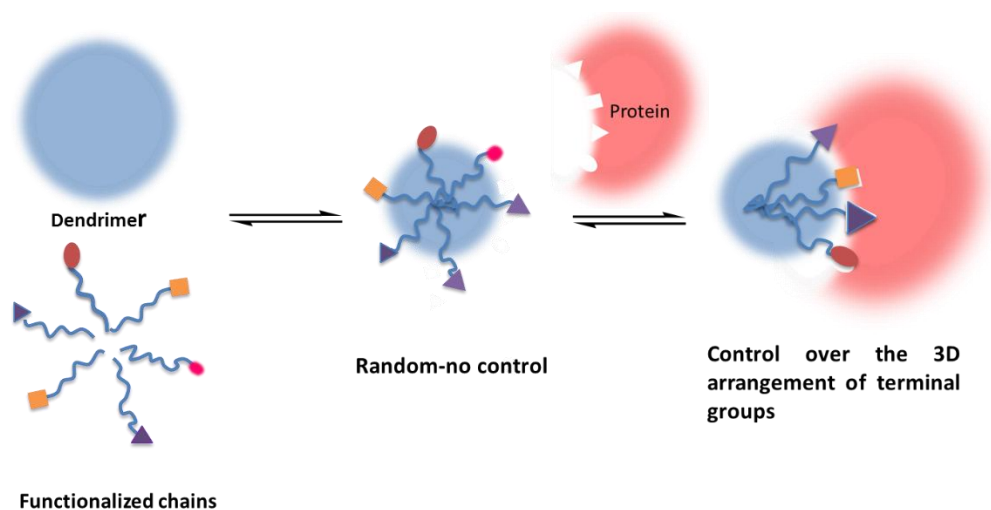


Figure 23: Covalently functionalized dendrimers as selective protein ligands.

All in all, the experiments attested to the critical role played by functionality and size in the process of creating macromolecular ligands for selective protein binding. Despite the success of the results, and although they provide an unambiguous proof of concept, covalent chemistry is time-intensive, particularly in terms of the need to incorporate core functionality and specific terminal groups. Additionally, design or synthesis errors are complex to correct, the implication being that, in the event that they take place, it is necessary to synthesise the dendrimer ligand once again. Moreover, while including a single/specific functional group on several occasions to the dendrimer surface (i.e., polyvalency) is quite straightforward, it is a highly complex affair to position moieties of this kind with a geometric level of accuracy in a way that is relative to one another. It is a yet more complicated task to include a varying number of functional groups to produce multivalency with control in terms of their relative positions. Needless to say, design accuracy of this kind is a fundamental requirement for the covalent synthesis of any therapeutically viable dendrimer.

This study aims to develop a proof of concept methodology for acquiring selective macromolecular ligands for specific proteins. The aim is to establish a system in which the protein can select its optimal ligand from an expansive set of functionalized macromolecular ligands. Thus, this study attempts to establish a non-covalent methodology for assembling targeting groups both around and inside a dendrimer framework. Controlling the relative positions of targeting groups relies on the use of a target protein (i.e., as a template), thus guiding the formation of an optimised macromolecular protein ligand.



**Figure 24:** Multivalent non-covalent method using a dynamic approach towards selectivity. On combining all constituents, self-selection of the optimised macro-ligand will occur.

We propose a novel non-covalent methodology based on the design shown in Figure 24. The first aim of this project was to establish parameters that would maximise the encapsulation of the linear chain. This would include hydrophobicity and the effect of any additional binding (e.g. hydrogen bonds, as illustrated in Figure 25). Another aim was to investigate how a linear chain functionalized with different amino acids could moderate binding. Additionally, we sought to study a mixture of linear chains with different amino acids. When investigating the

use of functionalized linear chains on binding, it will also be necessary to conduct various control experiments to determine what effect the dendrimer and non-encapsulated linear will have on binding.

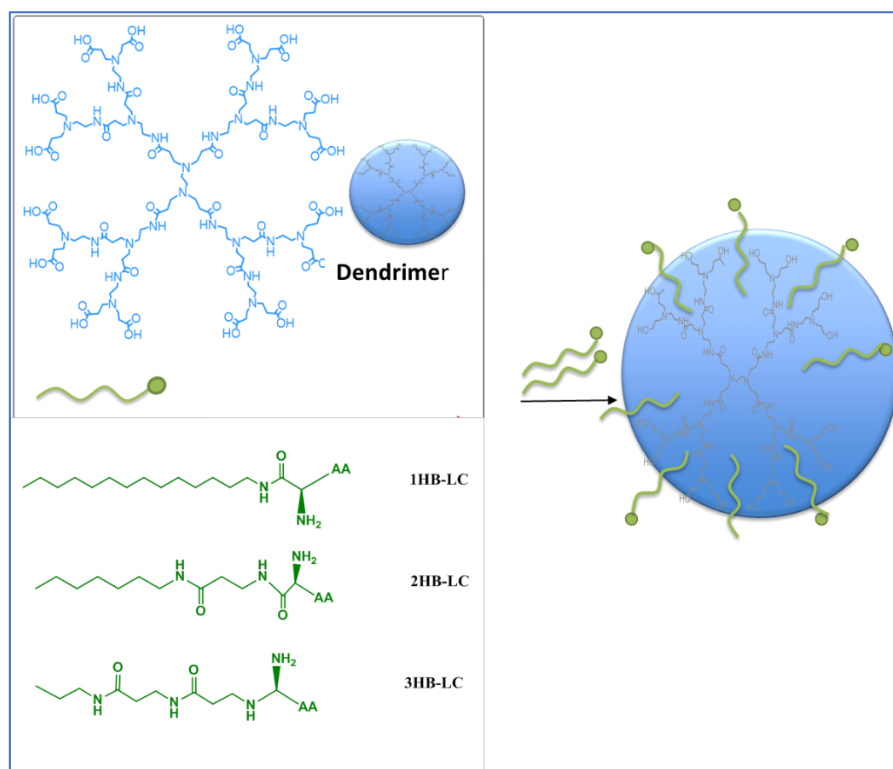


**Figure 25:** Proposed linear chains that including hydrophobicity and additional hydrogen bonds required to maximize encapsulation within the dendrimer

Another aim is to develop a protein binding system containing an additional molecule that can be used as a probe or sensor. This probe/sensor would be incorporated non-covalently, thereby producing a molecular design that can be modified conveniently for specific proteins by changing the linear chains and/or the probe/sensor. To be specific, this study pursues a novel paradigm that will utilise the modularised, non-covalent self-assembly of sensing and binding units within and around an inert dendrimer framework (Figure 26). Despite being contained

within the dendrimer, the binding units are characterised by their mobility. Hence, after adding a protein to the solution, the binding units change their position to heighten (cooperative) interactions with respect to the protein's binding surface. This process is protein-controlled because it regulates the formation of its own optimised macromolecular ligand by seeking the lowest energy system (protein/dendrimer complex). This aspect is the same as the one described in the introductory chapter. However, by incorporating the sensor units and binding units in the assembly programme, binding may also be identified and, moreover, measured. For this part of the research project, the aim is to develop a non-covalent approach by which targeting and sensing units can be assembled around and within a dendrimer framework.

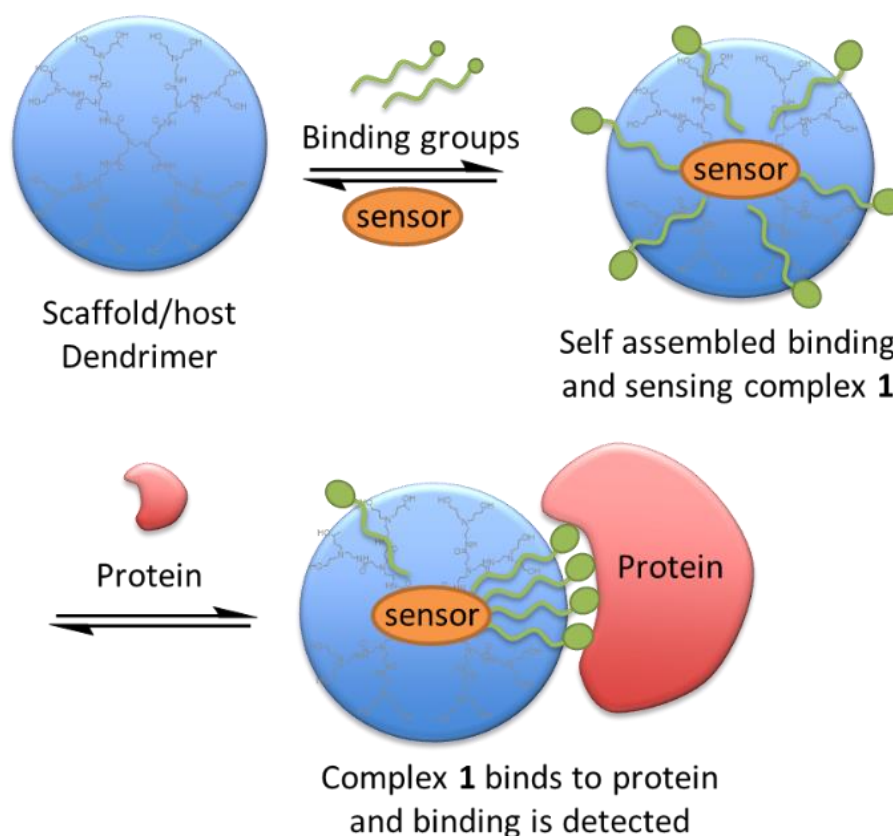


**Figure 26:** Proposed self-assembled protein binding complex **1** and its binding to a target protein. A neutral/non-binding dendrimer acts as a scaffold to support and encapsulate the binding and sensing units. The use of non-covalent chemistry allows the targeting groups to move and maximise their binding efficiency in the presence of a target protein.

## ***CHAPTER 3***

### ***Preparation of functionalized dendrimer***

### 3.1 INTRODUCTION AND AIMS

The complexes formed when proteins interact with each other or other biological macromolecules play essential roles in all biological processes.<sup>1</sup> Illness is typically the natural result of conditions that lead to protein mutations, or uncontrolled or unwanted interactions.<sup>2</sup> Notable illnesses include neurodegenerative diseases such as Alzheimer's and Huntington's disease.<sup>3</sup> Protein-protein interactions are also involved in viral and bacterial infections. For example, binding between proteins on the surface of bacteria and cells can facilitate the internalization of the bacteria within the host cell.<sup>4</sup> Using a similar mechanism, it has been demonstrated that viral proteins can bind to host proteins, resulting in internalization and infection.<sup>5</sup> As such, understanding how to modulate or inhibit protein-protein interactions is an emerging concept in drug design. The general concept of protein inhibition is illustrated in Figure 27.

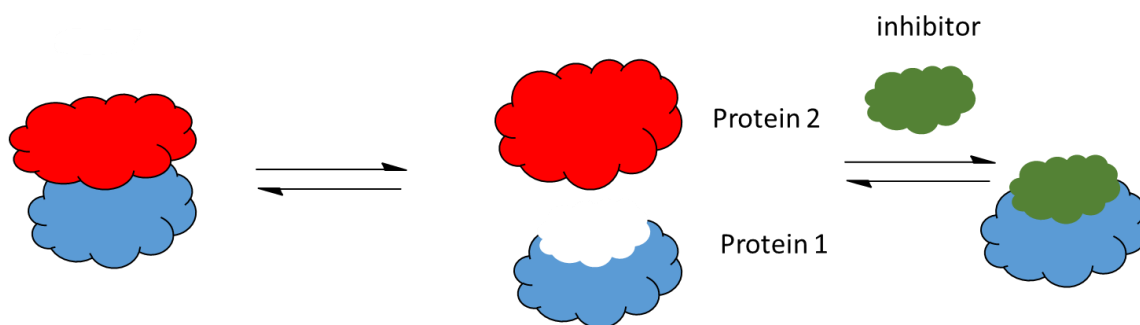


**Figure 27:** Protein inhibition

Complementary functionalities that are located at specific sites on large interacting surfaces, which can range from  $500 \text{ \AA}^2$  to  $5,000 \text{ \AA}^2$ , allow one protein to recognize another, and the main element is referred to as the interfacial area.<sup>6</sup> Hence, a difficulty that must be overcome in surface based inhibitor design relates to the establishment of architectures that are sufficiently

large to interact with a majority of a protein's interfacial area, and ideally all of it.<sup>7</sup> In addition to size, a range of non-covalent interactions are relevant to note in regards to the selectivity of an inhibitor. These non-covalent interactions include charge/charge, aromatic/ $\pi$ - $\pi$  interactions, hydrogen bonding, and hydrophobic interactions.<sup>8</sup> Research studies that have examined protein-protein interactions have reported on certain amino acids that contribute over 2 kcal/mol to the binding energy in a consistent way, all the while appearing at the interfacial surface with a frequency exceeding 10%.<sup>9</sup> Amino acids of this kind have the capability to engage in several interactions, and they include tyrosine (13%), arginine (14%), and tryptophan (21%). Hence, critical design elements to consider with respect to the acquisition of selective ligands for protein binding include functionality, charge, size, and multi/polyvalency. Given these requirements, it is not surprising that macromolecular ligands are associated with considerable promise with regards to protein binding. Examples include calixarene and porphyrin scaffolds,<sup>10,11</sup> nanomaterials,<sup>12</sup> and linear polymers.<sup>13,14</sup>

Functionalized calixarene and porphyrin scaffolds, supporting diverse amino acids, were traditionally used in the literature, which had a high level of affinity for a range of groups in binding to certain proteins.<sup>14</sup> Gilles et al. published the first study in which functionalized linear copolymers were used to bind enzymes with enhanced selectivity, which relied on the screening of co-monomers with varying types of amino acids.<sup>51</sup> The researchers established a library of inhibitors for binding to several serine proteases, and the functionalized co-monomers were used to inform selectivity. The co-monomer-amino residue interaction occurred on the surface of the protease and also inside the active site, as shown in Figure 23. Figure 23b indicates the collaboration among functionalized groups. Noteworthy, biphosphate co-monomers were identified as binding to the elastase surface, while an anchor monomer was found to direct an alanine terminal group to enter the active site and fill the elastase pocket.

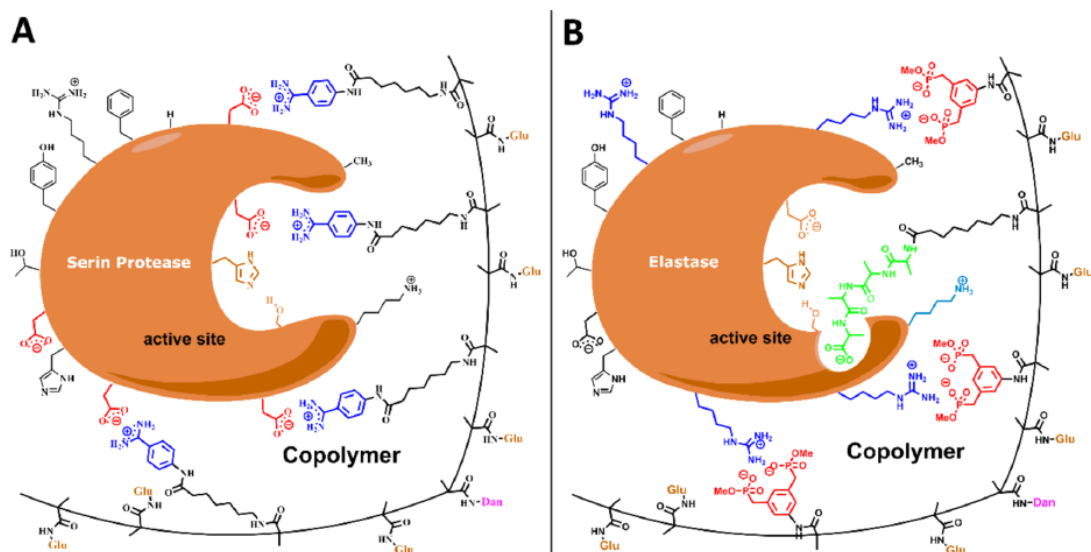


**Figure 23:** Illustration of interaction between enzyme-targeting co-polymers and (A) serine protease, and (B) elastase

Proteins are implicated in numerous biological processes, and the binding of a functionalized linear copolymer to a protein relies on the existence of complementarity between each partner's functional groups. In view of this, the aim is to establish a linear chain polymer of key functionality that can interact in a cooperative manner with a positively charged protein. In this case,  $\alpha$ -chymotrypsin is used. Additionally, the significance of a protein's charged regions cannot be overlooked. As a case in point, interactions can take place between positively charged ligands and negatively charged porcine pepsin,<sup>52</sup> or between negatively charged ligands and the positively charged serine protease hot spot. Hence, in the case of functional group interactions and targeting charge, both are consequential variables.

The extreme dynamism and flexibility of linear polymers is well-documented in the literature. In fact, polyvalent effects account for the interactions between linear polymers and proteins.

Given that linear polymers have the potential to improve binding by changing their shape in a flexible manner, size specificity is not a feature. As such, a directly proportional relationship exists between binding strength and the amount of charges. In view of this, interactions between linear polymers and proteins are regarded as lacking specificity.<sup>53</sup> Hence, this study determined that the employment of a rigid polymer would be viable as a scaffold for a functionalized linear chain, thereby heightening the binding affinity.

Dissimilar to hyperbranched polymers, the rapid and convenient synthesis of which is a core characteristic, dendrimers are complex to synthesise.<sup>54</sup> Therefore, any venture to synthesise dendrimers should be undertaken if and only if the properties of these molecules, and no other, would be satisfactory for a particular application. One of the qualities of dendrimers that makes them especially valuable in replicating protein binding partners is their spherical nature, which stems from the regular nature of their branches. Additionally, the rigid nature of a dendrimer's architecture means that binding is maximised only if the location of the complimentary functional groups on the protein and the dendrimer correspond to one another. Consequently, dendrimer binding is more cost-effective when compared to linear polymer binding in an entropic way, which is advantageous for molecule design initiatives because it promotes the enhancement of binding energy. Furthermore, dendrimers are distinct when compared to polymers due to the dense nature of their surface groups.<sup>55</sup> Generational synthesis offers quantised sizes, thereby promoting the formation of molecules that can bind selectively and specifically to target protein binding sites.

In view of the above considerations, dendrimers were chosen for this study's synthetic inhibitors. If the study is successful, it will be possible to design and produce macromolecules that can inhibit specific enzymes, bind and purify proteins, and open up new routes for drug delivery. Furthermore, the real-world application of the type of molecules studied in this

research project could solve problems relating to drug specificity and physical properties, particularly in view of the way they can contain and transport small active molecules to target proteins.<sup>41</sup>

## 3.2 Results and Discussion

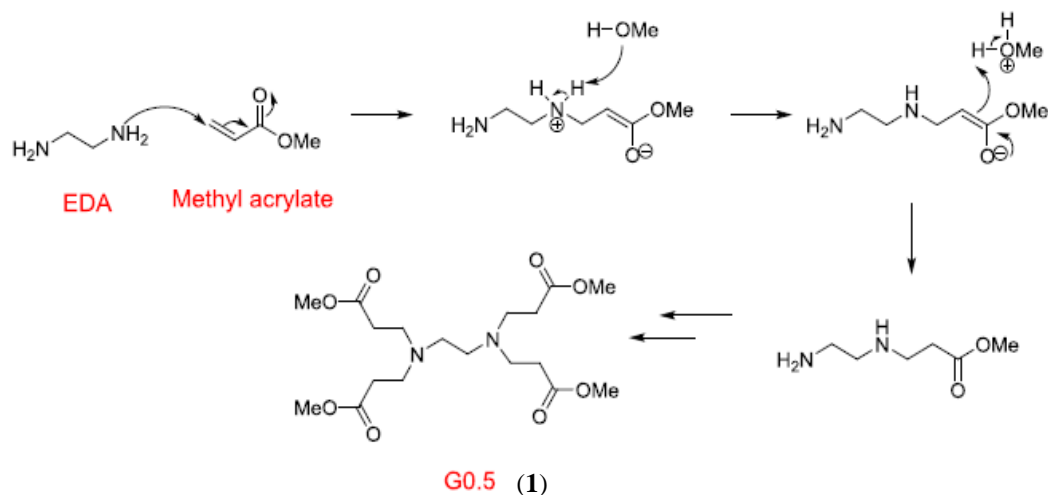
Therefore our initial aim to synthesis of various PAMAM dendrimers with discrete sizes was conducted to obtain the optimal dendrimer for binding a target protein (e.g.,  $\alpha$ -chymotrypsin), and also to create cavities for the encapsulation of functionalized linear chains. The divergent approach was used for the synthesis of dendrimers from generation 0.5 (**1**) to 3.5 (**7**) with 4 and 32 ester terminal groups, respectively.

## 3.3 Synthesis of PAMAM dendrimers

The purpose of the preliminary phase of the process is to determine whether dendrimer PAMAM can improve the solubility of linear chains. As mentioned before, PAMAM dendrimers are marked by their branched, well-defined structure and can be classified as monodispersed macromolecules. The literature indicates that they can effectively encapsulate small organic molecules within a hydrophobic interior or surface of dendrimers (interaction between dendrimers and drugs).<sup>18-19</sup> It is possible to change the terminal functional groups to achieve solubility in a particular solvent. The link between the linear chains and the dendrimer may occur based on non-covalent interactions (linear chains encapsulated inside the dendrimer)

Therefore, the synthesis of PAMAM dendrimer started with the G0.5 dendrimer (**1**) was synthesized by reacting ethylene diamine (EDA) with methyl acrylate at room temperature, as shown in Scheme 2. The reaction involves the nucleophilic conjugate addition to the

unsaturated carbonyl group of methyl acrylate using the amine on ethylenediamine (EDA). EDA has two amine groups, each of which has two hydrogens. Therefore, EDA can react with four molecules of methyl acrylate to give the G 0.5 dendrimer (**1**). Methyl acrylate was used in slight excess to ensure complete nucleophilic addition. The excess solvent and methyl acrylate was removed using a rotary evaporator.



**Scheme 2:** Mechanism for the synthesis of the half generation dendrimers

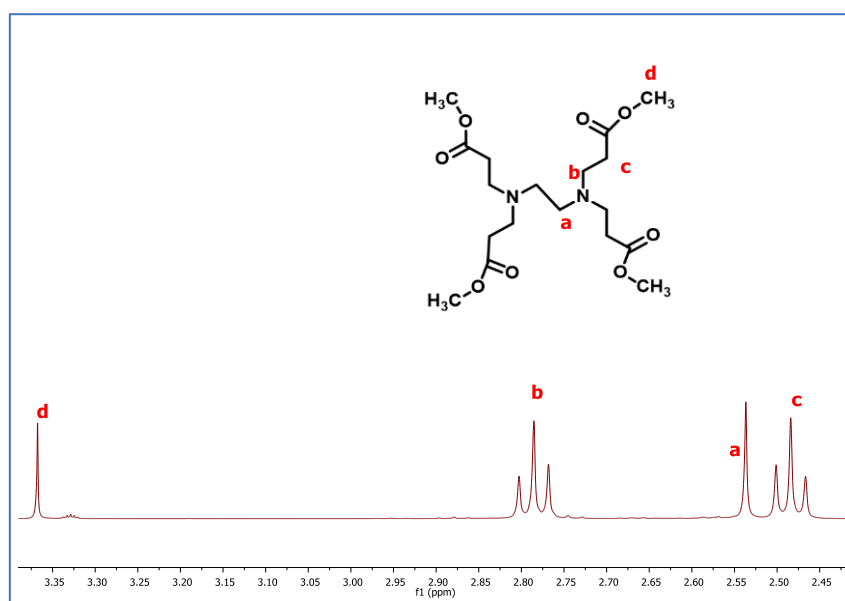
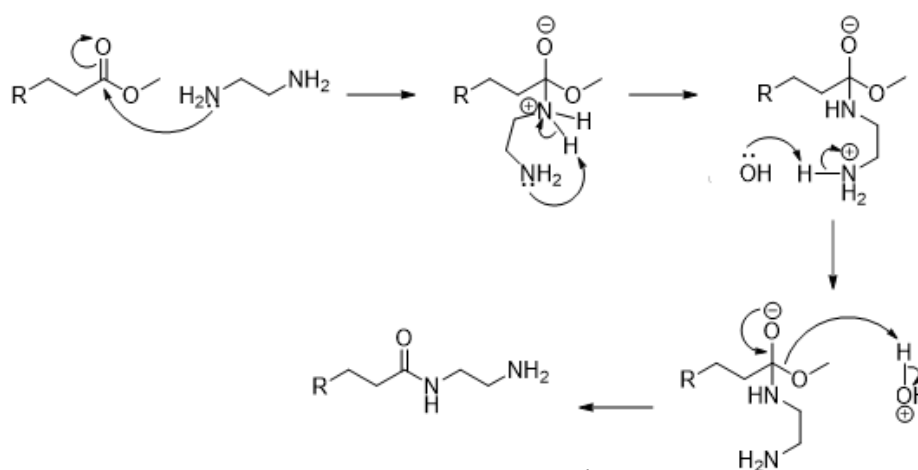


Figure 28:  $^1\text{H}$  NMR analysis for G 0.5 (1)

Confirmation that the reaction had completed came from  $^1\text{H}$  NMR analysis, as shown in Figure 28. The methoxy peak was visible as a singlet at 3.68 ppm, and a second singlet at 2.53 ppm, which integrated to 4H, was assigned to the core EDA protons. The excess methyl acrylate had been completely removed, as no signals were visible  $\approx$  5-6 ppm.  $^{13}\text{C}$  NMR and FTIR spectra showed an ester peak C=O at 172 ppm and  $1735\text{ cm}^{-1}$ . The mass spectrum supported the structure with a molecule ion at  $405\text{ (MH)}^+$ .

The full-generation dendrimers were synthesized by the reacting half-generation dendrimers with an excess amount of EDA. The lone pair of electrons on EDA's nitrogen atom reacted with the ester, resulting the electrophilic carbon resulted in the loss of methanol, as shown in Scheme 3.



**Scheme 3:** Mechanism of G 0.5 (1) into G 1.0 (2)

Excess EDA was used to ensure that the reaction reached completion. Remaining EDA was removed with an azeotropic mixture (9:1 v:v) of toluene and methanol, which is an effective competitor for EDA hydrogen bonding and has a higher boiling point than EDA.  $^1\text{H}$  NMR was used to check that EDA was completely removed, and this involved monitoring the EDA peak

at 2.71 ppm (Figure 29) If any EDA remained during the next step, it reacted with methyl acrylate to generate G 0.5 dendrimer (1). This created an impurity that can not be removed.

$^1\text{H}$  NMR spectra confirmed that a singlet peak at 2.71 ppm was no longer visible after washing with 2.0 L of an azeotropic solvent. These techniques were repeated to form G 3.5 (7) dendrimers. To confirm, the characterizations of half-dendrimers were summarized in Table 1.

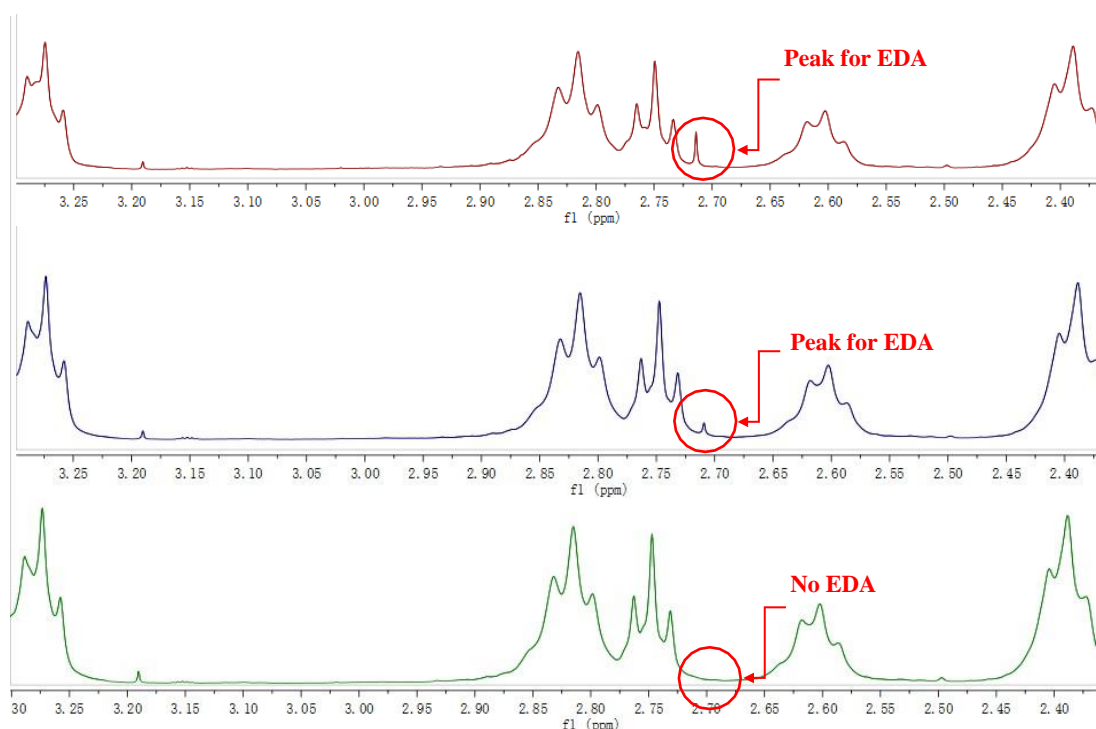
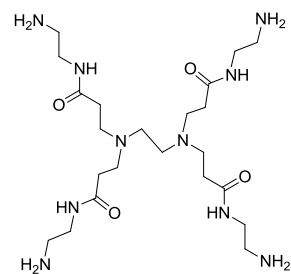


**Figure 29:** Comparison of  $^1\text{H}$  NMR spectra for G 3.0 after a series of washes with the azeotropic solvent.

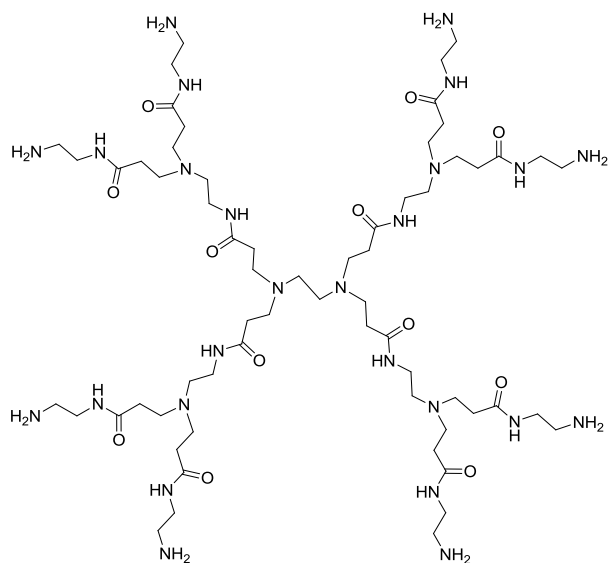
However, the ester dendrimer G3.5 (7) is not suitable for protein binding because esters rapidly hydrolyse to negatively charged carboxylic acids and the amine dendrimer are protonated. Therefore, as both are charged, neither are suitable for clinical and biological application. For that reason, we selected neutral G3.5-OH as our scaffold for functionalized liner chains.

Dendrimer generation	Molecular formula	Molecular weight (g/mol)	Terminal groups	Molecular ion (MH) <sup>+</sup> obtained
G 0.5 (1)	C <sub>18</sub> H <sub>32</sub> N <sub>2</sub> O <sub>8</sub>	406	4 esters	405
G 1.0 (2)	C <sub>22</sub> H <sub>48</sub> N <sub>10</sub> O <sub>4</sub>	516	4 amines	517
G 1.5 (3)	C <sub>54</sub> H <sub>96</sub> N <sub>10</sub> O <sub>20</sub>	1205	8 esters	1206
G 2.0 (4)	C <sub>62</sub> H <sub>128</sub> N <sub>26</sub> O <sub>12</sub>	1429	8 amines	1430
G 2.5 (5)	C <sub>126</sub> H <sub>224</sub> N <sub>26</sub> O <sub>44</sub>	2807	16 esters	2806
G 3.0 (6)	C <sub>142</sub> H <sub>288</sub> N <sub>58</sub> O <sub>28</sub>	3256	16 amines	3278
G 3.5 (7)	C <sub>270</sub> H <sub>480</sub> N <sub>58</sub> O <sub>92</sub>	6014	32 esters	6014

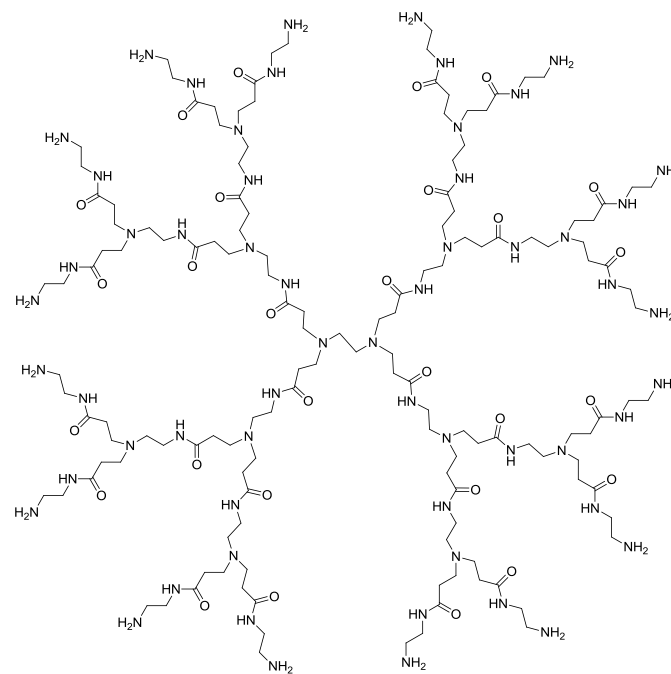
**Table 2:** Analysis of generation dendrimer



**G1.0 (2)**



**G2.0 (4)**



**G3.0 (6)**

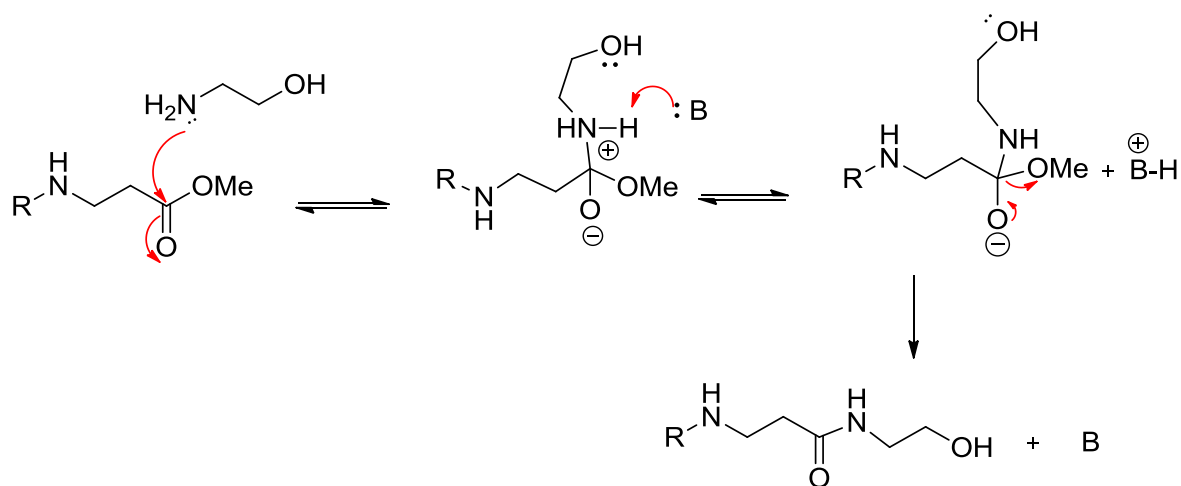
**Figure 30: Structure of full generation of PAMAM**

### 3.4 Synthesis of dendrimers with hydroxy terminal groups

To provide of this novel methodology, as well as a demonstration of how non-covalent combinatorial chemistry can be employed to facilitate the functionalization of the dendrimer with targeting groups at the same time. The exact process would rely on the use of non-functionalized dendrimers G3.5 PAMAM dendrimer (8149 Da) with OH terminal groups, on this will depends on the specific surface of the target protein of  $\alpha$ -chymotrypsin. Noteworthy, these can be created without difficulty, and they can be acquired commercially.

For the proposed design of our non-covalent unfactionalized dendrimer, the use a neutral dendrimer that cannot bind was also required. The dendrimer would need end groups that allow it to be water-soluble, and ethanolamine was selected as this would give dendrimers with OH end groups. The addition of ethanolamine was carried out using a process similar to that used for the full-generation dendrimers. The reaction and the mechanism of this conversion are shown in Scheme 4 . In this case, a base was required because the OH is not basic enough to deprotonate the charged intermediate.

Our previous studies reported that ethanolamine and dimethyl sulfoxide (DMSO) were difficult to remove. Attempts to avoid and maintain a basic environment were carried out using an excess amount of ethanolamine and potassium carbonate, without DMSO. However, the product was not soluble in water, thereby suggesting that the hydroxy groups were only partially attached. This is likely due to the poor solubility of the PAMAM dendrimers in ethanolamine.



**Scheme 4:** Mechanism of ethanolamine group with potassium carbonate (B) to produce hydroxyl terminal groups

To avoid the solubility problem, a minimum amount of DMSO (to solubilize dendrimer) was combined with the mixture. After purification, which was achieved by filtering under vacuum and trituration with acetone, the products were collected as a paste, allowed to settle before collection and then drying under vacuum. Crystals of potassium carbonate formed on the surface of the paste, and these were dissolved and removed by dissolution with small amounts of water. The product was then obtained using a second trituration with acetone. However, a singlet peak at 2.64 ppm and a triplet peak at 3.52 ppm, corresponding to DMSO and ethanolamine, respectively, were visible in the  $^1\text{H}$  NMR spectra of G 2.5-OH. Repeated trituration from water using acetone were carried out. The product was dried, and complete removal of impurities was confirmed in  $^1\text{H}$  NMR, as shown in Figure 31:  $^1\text{H}$  NMR spectra for G 2.5-OH. The same technique was used to build the G 1.5 and G 3.5-OH dendrimers (Figure 32). The characterization data of all OH terminated dendrimers is summarized in Table 3.

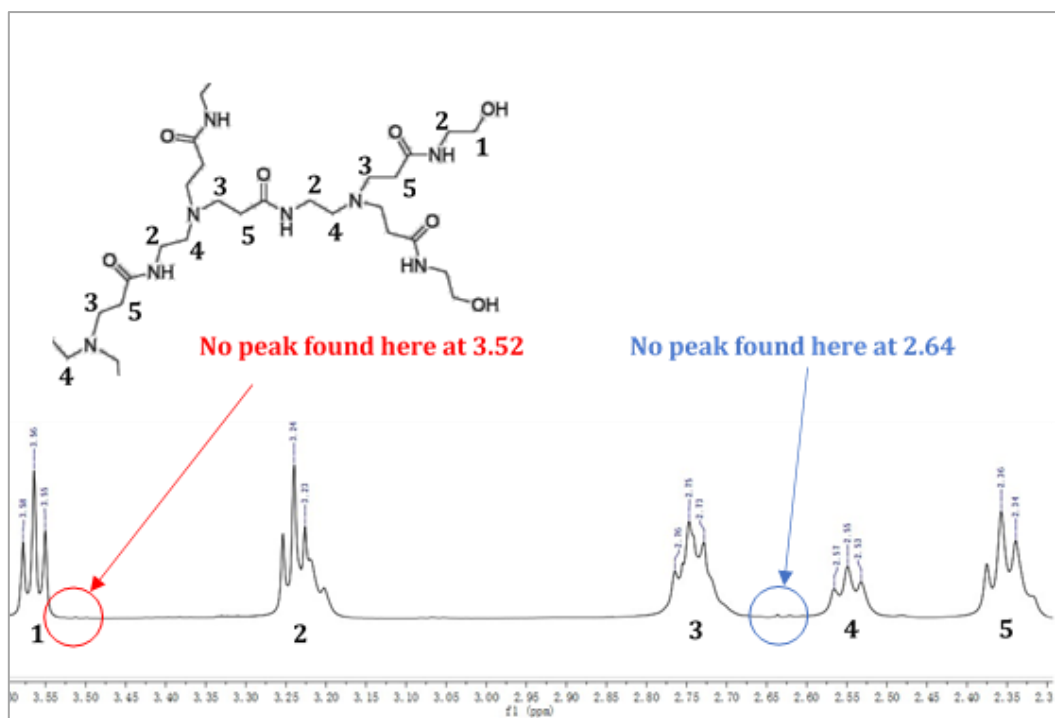


**Figure 31:** <sup>1</sup>H NMR spectra for G 2.5-OH

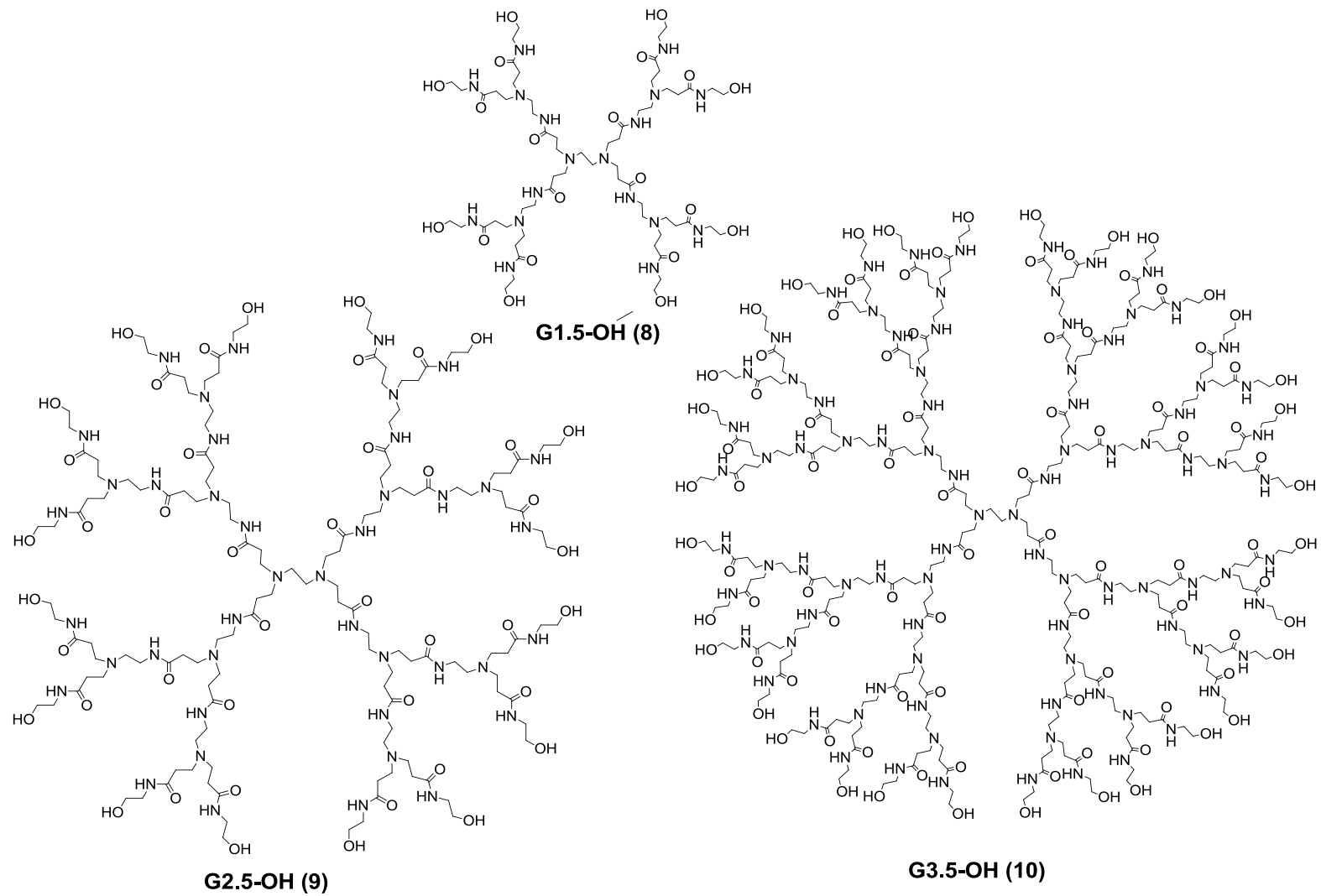


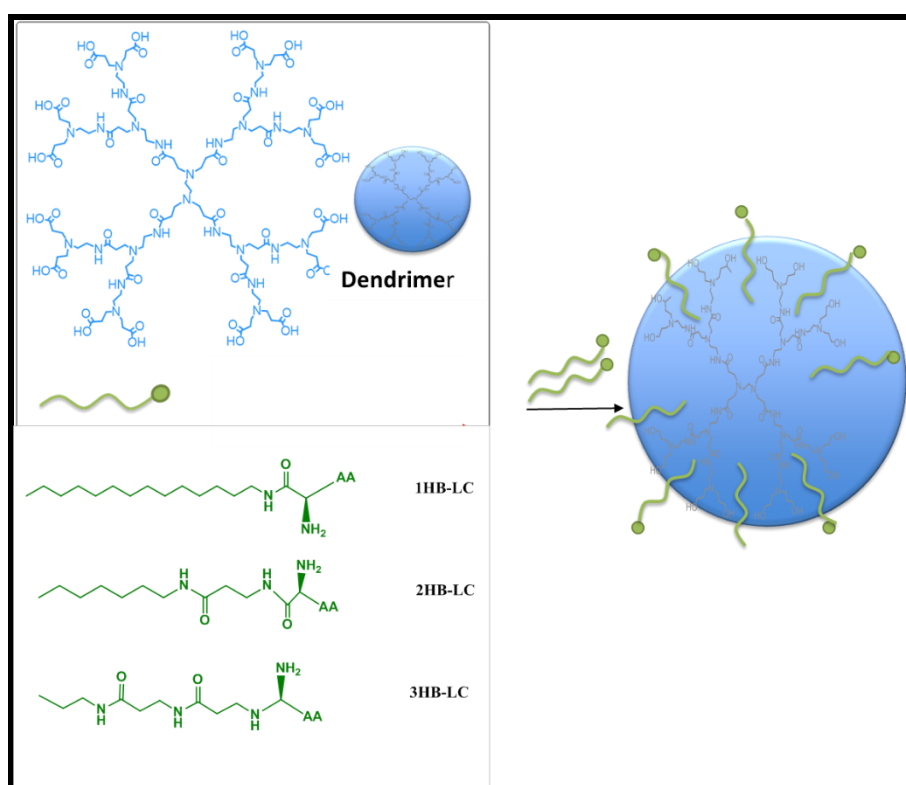
**Figure 32:** Chemical structure of PAMAM-OH

Dendrimer generation	Chemical formula	Expected molecular weight (g/mol)	Number of OH surface groups	Molecular ion (MH) <sup>+</sup>
G 1.5-OH (8)	C <sub>62</sub> H <sub>120</sub> N <sub>18</sub> O <sub>20</sub>	1438	8	1438
G 2.5-OH (9)	C <sub>142</sub> H <sub>272</sub> N <sub>42</sub> O <sub>44</sub>	3272	16	3272
G 3.5-OH (10)	C <sub>302</sub> H <sub>576</sub> N <sub>90</sub> O <sub>92</sub>	6940	32	6941

Table 3: Analysis of PAMAM-OHs

### 3.5 Synthesis of linear chain

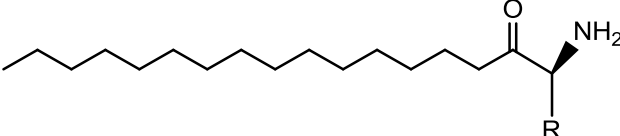
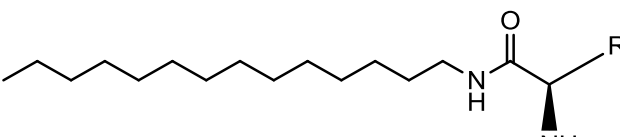
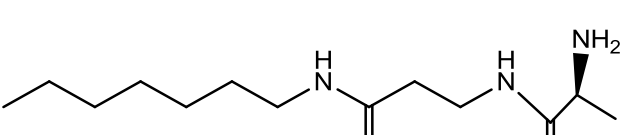
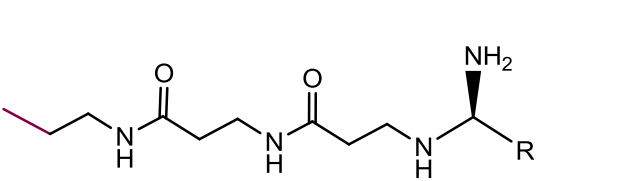
As noted above, a key element of the process was the non-covalent incorporation of the targeting groups. In particular, the amino acids that can bind to the dendrimer's interior using hydrogen and hydrophobic bonding interactions would be included at the end of a hydrophobic linear chain. It was possible to synthesize several of these functionalized linear chains and add them to a dendrimer to yield a functionalized system (Figure 33).



**Figure 33:** Proposed linear chains that include hydrophobic and hydrogen bond interactions to help encapsulation with the dendrimer.

This study aimed to exploit a series of macromolecules and develop a proof of principle methodology for obtaining selective ligands for specific proteins. The overall objective was to develop a system in which the protein can select its optimum ligand from a large pool of functionalized macromolecular ligands. Previous attempts by this research group using

hydrophobic linear chains and the level of encapsulation within the dendrimer have been very poor. Therefore, our initial step was to find the simplest method to synthesize functionalized and hydrophobic linear chains, with each having a different number of hydrogen bonding sites, and to investigate which encapsulated optimally within the PAMAM dendrimer. Therefore, we would then be able to determine which chain was best, based on the of synthesis versus the ability to bind reasonably to the dendrimer.

Linear chains R= Various amino acid functional groups	Number of hydrogen bonding / amide group (s)
(a) 	<b>0</b>
(b) 	<b>1</b>
(c) 	<b>2</b>
(d) 	<b>3</b>

**Scheme 5:** Proposed linear chain with hydrophobic site

### 3.5.1 Synthesis of the one amide H-bonding linear chain

The first synthetic route involves applying a simple method that provides one hydrogen bonding site. This was based on a prior study that demonstrated how hydrophobic drug molecules could be encapsulated within dendrimers to enhance their solubility. Based on these findings, our first attempt was the synthesis of a hydrophobic chain that possessed just 1 H-bonding group. The synthesis was between 1-tetradecylamine and tyrosine, to generate a Boc-Tyrosine chain (1HB-LC-Boc-Tyr). **11** The reaction was a simple amide coupling using the carboxyl activating coupling agent EDC.HCl. To avoid unwanted coupling, selective protection of the tyrosine's amine group was necessary. In this case, a tert-butyloxycarbonyl (Boc) protecting group was chosen. The Boc groups were removed using TFA and DCM. The synthetic route to 1HB-LC-Tyr is shown in Figure 35. <sup>1</sup>H NMR confirmed the attachment of 1-tetradecylamine based on the aromatic doublets at 7.0 ppm and 6.71 ppm. The protons on the chain resonated as a broad peak at 1.31 ppm, which integrated for 24 protons. The Boc peak was detected as a singlet at 1.41 ppm. Mass spectrometry indicated a molecular ion at 499.6 (MNa<sup>+</sup>), which confirmed the structure of Boc 1HB-LC-Boc.Tyr **11**

The deprotection of the Boc group was achieved using TFA in DCM. It was necessary to use a relatively high concentration of TFA to ensure complete removal of the Boc group. However, if insufficient deprotection takes place, it is clearly observable from the <sup>1</sup>H NMR spectrum (Figure 34). <sup>1</sup>H NMR confirmed the purity of the 1HB-LC-Tyr **12**. In addition, mass spectrometry indicated a molecular ion at 399 (MNa<sup>+</sup>), which confirmed the structure of 1HB-LC-Tyr

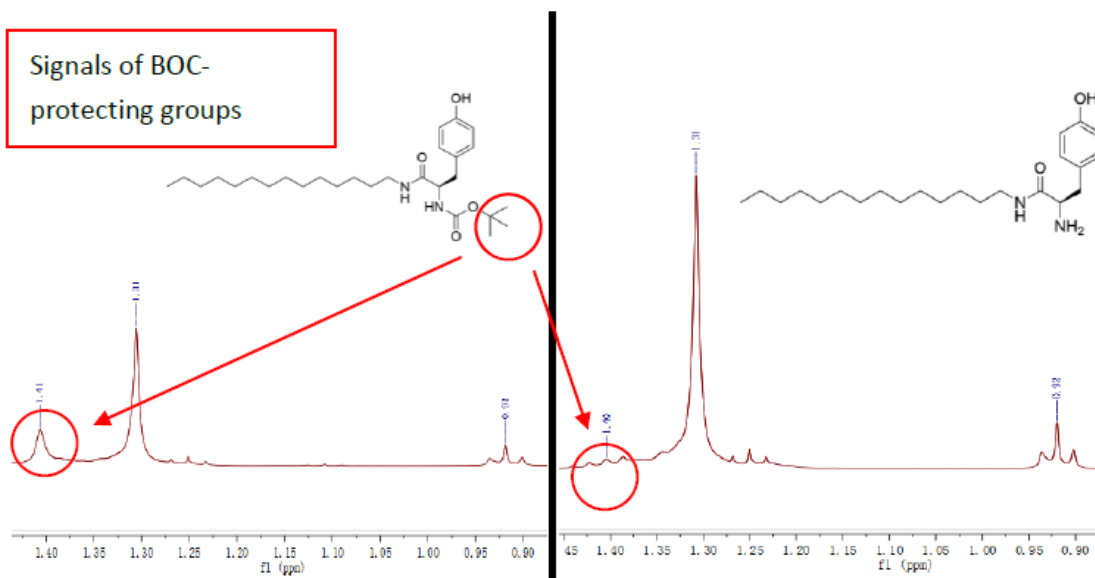


**Figure 34:**  $^1\text{H}$  NMR of 1 hydrogen bonding with protection and deprotection with tyrosine

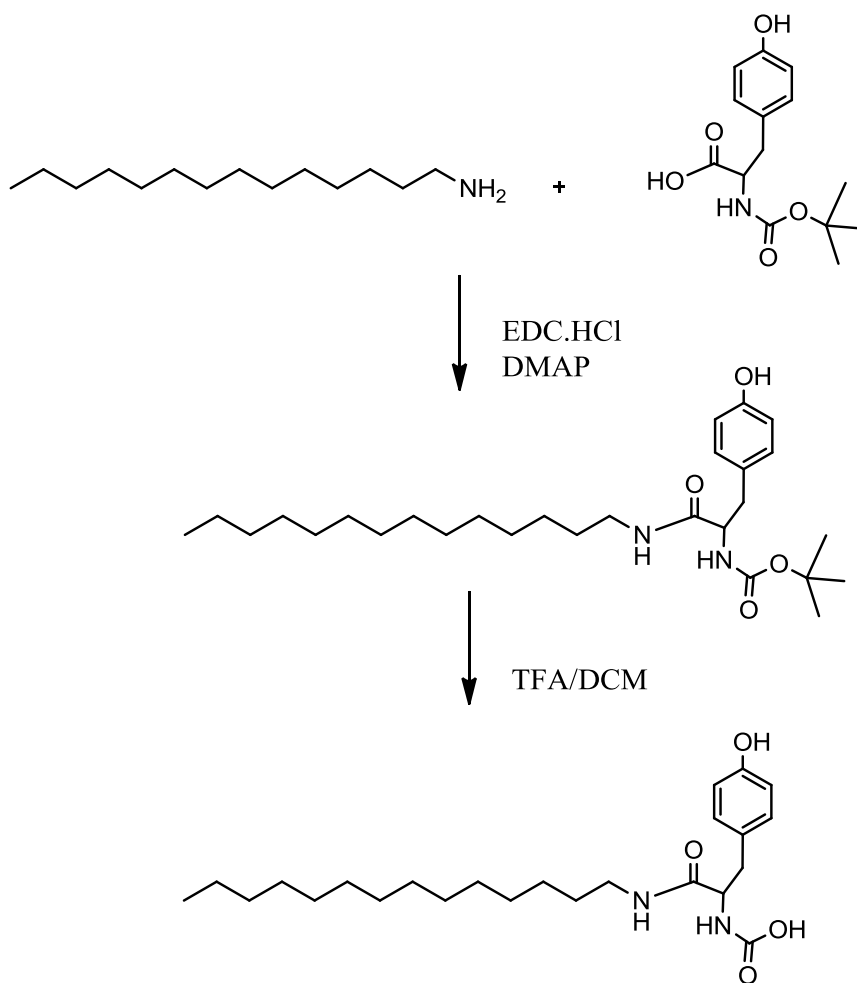
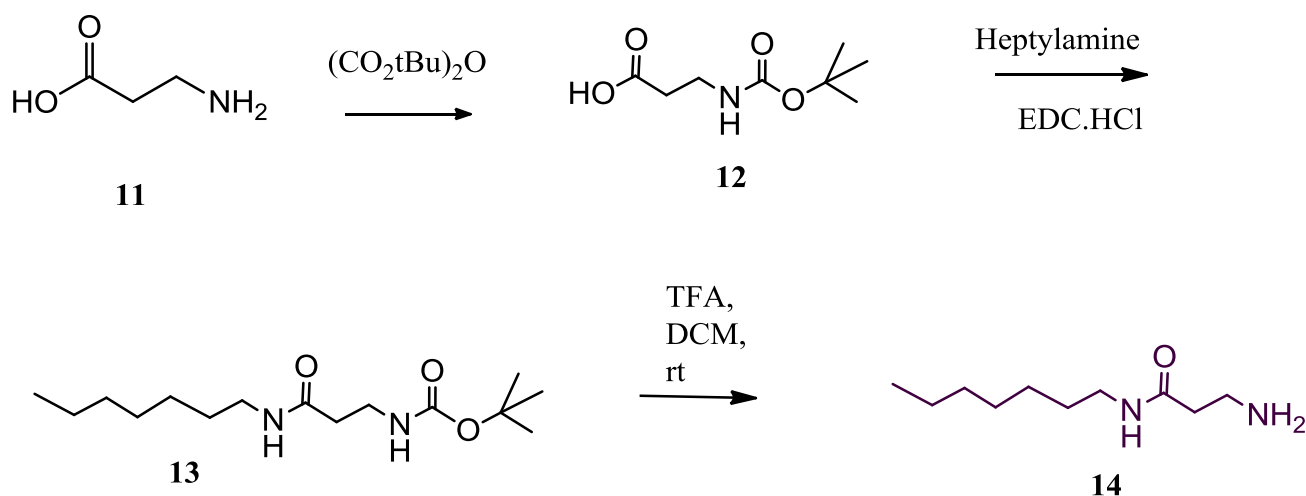


**Figure 35:** Preparation for 1 hydrogen bonding of linear chain, thereby providing more hydrophobic sites

### 3.5.2 Synthesis of the two amide H-bonding linear chains

The experiment was continued to prepare with 2 hydrogen bonding of linear chain that can provide the additional binding within dendrimer. The planned synthetic route for two hydrogen bonding **14** is shown in Scheme 6. The first step involved addition of a tert-butyloxycarbonyl (Boc) group to protect the amine group from unfavorable reactions. The Boc group was used as it is relatively easy to add and remove.

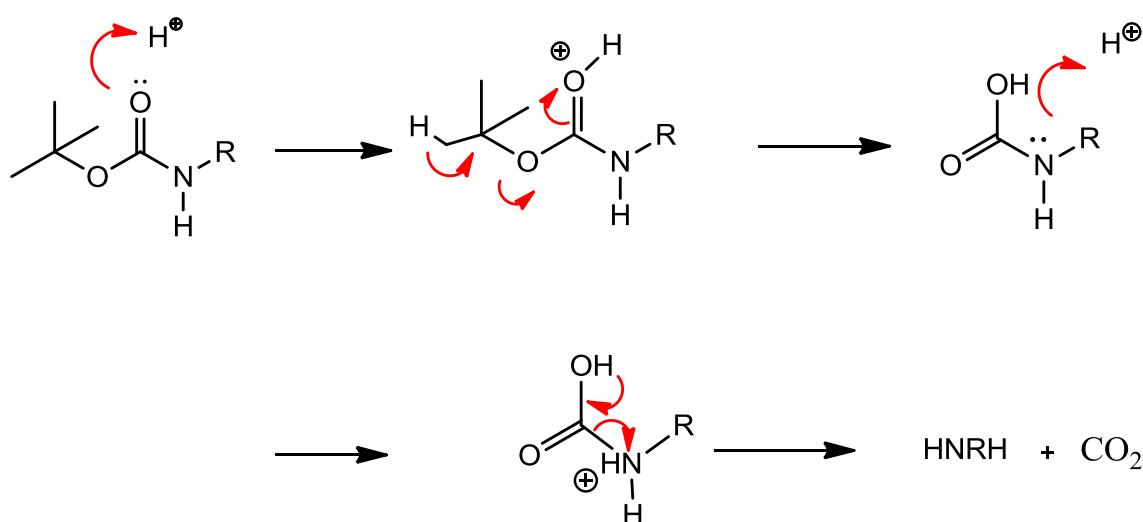
The attachment of the Boc group, which integrates as 9 protons, was confirmed by  $^1\text{H}$  NMR analysis, where a sharp singlet was visible around 1.40 ppm. The successful addition of  $\beta$ -alanine was also confirmed by integrating the broad singlets at 2.61 ppm and 3.42 ppm, which are assigned as for  $\text{CH}_2$  protons. Mass spectrometry had a molecule ion at 188 ( $\text{MH}^+$ ) and 212 ( $\text{MNa}^+$ ), which confirmed the structure of Boc amide (**12**)



**Scheme 6:** Planned synthetic route with two hydrogen bonding groups

The next step was coupling of Boc- $\beta$ -alanine with heptylamine, giving of Boc-heptylamine **13**. This was carried out using EDC.HCl and DMAP in a 1:2 ratio and the addition of base of 3 equivalent of basic triethylamine. Analysis by  $^1\text{H}$  NMR showed two doublets of doublet peaks between 7 and 8 ppm. The ES-MS spectrum had a signal at 123 ( $\text{MH}^+$ ), indicating the presence of DMAP in the product. Therefore, the crude product was dissolved in chloroform and rewashd with water and a concentrated sodium hydrogen carbonate solution to remove the impurities. The DMAP peaks were no longer visible in the  $^1\text{H}$  NMR and mass spectra,

indicating the washing was successful. White crystals were obtained and the yield was 55%. The  $^1\text{H}$  NMR spectrum had peaks at 3.28 ppm and 2.71 ppm each integrating as two protons, and these were assigned as the  $\underline{\text{CH}_2\text{CO}}$  and  $\underline{\text{CH}_2\text{NH}_2}$ , respectively. A triplet at 0.92 ppm was observed for the terminal methyl group and the integration of 8 protons at 1.30 ppm of  $\text{CH}_2$  for the remaining protons from heptylamine. The singlet at 1.45 ppm, which integrated as 9H, was assigned to the Boc group. The ES-MS spectrum showed a signal at 287 for the  $\text{MH}^+$  and 309 ( $\text{MNa}^+$ ) ion, confirming that synthesis of the pure protected chain **13** had been achieved. A further step was carried out to remove Boc using trifluoroacetic acid (TFA). This was undertaken based on the mechanism given Scheme 7, which allowed the carbon dioxide byproduct to bubble away.



**Scheme 7:** Mechanism of Boc deprotection

The Boc group was successfully removed to give amine **14** with few impurities, as confirmed by  $^1\text{H}$  NMR through the absence of the Boc peak  $\approx 1.45$  ppm. This resulted in the deprotected

chain **14**. TFA was removed by evaporation and solvent extraction, giving to the deprotected chain **14** in a yield 78 %. The pH of the solution was also monitored to ensure that no TFA remained, and multiple solvent extractions were carried out in order to remove TFA and all other impurities. An absence of the sharp singlet at 1.45 ppm for the Boc group in the  $^1\text{H}$  NMR indicated the successful removal of the Boc group (Figure 36). Mass spectrometry analysis confirmed the mass of amine **14** with a molecular ion at 187 ( $\text{MH}^+$ ). The next step involved addition of the amino acids.

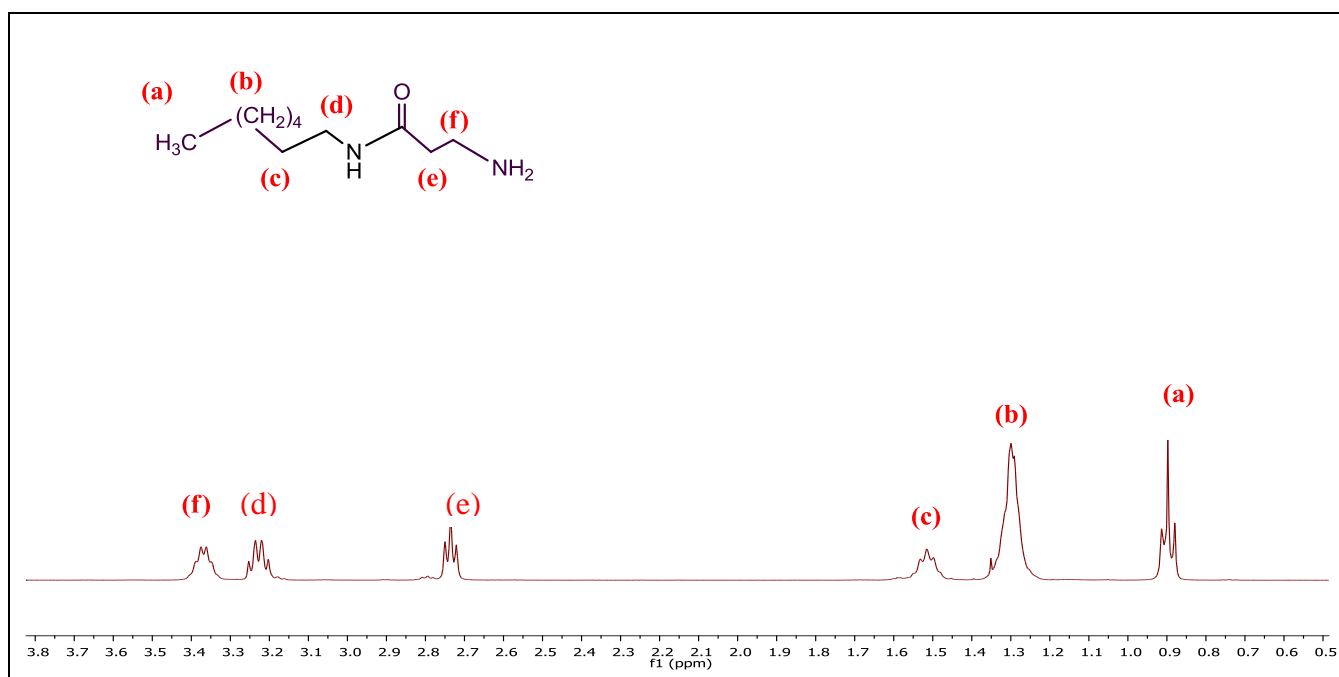
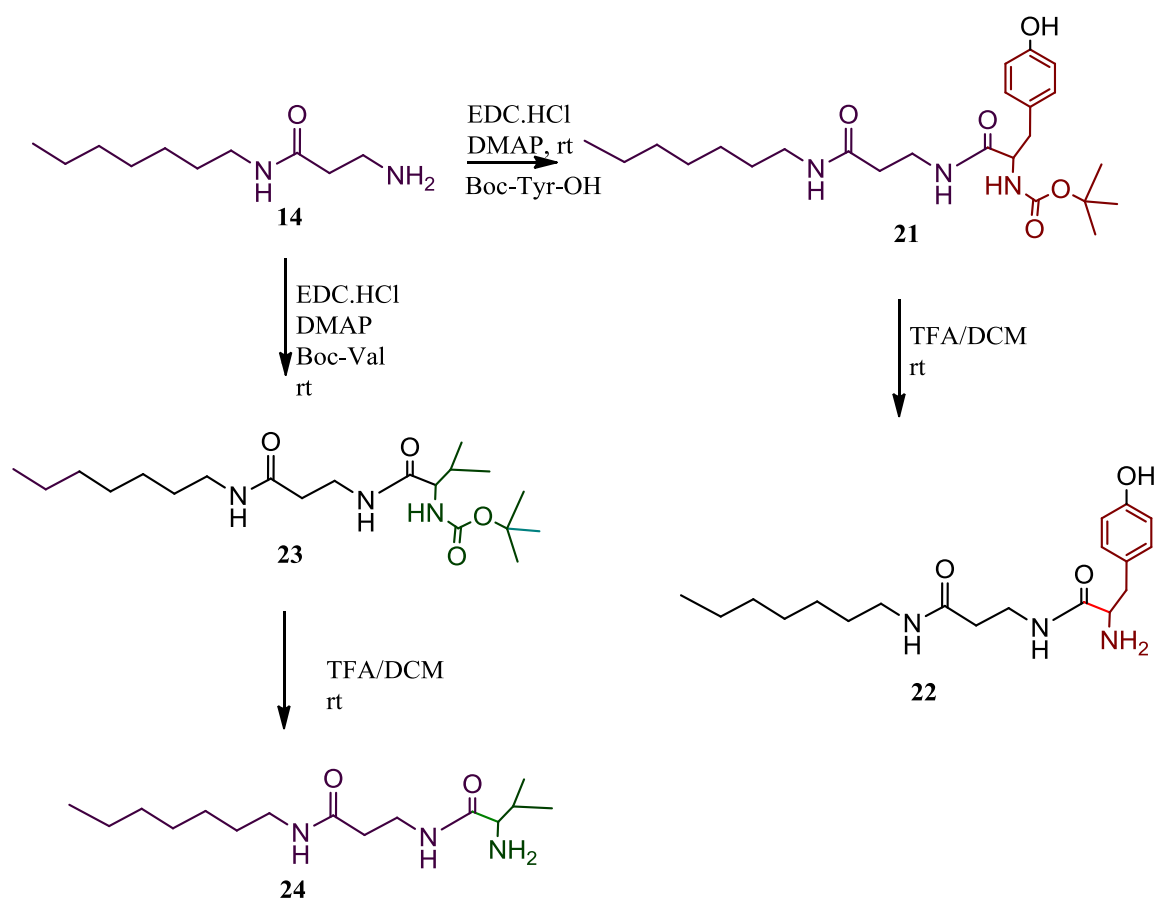


**Figure 36:**  $^1\text{H}$  NMR Boc-Heptylamine deprotection

### 3.5.3 Synthesis of two linear chains with tyrosine and valine

In a previous study, it was demonstrated that the functionalized dendrimer with tyrosine chain (3 hydrogen bonding) was associated with the greatest number of encapsulation/binding. In view of this, the same amino acids (i.e., tyrosine and valine) were chosen to examine the impact of different amino acids on binding, where these served as capping groups for the linear chain. Tyrosine was chosen because it plays a critical role in protein binding, while valine is documented as having a negligible impact on binding. Thus, when encapsulated into a dendrimer, our expectation was that the level of inhibition would be low.

Tyrosine was added to the linear chain as previously described by amide coupling of Boc-Tyr-OH to amine **14**. Scheme 8 to give 2HB-LC -Tyr **22** and 2HB-LC -Val **24**. Both reactions were carried out using the same procedure and characterizations, as mentioned before in Section 3.5. The first step involved an amide coupling reaction and the second step was a Boc deprotection.



**Scheme 8:** Addition of tyrosine and valine to 2 hydrogen linear chain by an amide coupling and Boc deprotection step

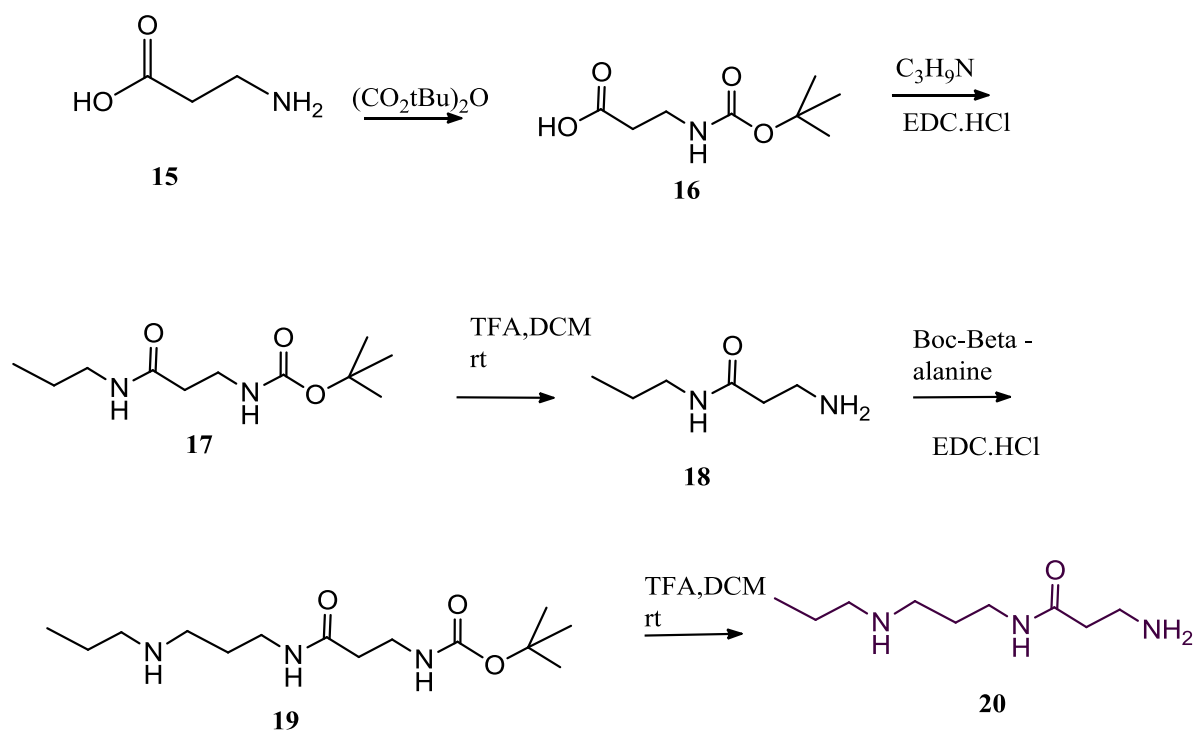
The confirmation of the addition of the tyrosine group for the synthesis of 2HB- Boc-tyrosine chain **15** was achieved after observing the peaks at 7.05 ppm and 6.72 ppm in the  $^1\text{H}$  NMR (corresponding to the aromatic protons of the tyrosine group) and the singlet peak at 1.4 ppm (corresponding to the Boc group). Additional mass spectrometry evidence confirmed the mass, where a molecular ion was observed at 450 ( $\text{MH}^+$ ). The Boc deprotection of tyrosine chain **21** with TFA was undertaken as before, and  $^1\text{H}$  NMR confirmed that the singlet peak at 1.4 ppm (from the Boc group) was no longer observed. To ensure complete removal of any remaining

TFA, 2HB-LC –Tyr **22** was placed under a vacuum for an extended for 5 days. The  $^1\text{H}$  NMR spectrum of 2HB-LC –Val **24** showed peaks at 5.28 ppm (N-H) and a peak for the stereogenic CH at 3.55 ppm. At the same time, a doublet 0.99 ppm and a septet at 2.26 ppm confirmed the presence of an iso-propyl group. The successful preparation of 2HB-LC Val **24** was confirmed from the mass spectrum which had molecular ion at 285 (MH) $^+$ .

### 3.5.2 Synthesis of the three amide H-bonding linear chains

Having successfully synthesised the one and two hydrogen bonding chains, the next step was preparation of a linear chain that could provide three hydrogen bond interactions within the dendrimer. The synthesis of the chain began from a smaller alkyl amine, and the chain was built up by repeated addition of  $\beta$ -alanine **14** using the same method previously used for the other linear chains.

The synthesis is similar to that used to prepare the two hydrogen bonding linear chain. In order to add the extra amide, and keep the chain length similar, the synthesis started with a shorter alkyl chain. As before, the same method was used for Boc protection of  $\beta$ -alanine **14** to give amide **16**. Confirmation of Boc protection came from  $^1\text{H}$  NMR, where the broad singlets observed at 2.61 ppm and 3.42 ppm, assigned as the  $\text{CH}_2$  protons, and a singlet at 1.39 ppm for the Boc group. Mass spectrometry was undertaken which had a molecule ion at 188 (MH $^+$ ) and a peak at 212 (MNa $^+$ ), thereby demonstrating that Boc amide **16** had been produced.



**Scheme 9:** Synthetic route of the linear chains

In the next reaction, propylamine was combined with chain **16** to give the diamide **17**, as shown in Scheme 8. The signal for the Boc group was observed at 1.45 ppm, which integrated as 9H,. Additionally, the synthesis of the pure protected chain **17** was indicated by the fact that the ES-MS spectrum displayed a molecular ion at 231 for the  $\text{MH}^+$  ion. Following the successful synthesis of the protected chain **17**, the Boc group needed to be removed. TFA removal took place as previously described and the deprotected chain **18** was obtained in a yield of 82%. Monitoring of the solution's pH was used to ensure removal of TFA. A lack of the Boc signal at 1.45 ppm in the  $^1\text{H}$  NMR analysis demonstrated Boc removal. In addition, mass spectrum ion at 131 confirming successful deprotection. Repetition of the EDC coupling was used to

combine a second Boc- $\beta$ -alanine group with the chain. In this case, DCM was not an effective solvent because the deprotected compound was more polar, and amide **18** was insoluble. Therefore, DCM was replaced with tetrahydrofuran (THF). The  $^1\text{H}$  NMR spectrum revealed peaks that were consistent with the product, namely a sharp singlet peak for the Boc group at 1.42 ppm and the terminal methyl group as a triplet at 0.93 ppm. Mass spectrometry supported the presence of the mass of amide **19** with a molecular ion at 302 ( $\text{MH}^+$ ). The deprotection of the compound was facilitated to generate amine **20**.

At this stage we had the linear chain and now needed to add the tyrosine and valine terminal groups. The synthesis of the tyrosine and valine chains is shown in Figure 37 and uses the same coupling/deprotection steps previously described ( *see section 3.5.3*). This resulted in 3HB-LC -Tyr **26** and 3HB-LC-Val **28**. The successful synthesis of the protected 3 hydrogen bond Boc-tyrosine chain **25** was confirmed by  $^1\text{H}$ NMR, where by peaks were observed at 7.05 ppm and 6.71 ppm, corresponding to the aromatic protons of the tyrosine group and a singlet at 1.39 ppm, corresponding to the Boc group. This was supported by mass spectrometry, which indicated aa molecular ion at 487.5 ( $\text{MNa}^+$ ). Boc deprotection using TFA was successful, as demonstrated by  $^1\text{H}$  NMR and mass spectrometry. The singlet at 1.4 ppm from the Boc group could no longer be observed in the NMR spectrum. The mass spectrum displayed a molecular ion at 299 corresponding to the molecular ion ( $\text{MH}^+$ ) along with a peak at 323 ( $\text{MNa}^+$ ). This confirmed the successful preparation of 3HB-LC -Tyr **26**.

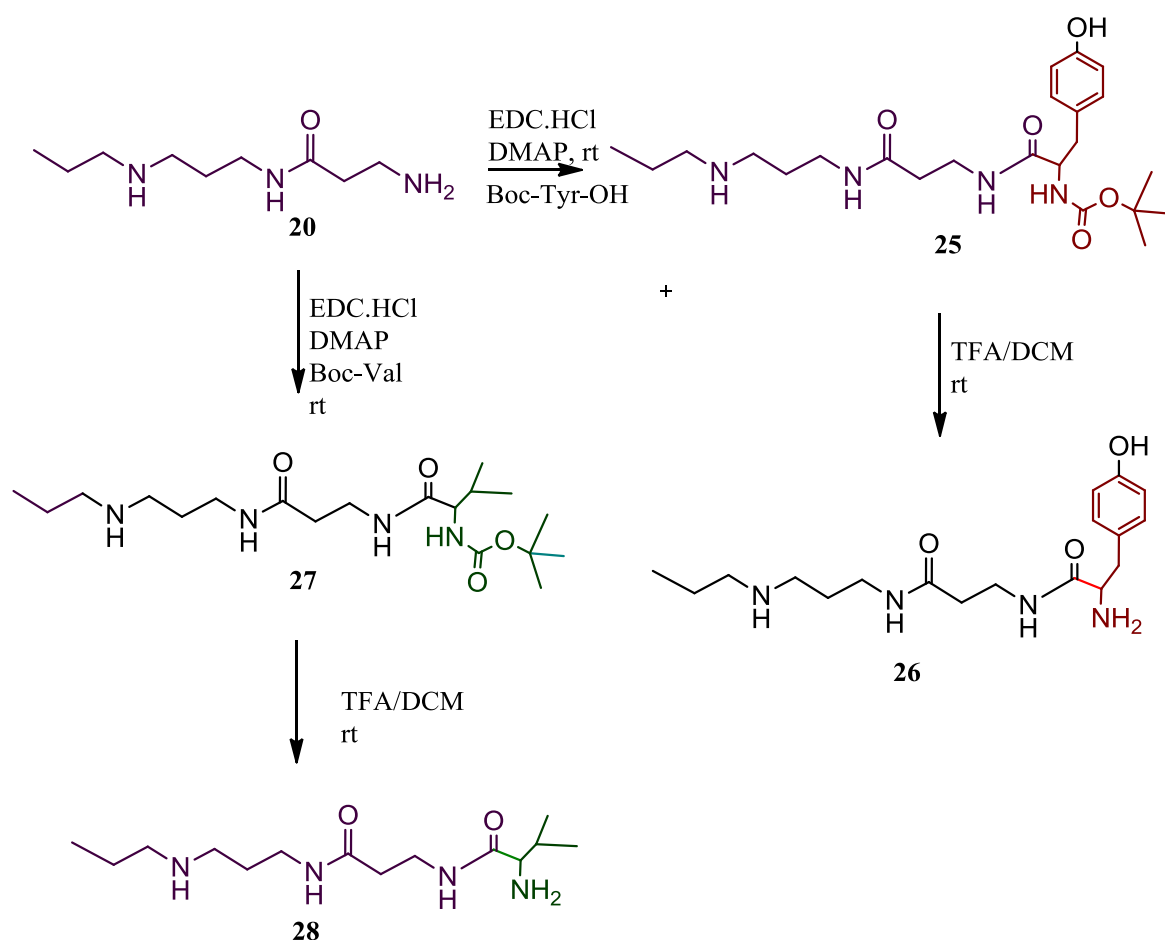


**Figure 37:** Synthesis route of three amide with valine and tyrosine

In conclusion, the 3 hydrogen bonding system was the hardest to synthesize, however, it does have the potential for better encapsulation within the dendrimer, and therefore better potential for protein binding. The next step will be to test how well the linear chains produced can be encapsulated within dendrimer.

### 3.6 Encapsulation of functionalized linear chain

As mentioned before, the encapsulation of hydrophobic molecules has been identified as a method for enhancing the solubility of drugs. In order to organize shape dendrimer as a scaffold for the functionalized linear chain, the selected dendrimer must be water-soluble. This ensures that the protein and the assembled ligand are in the same aqueous phase. In addition, the dendrimer's terminal groups must be neutral and inert. This is vitally important because the dendrimer must not react, bind, or interact with the protein's binding surface in the absence of any encapsulated functionality. Additionally, the dendrimer must be sufficiently large to address the full size of the target protein's interfacial area, whilst also ensuring that the incorporation of the binding is not prevented or limited by a dense shell or dense packed structure.<sup>19,20</sup> As such, the neutral G 3.5 PAMAM dendrimer **10**, with 32 terminal OH groups<sup>22</sup> and a maximum addressable area of  $1200 \text{ \AA}^2$  was selected as the scaffold unit.<sup>23,15</sup>

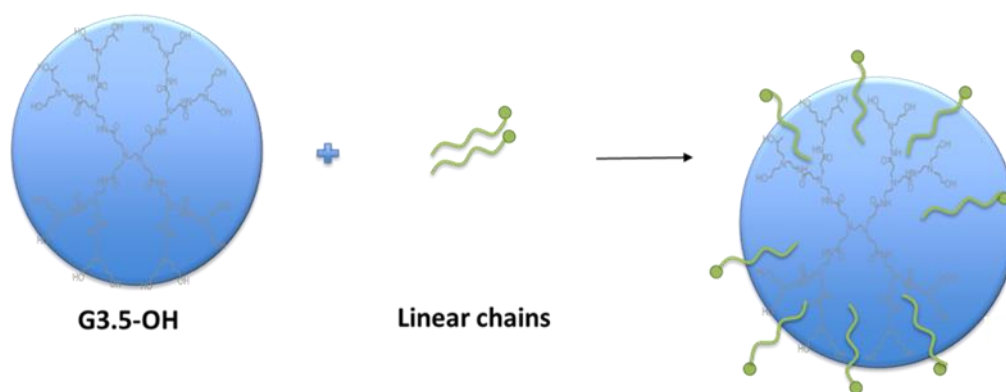


**Figure 38:** Encapsulation of linear chain (Tyr **22** and Val **24**) into G 3.5-OH to form functionalized dendrimer

The next step involved the targeting or binding units that needed to be encapsulated/incorporated within the dendrimer's interior. A cooperative combination of hydrophobic, electrostatic, and H-bonding interactions was chosen to drive encapsulation. To achieve this, a series of hydrophobic oligomeric amide chains, terminated with an amino acid (the binding functionality), were selected. For this proof of principle work, a tyrosine terminated chain **22** was selected as the binding/recognition motif, and a valine terminated chain **24** was selected as a control. These amino acids are known to contribute significantly well or extremely poorly, respectively, to protein-protein interactions.<sup>9</sup>

Encapsulation of the linear chains within the G 3.5-OH dendrimer **10** was achieved using a procedure similar to that used to solubilize and encapsulate hydrophobic drugs within water-soluble PAMAM dendrimers.<sup>25</sup> For the linear chains, 10 equivalents of each linear chains were added to methanolic solutions of dendrimer **10**. The methanol was removed and a known volume of buffer (0.01M PBS, pH 7.4) was added, to give a final dendrimer concentration of  $1 \times 10^{-6}$  M. The proportion of encapsulated chains within the dendrimer was calculated, as shown in Table 4. Each absorbance was divided by the extinction coefficient ( $\epsilon$ ) of the linear chains. To measure the loading encapsulation, the concentration of the dendrimer was divided by the concentration of the functionalized chain. The first experiment was involved 1 HB-LC-Tyr that showed a poor loading with 1 or 2 chain (s) per dendrimer.

Therefore, the experiment was continued with 2 hydrogen bonding sites (2HB-LC). Beer-Lambert analysis confirmed that all 10 linear chains had been encapsulated, giving a final concentration of  $2.5 \times 10^{-5}$  M for 2HB-LC-Tyr **22** (Table 4) and  $6.8 \times 10^{-5}$  M 2HB-LC-Val **24**

(Table 5). This is greater than the solubility of either linear chain without the dendrimer ( $1.16 \times 10^{-5}$  M for 2HB-LC-Tyr **22** and  $4.24 \times 10^{-5}$  M 2HB-LC-Val **24**).

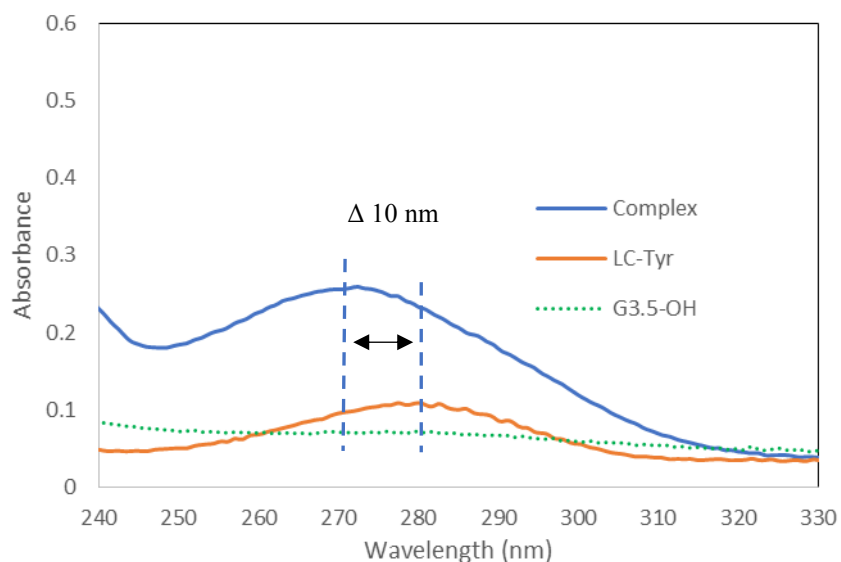


**Figure 39:** Complex of 2HB-LC-Tyr **22** Max concentration of linear chain  $1.16 \text{ E-}5 \text{ M}$

Generation dendrimer	Absorbance	Dendrimer conc / M	Molar absorption coefficient ( $\epsilon$ ) / $\text{M}^{-1}$	Calculated chain conc / M	Average number of chains encapsulated
Free 2HB-LC-Tyr <b>22</b>	0.1088	n/a	9326	$1.16\text{E-}05$	n/a
Complex	0.2332	$2.50\text{E-}06$	9326	$2.50\text{E-}05$	$5.34\text{E+}00$

**Table 4:** UV absorbance before and after encapsulation of G 3.5-OH with 2HB-LC-Tyr **22**

Generation dendrimer	Absorbance	Dendrimer conc / M	Molar absorption coefficient ( $\epsilon$ ) / M <sup>-1</sup>	Calculated chain conc / M	Average number of chains encapsulated
Free 2HB-LC-Val <b>24</b>	0.1014	n/a	2389.9	4.24E-05	n/a
Complex	0.1621	2.50E-06	2389.9	6.78E-05	5.08

**Table 5:** UV absorbance before and after encapsulation of G 3.5-OH with 2HB-LC-Val **24**

Furthermore, a 10-nm bathochromic shift was observed in  $\lambda_{\max}$  when either 2HB-LC-Tyr **22** or 2HB-LC-Val **24** were encapsulated within the dendrimer. This shift is consistent with a change in environment, as the water solvating the linear chains is replaced by the dendrimer's interior groups. Overall, the solubility and spectroscopic data confirm that all 10 linear chains were encapsulated within the dendrimer. It is assumed that the driving force for complexation was a cooperative process involving hydrophobic and H-bonding interactions (Figure 40). The methodology is similar to that used by Meijer to construct dendrimer complexes that can aggregate on dilution.<sup>26</sup>

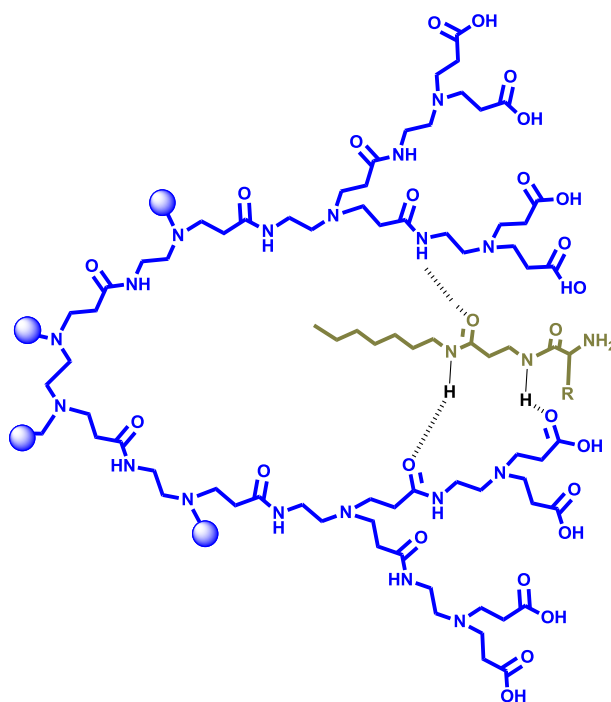


**Figure 40:** Schematic showing a segment of the G 3.5-OH dendrimer **10** and possible H-bonding motif to the linear chain, 2HB-LC-Tyr **22**

The same experiment was repeated for 3HB-LC-Tyr **26** and 3HB-LC-Val **28**, showing that, when the bathochromic shifted from 270 nm to 275 nm, this confirmed encapsulation within the dendrimer with six of chains encapsulated within the dendrimer through supramolecular/non-covalent interactions. It also confirmed that the neutral dendrimer's ability to operate as a scaffold for the linear chain. Having established and quantified the encapsulation of the various components, the next step involved a series of binding experiments to test whether or not the self-assembled complex could bind to protein and, moreover, be detected.

### 3.7 Conclusions

In conclusion, the synthesis of all dendrimers and linear chains proved to be successful. The experiments attested to the critical role played by functionality and size in the process of creating macromolecular ligands for selective protein binding. This study focuses on the use of OH-ended neutral dendrimers for encapsulation, which were synthesised from ester-terminated dendrimers, followed by addition of ethanolamine to provide terminal OH groups. To identify the dendrimer's maximum loading capacity, a 10 fold excess of linear chains was used with a constant dendrimer concentration of  $1 \times 10^{-5}$  M. The level of encapsulation was estimated using UV spectroscopy, which showed that more of the 3 H-bonding chains could be encapsulated relative to the other chains. Specifically, all 10 linear chains could be encapsulated for the 3 H-bonding system, versus 5-6 for the 2 H-bonding system. Only 1-2 chains could be encapsulated for the 1 H-bonding linear chain. The methodology is similar to that used by Meijer to construct dendrimer complexes that can aggregate on dilution.. Therefore future studies would concentrate on the 3 and 3 H-bonding systems to see which would bind better to the target protein. Overall we wanted to see which would perform best with respect to a compromise between protein binding and ease of synthesis. Therefore, our next aim was to test the inhibition properties of these complexes.

## ***CHAPTER 4***

### ***Non-covalent functionalized dendrimers to inhibit $\alpha$ -chymotrypsin***

## 4.0 Introduction and Aim

Macromolecular scaffolds are associated with a range of structural characteristics that lend themselves effectively to protein surface binding. In the presence of several surface contacts between the polymer and the protein, the efficiency of the binding can be increased.<sup>43, 44</sup> The flexible nature of polymers, as well as their status as large molecules, provides a sufficiently sizeable area for contacting with a target protein, which generates numerous applications in the field of identifying protein external surfaces.

Protein surface targeting has multiple practical uses, one of the main ones being enzyme inhibition. The protease enzyme family includes many proteins that have the capability to hydrolyse amides and esters. Additionally, an expansive group of natural protein inhibitors has been identified as binding to the active sites and surface regions of elastase,  $\alpha$ -chymotrypsin, trypsin, and other serine proteases.<sup>45</sup> Most protein inhibitors that have been identified and characterised in the literature are oriented towards  $\alpha$ -chymotrypsin.  $\alpha$ -Chymotrypsin was used as this study's target for testing the inhibition potency of a synthetic protein receptor. This study sought to synthesise inhibitors for targeting the active sites, but the active sites are marked by considerable similarity. Hence, it is a complex affair to find a specific inhibitor that corresponds to every protease enzyme. In view of this, creating inhibitors for surface binding represents a new strategy. Structurally speaking,  $\alpha$ -chymotrypsin is a ring of positively charged residues organised around an active pocket and scattered surface hot spots.<sup>12</sup>

It is possible to target these hot spots as part of a strategy to formulate a surface-based inhibitor.  $\alpha$ -chymotrypsin leverages its cationic residues to connect with anionic synthetic inhibitors and receptors, including polymeric micelles,<sup>45</sup> dendrimers,<sup>46</sup> porphyrins,<sup>47</sup> gold nanoparticles,<sup>48</sup>

and – more recently – graphene oxide.<sup>49</sup> Nevertheless, due to the additional non-covalent interactions stemming from amino acid functionality, protein binding is marked by specificity and high affinity. This is the case even in spite of the main interaction's electrostatic nature. A research project that sought to examine the effect of amino acid preferences and functionality on interfacial areas and hot spots revealed that arginine, tyrosine, and tryptophan – if present – were often identified with hot spots.<sup>12</sup> Although these amino acids are relatively rare in protein structures,<sup>50</sup> they are largely responsible for non-covalent interactions.

Despite the fact that it was not possible to detect binding with only the neutral dendrimer, the assessment of binding will occur when functionalized chains are included. This will suggest that control of the three-dimensional arrangement of terminal groups to lock on the template of protein of  $\alpha$ -chymotrypsin. Therefore, , an enzyme inhibition assay was used to evaluate the functionalized dendrimer's protein binding

#### **4.1 Assessment of Protein Binding Using an Enzyme Inhibition Assay**

As mentioned before, the key assumption underpinning this process was that access of the substrate to the active site could be prevented or inhibited by binding to the enzyme surface. The relevance of this is strong in relation to  $\alpha$ -chymotrypsin, where the active site entrance is within the hot spot binding surface as shown in Figure 41.<sup>31</sup>

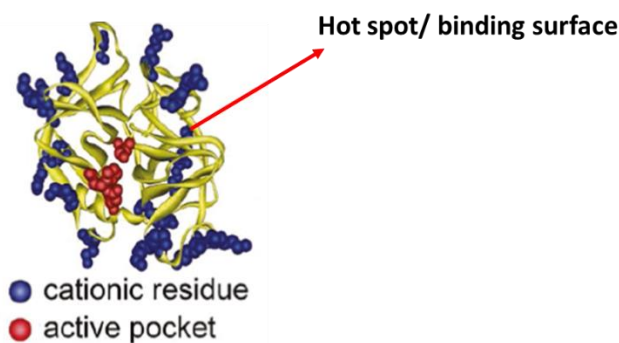


**Figure 41:** The surface of  $\alpha$ -chymotrypsin (Chy). Image reprinted with permission from [De, M., Chou, S. S. and Dravid, V. P. J. Am. Chem. Soc. 133, 17524–17527 (2011)]<sup>31</sup>

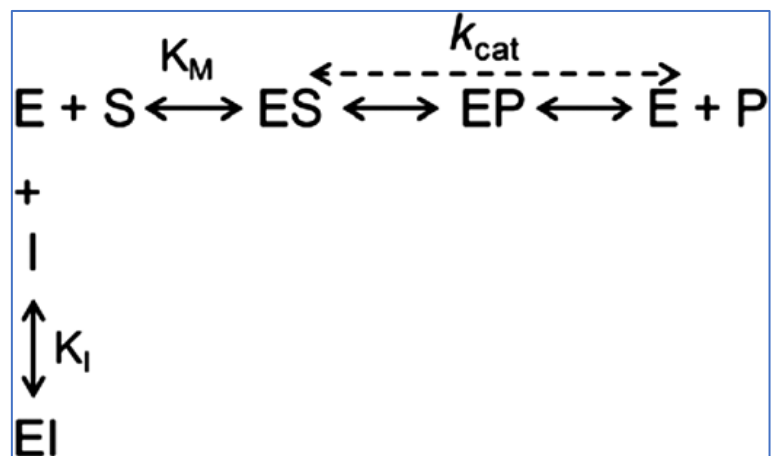
In a prior study, our group leveraged this principle in order to demonstrate that a size-based relationship existed between protein binding and dendrimers.<sup>17, 34</sup> Additionally, in the study conducted by De and Dravid, the researchers drew on the same assumption to show that unfunctionalized graphene oxide, which is negatively charged, has the capability to interact in an electrostatic way with  $\alpha$ -chymotrypsin.<sup>31</sup>

Initial rates for every species were identified at a range of substrate and inhibitor concentrations (*see equation 1*) for the purpose of generating more comprehensive kinetic and inhibition data, and also to identify the mode of inhibition. In turn, the initial rates were plotted against the inverse of substrate concentration using GraphPad,<sup>36</sup> and the plots for every experiment were fitted to an inhibition model using the following equation:

$$V = \frac{V_{max}[S]}{[S] \left( 1 + \frac{[I]}{\alpha K_i} \right) + K_m \left( 1 + \left( \frac{[I]}{K_i} \right) \right)}, \quad [\text{equation 1}]$$

where  $K_m$  is the Michaelis-Menten constant (concerned with the binding effectiveness of the substrate to the enzyme),  $V_{max}$  is the maximum enzyme velocity upon saturation with the substrate, and  $K_i$  denotes the inhibition constant (concentration must inhibit 50%). It is also noteworthy that the parameter  $\alpha$  can be generated from this model, and it provides valuable information about the inhibition mechanism as shown in Figure 41.<sup>37</sup>

The objective of this study is to increase the dissociation constant ( $K_I$ ) of the enzyme-inhibitor complex for the purpose of desensitising the enzyme to an inhibitor (Scheme 10). The equilibrium expression for enzyme, inhibitor and the EI complex re-arranges to the form  $[E]/[EI] = [K_I][I]$ . Therefore, as the size of  $K_I$  increases, the quantity of  $[E]$  available for catalysis is also larger.



Scheme 10: Kinetic parameters available for improving reaction velocity in the presence of a competitive inhibitor.

To arrive at the Michaelis constant  $K_m$ ,  $V_{max}$  (maximum velocity) is halved. If  $K_m$  changes from 100  $\mu\text{M}$  (uninhibited) to 400  $\mu\text{M}$  (inhibited), then  $\alpha$  is 4. In other words, stronger enzyme-inhibitor binding is indicated by higher  $K_m$  and  $\alpha$  values. A mixed-model inhibition plot shows how the the initial velocity of the enzyme varies with the concentration of substrate (Figure 42a). Transforming these data to a Lineweaver-Burk or double reciprocal plot, shows that the reciprocal of initial velocity varies according to the reciprocal of the concentration of substrate (Figure 42(b)).

Based on the value of  $V_{max}$ , Lineweaver-Burk plots were also used to establish the mode of inhibition. Competitive inhibition is indicated by an unchanged  $V_{max}$  and the same y-intercept (with or without the inhibitor) (Figure 43). In that instance, the inhibitor and substrate compete for the same active site. Where the inhibitor binds before substrate, the reaction rate is reduced leading to an increase in  $K_m$ . As raised previously, higher  $K_m$  values are indicative of weak binding interactions between the enzyme and substrate, and the converse where  $K_m$  is low. The  $V_{max}$  value differs with uncompetitive and non-competitive inhibitors. There is no effect upon  $K_m$  in non-competitive inhibition, but in uncompetitive inhibition,  $K_m$  values are reduced.

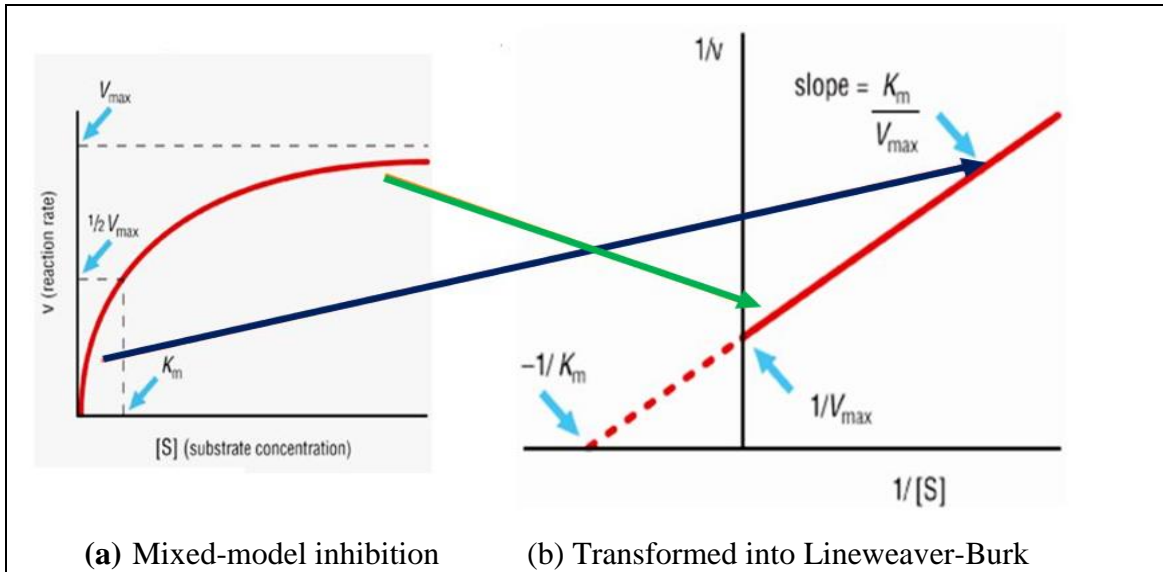


Figure 42: Mixed inhibition data transformed into double reciprocal Lineweaver-Burk analysis using GraphPad Prism 7.03

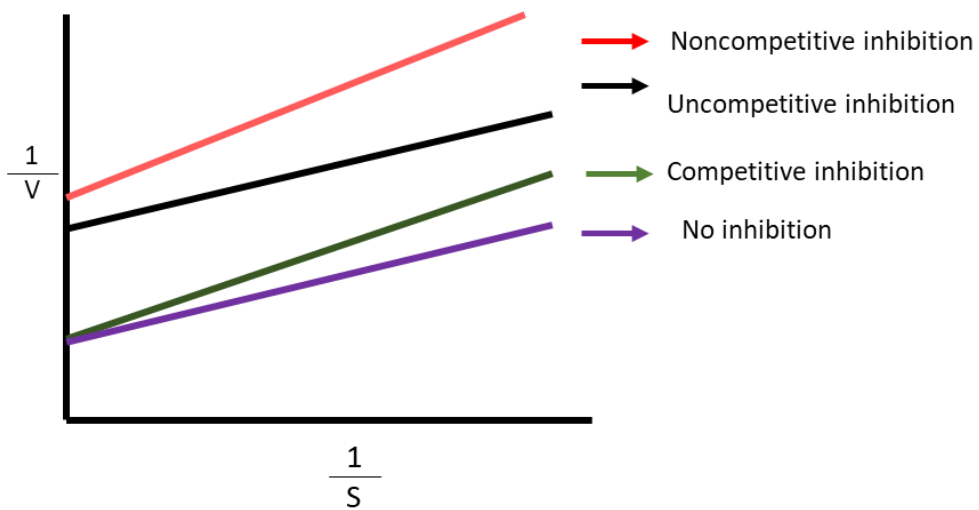
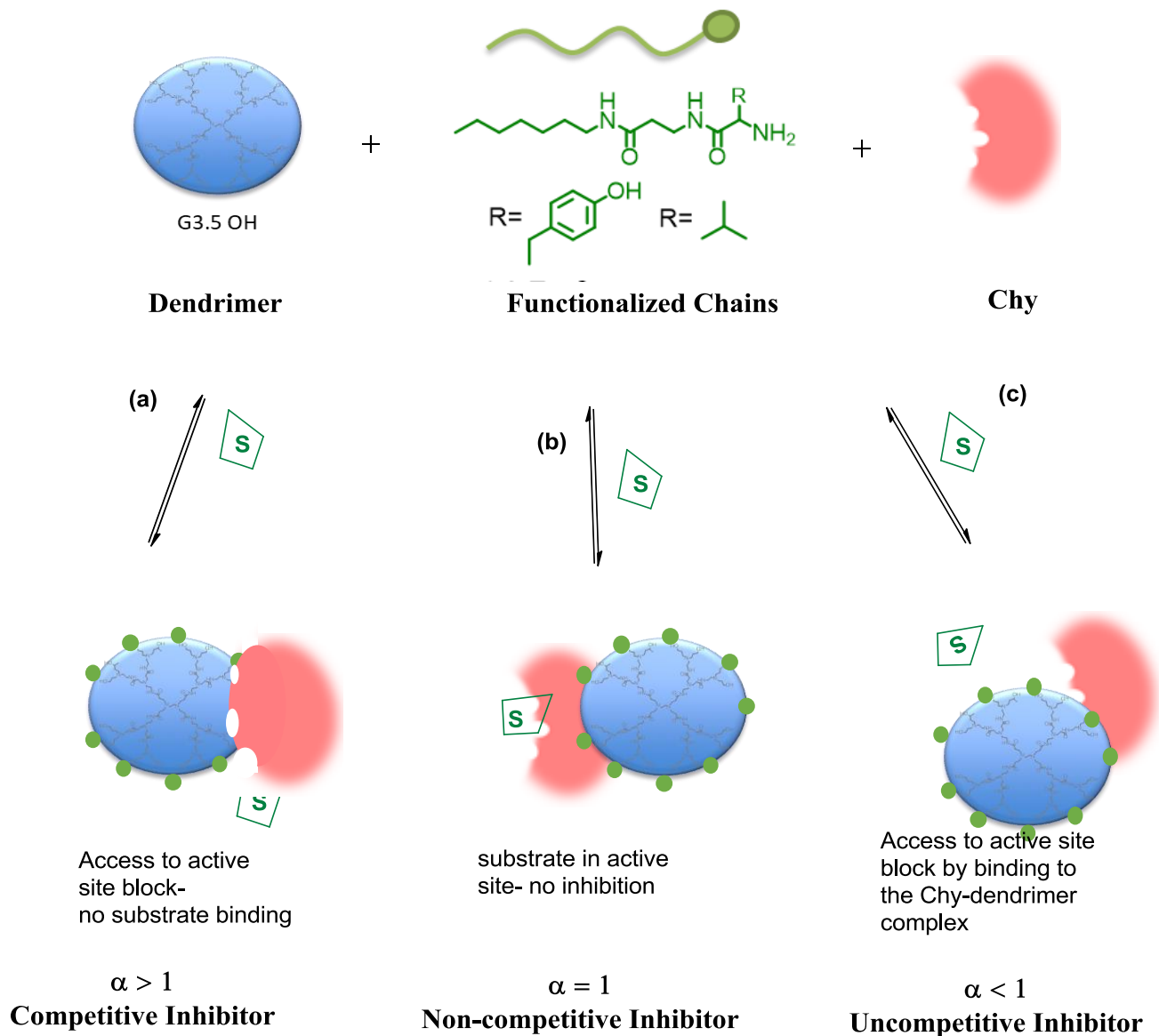
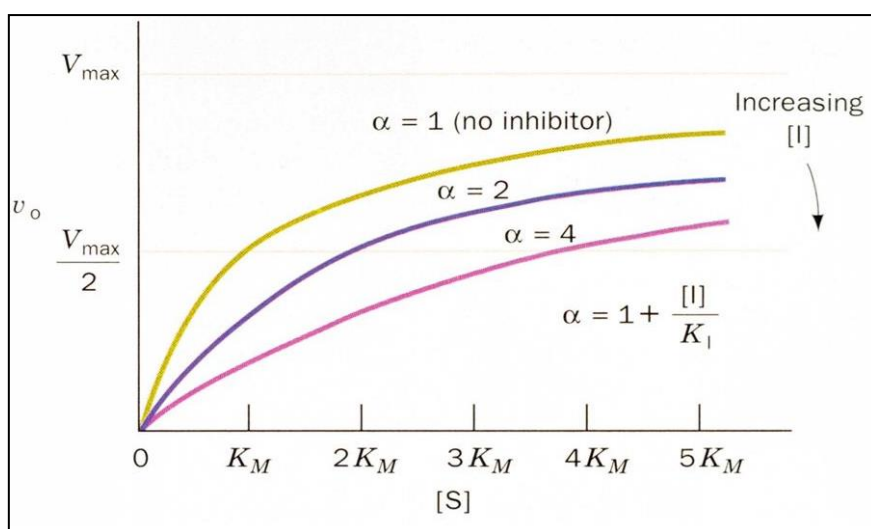


Figure 43: Lineweaver-Burk distinguishes between the three categories of reversible inhibition



**Figure 44:** The type of inhibitor present can be explained by its effect on the degree of inhibition. a) When  $\alpha > 1$ , binding of the substrate to the enzyme is prevented by the inhibitor, this condition is referred to as competitive inhibition; b) when  $\alpha = 1$  is the condition in which the substrate binding to the enzyme is unaffected by the inhibitor called non-competitive inhibition; c) When  $\alpha < 1$ , the inhibitor binds to the enzyme-substrate (ES) complex preventing formation of product corresponds to uncompetitive inhibitor.

In the event that the value of  $\alpha$  is greater than 1.0, the substrate and the inhibitor compete for the enzyme in a process known as competitive inhibition. Additionally, the size of  $\alpha$  is indicative of the relative binding affinity for the dendrimer substrate inhibitors. Contrastingly, when the value of  $\alpha$  is less than 1.0, a non-productive ternary complex is formed after the inhibitor's binding to the enzyme/substrate complex. This process is referred to as uncompetitive inhibition. Lastly, when the value of  $\alpha$  is equivalent to 1.0, non-competitive inhibition takes place, where the substrate and inhibitor binding to the enzyme are not dependent on one another, but the enzyme/substrate complex is not productive.



**Figure 45:** The degree of inhibition ( $\alpha$ ) dependent/related parameters with the  $V_{max}$ ,  $K_m$ ,  $[I]$  and  $K_i$ .

Nevertheless, a range of interactions other than electrostatics are involved in protein binding. The active site entrance of  $\alpha$ -chymotrypsin also incorporates functionality that has the capacity to engage H-bonding,  $\pi$ - $\pi$ , hydrophobic interactions, and others.<sup>35</sup>

## 4.2 Inhibition using 2 hydrogen bonding chain

The intention of this part of the study is to determine how important and strong the polyvalent interactions from the amino acids of 2 hydrogen bonding are when binding proteins. If this methodology is valid, then the dendrimers functionalized with amino acids known to be involved in protein-protein binding, should bind well to the surface of  $\alpha$ -chymotrypsin and inhibit its function. On the other hand, a dendrimer functionalized with valine, which is not associated with protein binding, would result in weaker binding and less inhibition. This is the same hypothesis used in the previous work described by Bogan and Twyman.<sup>12,67</sup> If polyvalent interactions are not observed or if the orientation of the chains is not compatible with binding, then there will be no change in binding. In that instance, the kinetic and inhibition data would be the same as that measured in the G3.5-OH **10** control reaction/experiment.

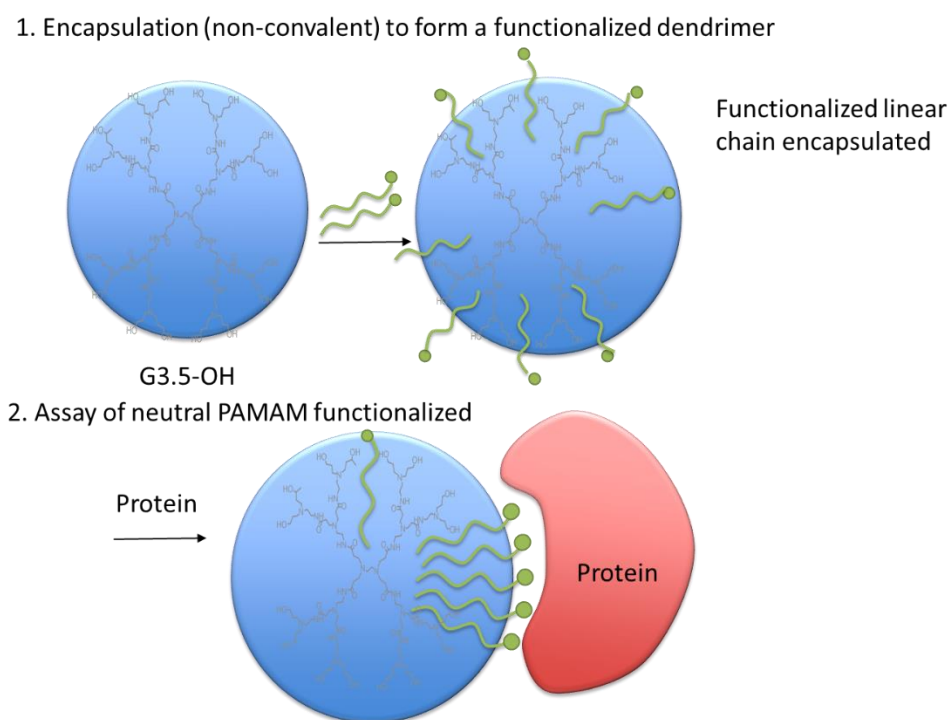
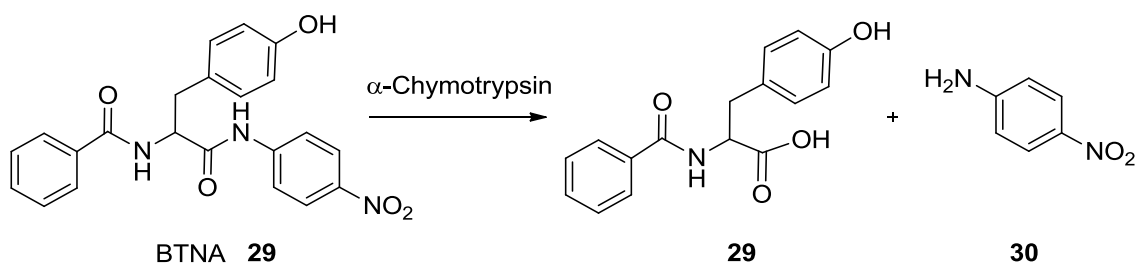


**Figure 46:** Cooperative interactions of the amino acid with the  $\alpha$ -chymotrypsin's surface.



**Scheme 11:** Enzyme-mediated reaction for assessing relative binding to  $\alpha$ -chymotrypsin

In view of this, adding complimentary functionality to the dendrimer's surface was expected to enhance selectivity. For the purpose of evaluating binding, the inhibition of  $\alpha$ -chymotrypsin to conduct the hydrolysis of the enzyme substrate N-benzoyl tyrosine p-nitroanilide (BTNA) was studied. Following hydrolysis, BTNA produces an aromatic species **30** that is characterized by a yellow hue, and which can be employed to follow the hydrolysis over time. It is then possible to determine the initial rates based on the plots of concentration against time for the nitro aniline product **30**. This will allow us to study binding by plotting initial rates at various substrate's concentration to get the kinetic parameters (Such as  $K_i$ ,  $\alpha$  etc). At the outset, BTNA as a substrate was used to generate a baseline/control for  $\alpha$ -chymotrypsin activity without the presence of inhibitor. This is in order to determine the conditions of the experiments and to verify that there was no interaction or reaction between BTNA . Thus, all inhibition was a direct consequence of interaction between the inhibitor and the protein. .

For the control reaction, 2.0  $\mu$ M BTNA and 0.4  $\mu$ M  $\alpha$ -chymotrypsin in 0.1 M phosphate buffer was employed for the reaction, and 0.4  $\mu$ M  $\alpha$ -chymotrypsin pre-incubated with 0.4  $\mu$ M of the specific inhibitor was used to examine the impact on the background rate for G3.5-OH, the

G3.5-OH-Val, and G3.5-OH-Tyr. In every experiment, the hydrolysis product's **30** concentration was plotted versus time, as shown in Figure 47. GraphPad was used to identify initial velocities,<sup>36</sup> and the data were fit with linear regression. This permitted an assessment of whether or not it was possible for the neutral dendrimer to bind. In turn, the reaction was undertaken again with G3.5-OH, where the final concentration was the same as the enzyme (i.e., 0.4  $\mu$ M). In line with expectations, the profile remained unchanged, thereby verifying that G3.5-OH does not inhibit the reaction or bind to the protein. This can be accounted for by referencing the fact that the dendrimer lacks groups that can interact with the other groups present on the protein or the charged surface.

20% of the enzyme's activity in relation to the control was inhibited by 2HB-Tyr (inhibited reaction). The results given in Figure 45 the effectiveness of the neutral dendrimer as an inhibitor upon functionalization with tyrosine. Contrastingly, valine-functionalized dendrimers were associated with the lowest level of inhibition, and thus the weakest binding. Valine is frequently found in protein structures, but there is limited availability of valine at the binding/interfacial areas. As a consequence, binding after the addition of functionalized chains can be linked to polyvalent interactions between the protein surface and the amino acids.

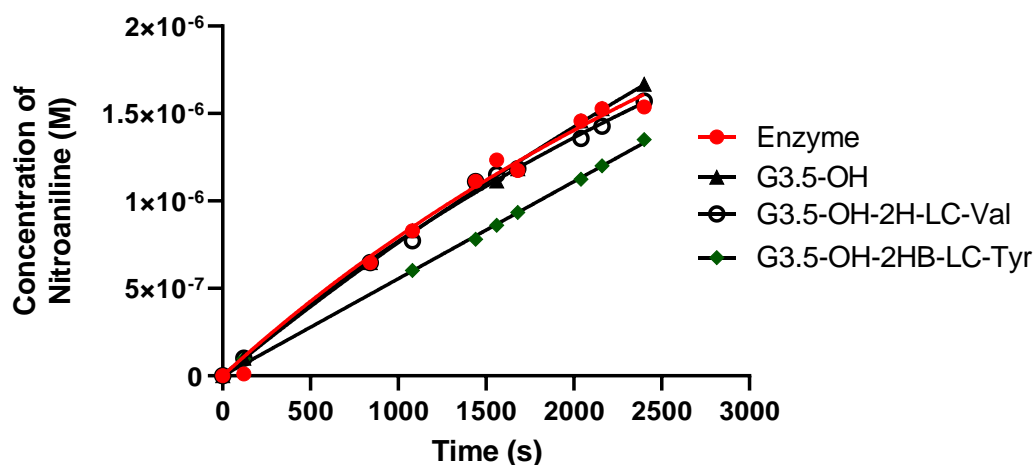


**Figure 47:** Rate plots employed to identify initial velocities ( $V$ ) for the hydrolysis of  $2.0 \mu\text{M}$  BTNA with  $0.4 \mu\text{M}$  chymotrypsin in the absence and presence of  $0.4 \mu\text{M}$  dendrimer inhibitors

Inhibitor	No inhibitor	G3.5-OH/non functionalized	2HB-LC-Val	2HB-LC-Tyr
Initial rate ( $\text{nMs}^{-1}$ )	0.716	0.718	0.670	0.575

**Table 6:** Provides an overview of the plots for the G3.5-OH-Tyr.

BTNA concentration ( $\mu\text{M}$ )	2.0	4.0	6.0	8.0
No Inhibitor ( $0.0 \mu\text{M}$ )	0.716 ( $\pm 0.143$ )	1.180 ( $\pm 0.112$ )	1.562 ( $\pm 0.121$ )	2.010 ( $\pm 0.312$ )
2HB-LC-Val $0.4 \mu\text{M}$	0.670 ( $\pm 0.012$ )	1.004 ( $\pm 0.013$ )	Not applicable	1.522 ( $\pm 0.013$ )
2HB-LC-Val $0.8 \mu\text{M}$	0.71 ( $\pm 0.021$ )	1.078 ( $\pm 0.120$ )		1.471 ( $\pm 0.145$ )
2HB-LC-Val $1.6 \mu\text{M}$	0.625 ( $\pm 0.003$ )	1.008 ( $\pm 0.032$ )		1.309 ( $\pm 0.643$ )
3HB-LC-Tyr $0.4 \mu\text{M}$	0.575 ( $\pm 0.039$ )	0.982 ( $\pm 0.034$ )	1.338 ( $\pm 0.210$ )	1.654 ( $\pm 0.213$ )
3HB-LC-Tyr $0.8 \mu\text{M}$	0.450 ( $\pm 0.003$ )	0.784 ( $\pm 0.068$ )	1.030 ( $\pm 0.081$ )	1.363 ( $\pm 0.100$ )
3HB-LC-Tyr $1.6 \mu\text{M}$	0.343 ( $\pm 0.005$ )	0.627 ( $\pm 0.031$ )	0.780 ( $\pm 0.021$ )	1.030 ( $\pm 0.021$ )

**Table 7:** Initial rates identified with different inhibitor and substrate concentrations, with experiments undertaken using 0.4  $\mu\text{M}$  chymotrypsin

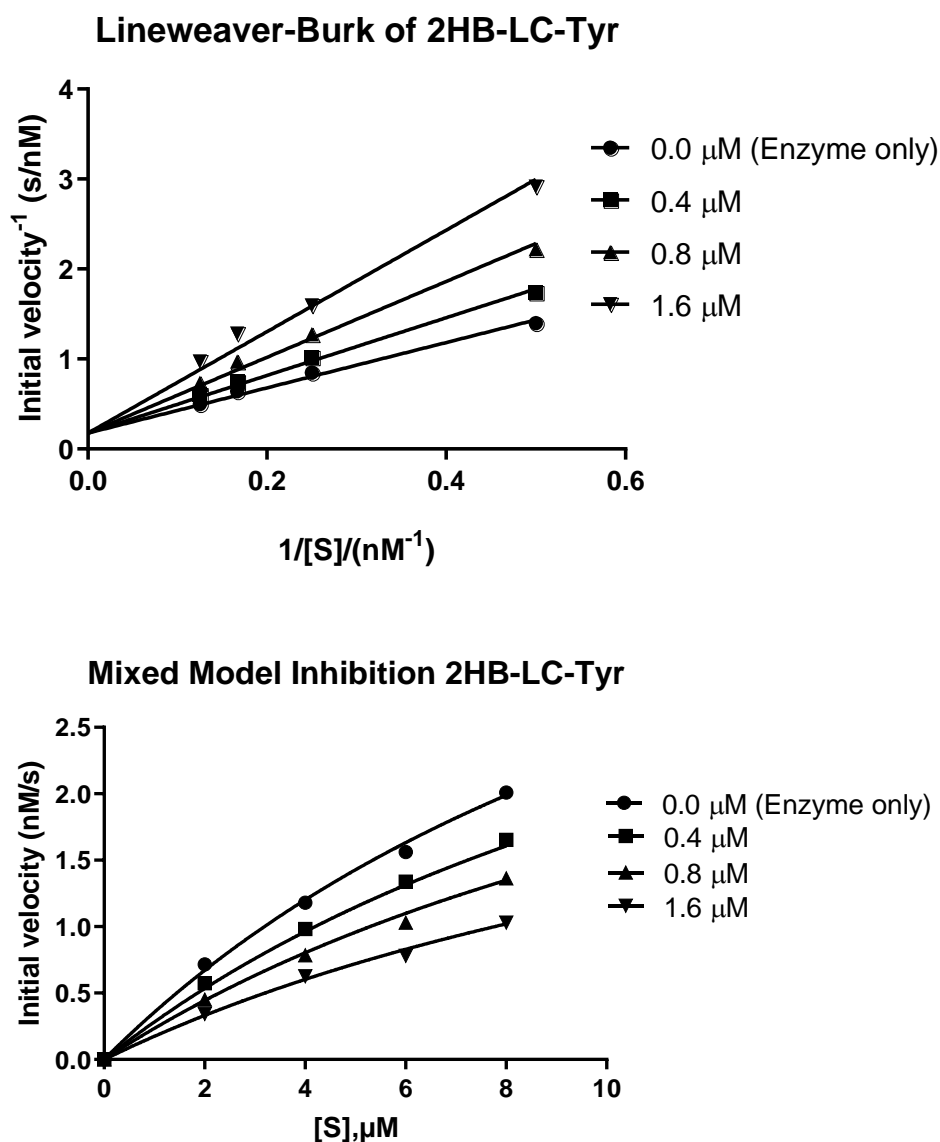


**Figure 48:** (Top) Plot of BTNA concentration against initial rate at several functionalized G3.5-OH concentrations. Values for  $\alpha$ ,  $K_i$ ,  $K_m$ , and  $V_{max}$  were generated by fitting data to equation 1 (fitted to the inhibition model within GraphPad, where Table 2 provides an overview of the initial rates). (Bottom) Lineweaver-Burk plots indicating a shared intercept for every inhibitor concentration, thereby supporting the kinetic analysis regarding the existence of a competitive inhibition mechanism. Every experiment involved 0.4  $\mu\text{M}$  chymotrypsin.

Using the graphical analysis and fits, the kinetic parameters were identified for every inhibitor (see Table 7). In this experiment, the value of  $K_m$  rose for every functionalized dendrimer inhibitor, and the value was greatest for the tyrosine system. In this way, the highest level of inhibition was associated with the use of the G3.5-OH-Tyr system, where  $K_m$  was related in an inversely proportional way to enzyme affinity for the substrate as illustrated in Figure 48. The values of  $K_i$  supported this, which were 95% lower than the inhibition determined for the unfunctionalized dendrimer (for the valine and tyrosine systems, respectively). These data demonstrate that dendrimer functionalization with tyrosine promotes inhibition. Since  $\alpha > 1.0$ , the tyrosine dendrimer system evidently operated based on a competitive inhibition mechanism. Additionally,  $\alpha$  was large, and the trend regarding the size was the same as that observed for  $K_m$ , which was the greatest for the tyrosine system. This demonstrates that the enzyme and the inhibitor bind strongly, where the tyrosine dendrimer system (G3.5-OH-Ty) was associated with the strongest binding. Figure 48's Lineweaver-Burk plot, specifically the outcome for G3.5-OH-Tyr, provides further support for competitive inhibition.

From our overall results (Table 8), the data that indicates poor inhibition and therefore, poor binding. The valine initial rates for all the substrate and concentrations used were very similar to those obtained for the control data. It is clear from Table 9 that the valine dendrimers do not bind or inhibit chymotrypsin. Nevertheless, the plots relating to valine concentrations did not have the intercept in common Figure 50, thereby verifying uncompetitive inhibition.

BTNA ( $\mu\text{M}$ )	Control	0.4	0.8	1.6
2.0	0.7158	0.67	0.71	0.625
4.0	1.18	1.004	1.078	1.008
8.0	1.562	1.522	1.471	1.309

**Table 8:** The summary of initial velocity data in the absence and presence of G3.5-OH-Val . Chy at 0.4  $\mu\text{M}$

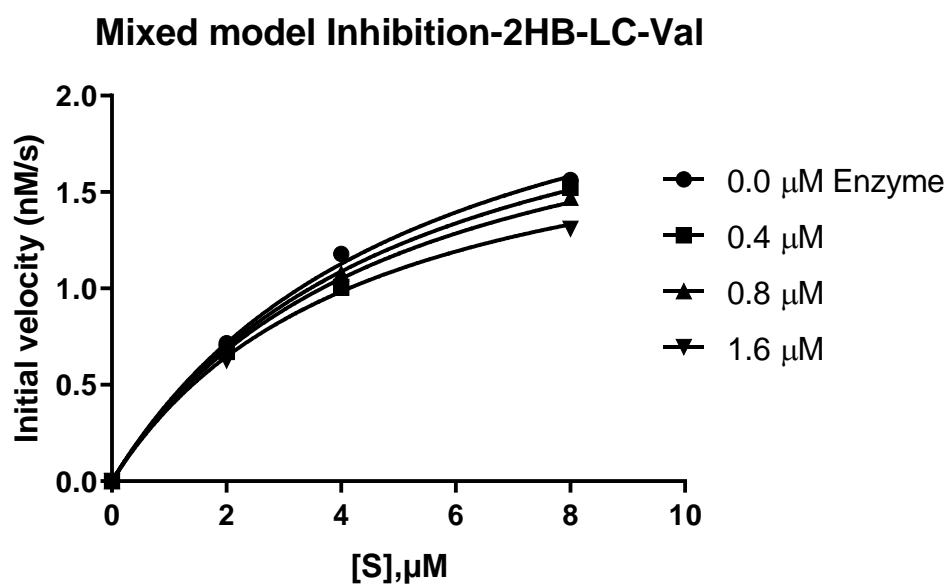


**Figure 49:** Mixed mode inhibition plots of [BTNA] at various concentrations of G3.5-OH-Val 40 at 0.4  $\mu\text{M}$  of Chy.

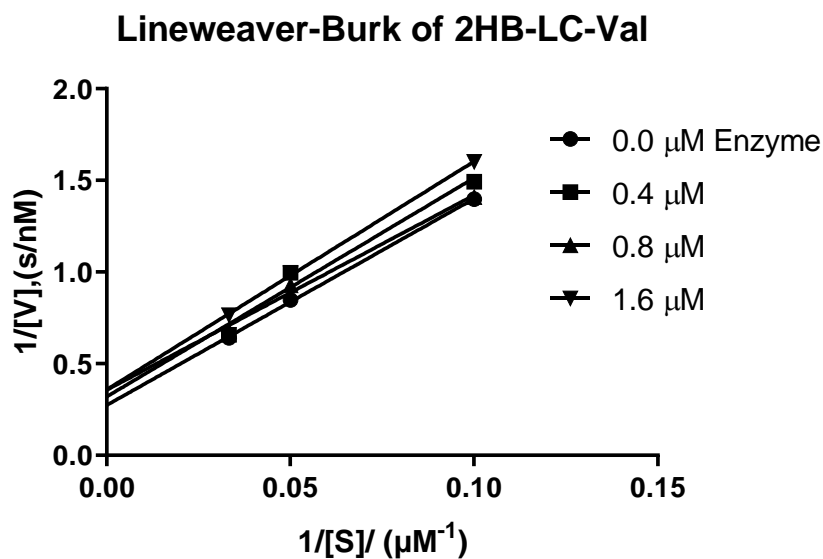


**Figure 50:** Lineweaver-Burk plots of [BTNA] at various concentrations of G3.5-OH-2HB-LC-Val at 0.4 μM of Chy. Lineweaver-Burk plots indicating a unshared intercept for every inhibitor concentration, thereby indicating the kinetic analysis regarding the existence of a uncompetitive inhibition mechanism.

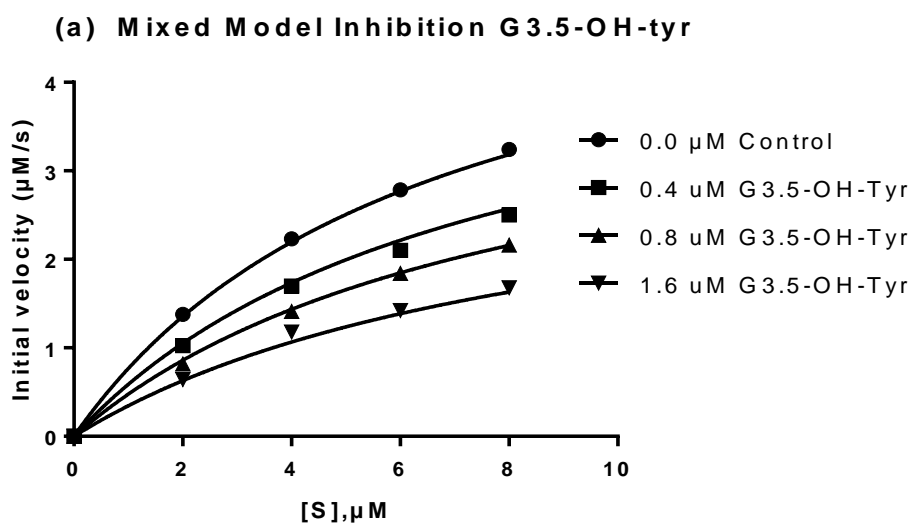
No appropriate functionality is associated with valine that has the capacity to interact (i.e., H-bonding,  $\pi$ - $\pi$ , electrostatically), and only weak hydrophobic binding was identified, offering an elevated value of  $K_i$  amounting to 36.43 μM. These results attest to the significance of functionality on molecular interactions regarding binding to the protein surface of Chy, and they reflect the importance of the linear chain's head group. In particular, they show that the aromatic group of tyrosine leads to stronger binding when compared to valine.

Inhibitor	$K_m, \mu\text{M}$	$K_i, \mu\text{M}$	$\alpha$
2HB-LC-Val	5.41	36.43	0.16
2HB-LC-Tyr	15.17	1.51	1.45

**Table 9:** Overview of kinetic parameters for every functionalized dendrimer inhibitor

### 4.3 Inhibition using 3 hydrogen bonding chain

The inhibition and binding experiments used were the same as applied to the 2 hydrogen bonding system and were carried out by a colleague in the group (Dr Azrah Abdul Aziz). The first experiment was a control to establish the maxim enzyme velocity using only BTNA and Chy in buffer (pH 7.46). This provided the initial rate of the uninhibited reaction (nitroaniline production). We then carried out binding and inhibition experiments using the 3 H-bonding linear chains to establish the kinetic data. The data is shown below in **Figure 51.**, presented in Tables 8 and 9.



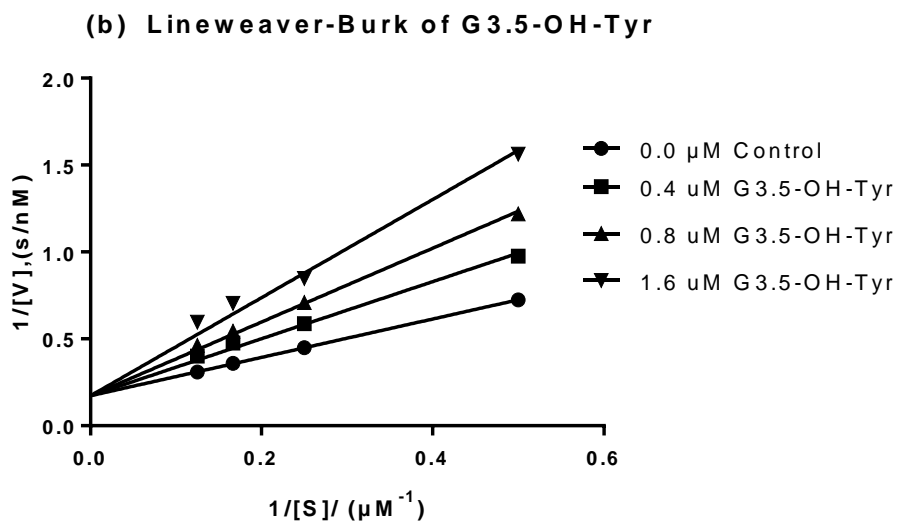


**Figure 51:** (a) Mixed mode inhibition and (b) Lineweaver-Burk plots for 3HB-LC-Tyr-Tyr at 0.4  $\mu\text{M}$  of Chy.

Overall, the data confirmed our predictions regarding amino acid availability and population sizes at interfacial/binding areas. In addition, the binding affinity of functionalized dendrimers also showed that the 3HB-LC-Tyr bound chymotrypsin much more strongly than the 2HB-LC-Tyr. As before, the 3HB-LC-Val functionalized dendrimers exhibited very little inhibition and therefore the weakest binding. Table 10 shows the initial rates at the highest substrate concentrations. At these concentration the tyrosine systems inhibited 48% . However, the valine system bound very weakly, only inhibiting 8% ( $\pm 5\%$ ).

Inhibitor Kinetic inhibition data	Control / non-functionalized <b>G3.5-OH</b>	3HB-LC-Val	3HB-LC-Tyr
Initial velocity (V), nMs <sup>-1</sup>	3.240 (±0.217)	2.995 (±0.321)	1.680 (±0.771)
Percentage Inhibition (%)	0	8	48

**Table 10:** Initial velocity translated into percentage inhibition

Inhibitor	$K_m$ , $\mu\text{M}$	$K_i$ , $\mu\text{M}$	$\alpha$
3HB-LC-Val	5.50	24.60	0.85
3HB-LC-Tyr	6.56	1.23	1.23

**Table 11:** Kinetic parameters obtained for all functionalized G3.5-OH with 3 hydrogen bonding linear chain

Table 11 summarises the kinetic and inhibition results which were obtained by varying substrate concentrations and applying the same kinetic analysis described for the 2 H-bonding systems. The  $K_m$  values obtained were lower for 3HB-LC-Val and 3HB-LC-Tyr, indicating that the 3 H-bonding systems bind to the protein more strongly than the 2 H-bonding systems. Furthermore, the  $\alpha$  values and Lineweaver-Burk plots also confirmed that the 3 H-bonding systems were competitive inhibitors, with the 3HB-LC-Tyr having an  $\alpha$  value of 1.23.

Dendrimers functionalized with the valine chain showed very weak binding and uncompetitive inhibition ( $\alpha = 0.85$ ). As before, this was expected. Valine does not contain suitable functionality that can interact, whether electrostatically or in terms of H-bonding, aromatic,  $\pi$ - $\pi$  interaction, and is only capable of weak hydrophobic binding, which gave a high  $K_i$  value of

24.60  $\mu\text{M}$ . In contrast, Tyr exhibited a  $K_i$  value of 1.93  $\mu\text{M}$ . The uncompetitive binding mechanism was also confirmed from a Lineweaver-Burk plot, which did not show a common y-intercept. As before, tyrosine binding was stronger than valine and can be attributed to the  $\pi$ - $\pi$  interactions, and hydrogen bonding interactions, provided by the tyrosine functionality. In addition, the linear chain has an extra hydrogen bond, which maximises its interaction with the dendrimer. Overall, the results confirm the importance of amino acid functionality and the level of hydrogen bonding (provided by the chain) on the overall interactions with respect to encapsulation and protein binding.

#### **4.4 Comparison of the 1, 2 and 3 hydrogen bonding linear chains**

At this stage, it is worth comparing the results obtained so far with respect to the number of H bonding group along the linear chain and the effect on binding affinity. The 1HB-LC-Tyr did not encapsulate into the dendrimer very well and was not used in any protein binding experiments. However, comparing the 2HB-LC results against those obtained for the 3HB-LC systems conformed the importance of maximising dendrimer/linear chain interactions. Comparing the results from these two systems allows us to qualitatively determine the contribution of the H bonding chains to any overall involved in protein binding (enzyme inhibition). When comparing the valine systems, it is clear that there is no significant difference between 3HB-LC and 2HB-LC when inhibiting or binding the protein. This is due entirely to the overall poor protein binding demonstrated for both systems. However, there was a significantly different result for the tyrosine systems. Although reasonable levels of inhibition were observed for the 2HB-LC-Tyr chain (with  $\alpha$  and  $K_i$  values of 1.45 and 1.51  $\mu\text{M}$ , respectively), significantly higher values were observed for the 3HB-LC-Tyr (with  $\alpha$  and  $K_i$

values of 1.95 and 1.23  $\mu\text{M}$ , respectively - Table 10). The difference in  $K_i$  for the 2 and 3 H-bonded tyrosine chains was nearly 25%. This confirms that the number of H-bonds along the linear chain is an important factor with respect to protein binding and complex stability.

Inhibitor	Head Group of amino acid	$K_m, \mu\text{M}$	$K_i, \mu\text{M}$	$\alpha$
2HB-LC	Val	5.41	36.43	0.16
	Tyr	15.17	1.51	1.45
3HB LC	Val	5.50	24.60	0.85
	Tyr	6.56	1.23	1.95

**Table 12:** Kinetic parameters obtained from a linear fit of data for the enzyme catalysed hydrolysis BTNA with functionalized 2HB-LC and 3HB-LC with tyrosine and valine respectively.

## 4.5 Conclusions

This study's aim was to exploit non-functionalized dendrimers and to incorporate targeting and binding groups non-covalently into the dendrimer surface. . This included hydrophobicity and the effect of any additional binding with one hydrogen bonding linear chain (1HB-LC), two (2HB-LC) and three hydrogen bonding (3HB-LC) were studied. Another aim was to investigate how these linear chain functionalized with different amino acids could moderate binding. Several linear chains were synthesised and encapsulated within the dendrimer to give the functionalized system. . A 10-nm bathochromic shift was observed in  $\lambda_{\text{max}}$  when 2HB-LC-Tyr or 2HB-LC-Val were encapsulated within the dendrimer and a 5 nm bathochromic shift was observed for 3HB-LC-Tyr and 3HB-LC-Val. This shift is consistent with a change in environment, as the water solvating the linear chains is replaced by the dendrimer's interior groups. The encapsulation levels depended on the number of hydrogen bonding sites along the chain, with the 3 H-bonding system being encapsulated better than the 2 H-bonding systems. The importance of maximising hydrogen bonding interactions between the linear chain and the dendrimer were also observed in protein binding experiments (enzyme inhibition). Overall the best system was the dendrimer encapsulated 3HB-LC-Tyr system, which had a  $K_i$  value of 1.23  $\mu\text{M}$ , which was 25% better than any other system. In addition, the results verified the significance of tyrosine as a protein targeting group. It was important to confirm that the individual components did not inhibit the enzyme. This was achieved through control experiments, which showed that the both dendrimer and linear chain were required for binding. No binding could be detected if either were used alone.

The results support our original hypothesis that a neutral dendrimer can be functionalized non-covalently using a targeting group that can be encapsulated within a neutral (non-binding) dendrimer. The next stage of the study will be examination of other targeting groups, as well as targeting and binding other proteins.

#### 4.6 Future works

Further studies in this field should seek to develop novel, multivalent dendrimer chain complexes containing 3 H-bonding groups functionalized with a series of different amino acids, as well as different dendrimers, which can then be mixed together to form optimized dendrimer/protein complexes, as shown in Figure 52. After successful encapsulation, the system will need to be cross-linked to fix the structure of the dendrimer bound ligand and the protein removed, thereby generating a protein ligand that can be collected and used as a protein ligand for a number of different applications, including use as a therapeutic molecule.

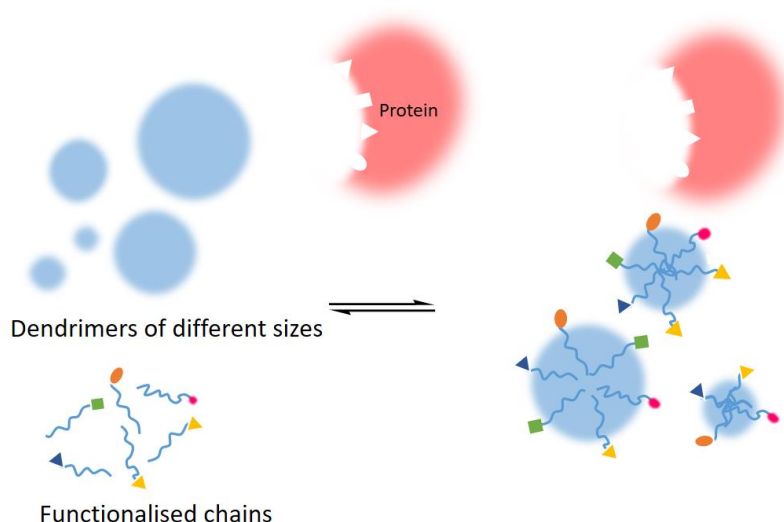


**Figure 52:** Dynamic Combinatorial Library to self-selected dendrimer-protein complex.

## 4.7 References

1. Chothia, C. & Janin, J. Principles of protein-protein recognition. *Nature* **256**, 705–708 (1975).
2. Hashimoto, M., Rockenstein, E., Crews, L. & Masliah, E. Role of protein aggregation in mitochondrial dysfunction and neurodegeneration in Alzheimer's and Parkinson's diseases. *NeuroMolecular Med.* **4**, 21–35 (2003).
3. Tao, S. C., Li, Y., Zhou, J., Qian, J., Schnaar, R. L., Zhang, Y., Goldstein, I. J., Zhu, H. & Schneck, J. P. Lectin microarrays identify cell-specific and functionally significant cell surface glycan markers. *Glycobiology* **18**, 761–769 (2008).
4. Whitford, D. *Proteins: Structure and Function*. (John Wiley and Sons Ltd, 2005).
5. Jones, S. & Thornton, J. M. Principles of protein-protein interactions. *Proc. Natl. Acad. Sci* **93**, 13–20 (1996).
6. Stefan, M. I. & Nove, N. Le. Cooperative Binding. *PLOS Comput. Biol.* **9**, 2–7 (2013).
7. Stites, W. Protein-protein interactions: interface structure, binding thermodynamics, and mutational analysis. *Chem. Rev.* **97**, 1233–1250 (1997).
8. Conte, L. Lo, Chothia, C. & Janin, È. The Atomic Structure of Protein-Protein Recognition Sites. *J. Mol. Biol.* **285**, 2177–2198 (1999).
9. Reichmann, D., Rahat, O., Cohen, M., Neuvirth, H. & Schreiber, G. The molecular architecture of protein-protein binding sites. *Curr. Opin. Struct. Biol.* **17**, 67–76 (2007).
10. Argos, P. An investigation of protein subunit and domain interfaces. *Protein Eng. Des. Sel.* **2**, 101–113 (1988).
11. Tsai, C. J., Lin, S. L., Wolfson, H. J. & Nussinov, R. Studies of protein-protein interfaces: a statistical analysis of the hydrophobic effect. *Protein Sci.* **6**, 53–64 (1997).
12. Bogan, A. A. & Thorn, K. S. Anatomy of hot spots in protein interfaces. *J. Mol. Biol.* **280**, 1–9 (1998).
13. Clarkson, T. & Wells, J. a. A hot spot of binding energy in a hormone-receptor interface. *Science* . **267**, 383–386 (1995).
14. Jain, R. K. & Hamilton, A. D. Protein surface recognition by synthetic receptors based on a tetraphenylporphyrin scaffold. *Org. Lett.* **2**, 1721–1723 (2000).
15. Yin, H. & Hamilton, A. D. Strategies for targeting protein-protein interactions with synthetic agents. *Angew. Chemie - Int. Ed.* **44**, 4130–4163 (2005).
16. Fry, D. C. Protein – Protein Interactions as Targets for Small Molecule Drug Discovery.

- 84**, 535–552 (2006).
17. D. Kuritzkes, S. K. and P. K. Fresh from the Pipeline: Maraviroc. *Nat. Rev. Drug Discov.* **7**, 15–16 (2008).
  18. Arkin, M. R., Tang, Y. & Wells, J. A. Small-Molecule Inhibitors of Protein-Protein Interactions: Progressing toward the Reality Michelle. *Chem. Biol.* **21**, 1102–1114 (2014).
  19. Alderton, W. K., Cooper, C. E. & Knowles, R. G. Nitric oxide synthases : structure , function and inhibition. *Biochem. J* **615**, 593–615 (2001).
  20. Carrington, B., Myers, W. K., Horanyi, P., Calmiano, M. & Lawson, A. D. G. Natural Conformational Sampling of Human TNF  $\alpha$  Visualized by Double Electron-Electron Resonance. *Biophys. J.* **113**, 371–380 (2017).
  21. Miller, S. E., Thomson, P. F. & Arora, P. S. Synthesis of Hydrogen- Bond Surrogate  $\alpha$ - Helices as Inhibitors of Protein- Protein Interactions. in *Curr. Protoc. Chem. Biol* **6**, 101–116 (John Wiley & Sons, Inc, 2014).
  22. Wang, D., Lu, M. & Arora, P. S. Inhibition of HIV-1 Fusion by Hydrogen-Bond-Surrogate-Based  $\alpha$  Helices. *Angew. Chemie - Int. Ed.* **47**, 1879–1882 (2008).
  23. Renner, C., Kusebauch, U., M. Löweneck, Milbradt, A. G. & Moroder, L. Azobenzene as photoresponsive conformational switch in cyclic peptides. *Chem. Biol. Drug Des.* **65**, 4–14 (2005).
  24. Akio Ojida, Masa-aki Inoue, Yasuko Mito-Oka & Itaru Hamachi. Cross-Linking Strategy for Molecular Recognition and Fluorescent Sensing of a Multi-phosphorylated Peptide in Aqueous Solution. *J. Am. Chem. Soc.* **125**, 10184–5 (2003).
  25. Leung, D. K., Yang, Z. & Breslow, R. Selective disruption of protein aggregation by cyclodextrin dimers. *Proc. Natl. Acad. Sci* **97**, 5050–5053 (2000).
  26. Tomalia DA, Frechet JMJ. Discovery of dendrimers and dendritic polymers: a brief historical perspective. *J Polym Sci A Polym Chem.*; **9**, 2719–2728 (2002)
  27. Emerson SD, Palermo R, Liu CM, et al. NMR characterization of interleukin-2 in complexes with the IL-2R $\alpha$  receptor component, and with low molecular weight compounds that inhibit the IL-2/IL-R $\alpha$  interaction. *Protein Sci.*; **12**(4):811–822. (2003)
  28. Lee, J. H., Zhang, Q., Jo, S., Chai, S. C., Oh, M., Im, W., Lu, H. & Hyun-Suk Lim. Novel Pyrrolopyrimidine-Based  $\alpha$ -Helix Mimetics: Cell-Permeable Inhibitors of Protein–Protein Interactions. *J. Am. Chem. Soc.* **133**, 676–679 (2010).
  29. Guo, W., Wisniewski, J. A. & Ji, H. Hot spot-based design of small-molecule inhibitors for protein – protein interactions. *Bioorg. Med. Chem. Lett.* **24**, 2546–2554 (2014).

30. Srivastava, S., Verma, A., Frankamp, B. L. & Rotello, V. M. Controlled assembly of protein-nanoparticle composites through protein surface recognition. *Adv. Mater.* **17**, 617–621 (2005).
31. De, M., Chou, S. S. & Dravid, V. P. Graphene oxide as an enzyme inhibitor: Modulation of activity of  $\alpha$ -chymotrypsin. *J. Am. Chem. Soc.* **133**, 17524–17527 (2011).
32. Ahmada, I., Mozhia, A., Yanga, L., Hana, Q., Lianga, X., Lia, C., Yanga, R. & Chen Wang. Graphene oxide-iron oxide nanocomposite as an inhibitor of A $\beta$  42 amyloid peptide aggregation. *Colloids Surfaces B Biointerfaces* **159**, 540–545 (2017).
33. Svenson, S. & Tomalia, D. A. Dendrimers in biomedical applications - Reflections on the field. *Adv. Drug Deliv. Rev.* **57**, 2106–2129 (2005).
34. Moiani, D., Salvalaglio, M., Cavallotti, C., Bujacz, A., Redzynia, I., Bujacz, G., Dinon, F., Pengo, P. & Fassina, G. Structural Characterization of a Protein A Mimetic Peptide Dendrimer Bound to Human IgG. *J. Phys. Chem* **113**, 16268–16275 (2009).
35. Chiba, F., Hu, T. C., Twyman, L. J. & Wagstaff, M. Dendrimers as size selective inhibitors to protein-protein binding. *Chem Commun* 4351–4353 (2008). doi:10.1039/b806517a
36. Kim, R. M., Manna, M., Hutchins, S. M., Griffin, P. R., Yates, A., Bernick, A. M., Chapman, K. T., Griffin, P. R., Yates, N. A., Bernick, A. M. Y. M. & Chapman, K. T. Dendrimer-Supported Combinatorial Chemistry Published. *Proc. Natl. Acad. Sci. U. S. A.* **93**, 10012–10017 (1996).
37. Li, J., Nowak, P. & Otto, S. Dynamic Combinatorial Libraries : From Exploring Molecular Recognition to Systems Chemistry. *J. Am. Chem. Soc* **135**, 9222–9239 (2013).
38. Huang, R. & Leung, I. K. H. Protein-Directed Dynamic Combinatorial Chemistry : A Guide to Protein Ligand and Inhibitor Discovery. *Molecules* **27**, 910 (2016).
39. Liu, R., Li, X. & Lam, K. S. Combinatorial Chemistry in Drug Discovery. *Curr. Opin. Chem. Biol.* **38**, 117–126 (2017).
40. Fletcher, S. & Hamilton, A. D. Targeting protein – protein interactions by rational design : mimicry of protein surfaces. *J. R. Soc. Interface* **3**, 215–233 (2006).
41. Toogood, P. L. Inhibition of Protein–Protein Association by Small Molecules: Approaches and Progress. *J. Med. Chem.* **45**, 1543–1558 (2002).
42. Babine, R. E. & Bender, S. L. Molecular Recognition of Protein – Ligand Complexes : Applications to Drug Design. *Chem. Rev.* **97**, 1359–1472 (1997).
43. Shaunak, S., Thomas, S., Gianasi, E., Godwin, A., Jones, E., Teo, I., Mireskandari, K., Luthert, P. *et al.* Polyvalent dendrimer glucosamine conjugates prevent scar tissue

- formation. *Nat. Biotechnol.* **22**, 977–984 (2004).
44. Palen, E. The Enzyme Kinetic Activity of Chymotrypsin : Temperature and pH Effects , Determination of  $K_m$  ,  $V_{max}$  , and Inhibitor Effects. 1–11 (2011).
  45. Torchilin, V. P. Drug targeting. *Eur. J. Pharm. Sci.* **11**, S81–S91 (2000).
  46. Abbasi, E., Aval, S., Akbarzadeh, A., Milani, M., Nasrabadi, H., Joo, S., Hanifehpour, Y., Nejati-Koshki, K. & Pashaei-Asl, R. Dendrimers: synthesis, applications, and properties. *Nanoscale Res. Lett.* **9**, 247 (2014).
  47. Tsou, L. K., Jain, R. K. & Hamilton, A. D. Protein surface recognition by porphyrin-based receptors. *J. Porphyr. Phthalocyanines* **08**, 141–147 (2004).
  48. Nanoparticles, A. A. G., You, C., De, M., Han, G. & Rotello, V. M. Tunable Inhibition and Denaturation of  $\alpha$ -Chymotrypsin with Fabrication of Amino Acid-Functionalized Gold Nano-. 12873–12881 (2005).
  49. Gao, W. The chemistry of graphene oxide. *Graphene Oxide Reduct. Recipes, Spectrosc. Appl.* 61–95 (2015).
  50. Jha, A. N., Vishveshwara, S. & Banavar, J. R. Amino acid interaction preferences in proteins. *Protein Sci.* **19**, 603–616 (2010).
  51. Gilles, P., Wenck, K., Stratmann, I., Kirsch, M., Smolin, D. A., Schaller, T., De Groot, H., Kraft, A. & Schrader, T. High-Affinity Copolymers Inhibit Digestive Enzymes by Surface Recognition. *Biomacromolecules* **18**, 1772–1784 (2017).
  52. Ciolkowski, M., Rozanek, M., Bryszewska, M. & Klajnert, B. The influence of PAMAM dendrimers surface groups on their interaction with porcine pepsin. *Biochim. Biophys. Acta - Proteins Proteomics* **1834**, 1982–1987 (2013).
  53. Munro, P. D., Jackson, C. M. & Winzor, D. J. Consequences of the non-specific binding of a protein to a linear polymer: Reconciliation of stoichiometric and equilibrium titration data for the thrombin-heparin interaction. *J. Theor. Biol.* **203**, 407–418 (2000).
  54. Smith, K. & Twyman, L. J. A comparison of dendrimers and hyperbranched polymers for the encapsulation of poorly soluble drugs. **MChem**, (University of Sheffield, 2012).
  55. Ficker, M., Petersen, J. F., Hansen, J. S. & Christensen, J. B. Guest-host chemistry with dendrimers-binding of carboxylates in aqueous solution. *PLoS One* **10**, 1–12 (2015).
  56. Esfand, R. & Tomalia, D. a. Poly(amidoamine) (PAMAM) dendrimers: From biomimicry to drug delivery and biomedical applications. *Drug Discov. Today* **6**, 427–436 (2001).
  57. Tomalia, D. A., Baker, H., Dewald, J., Hall, M., Kallos, G., Martin, S., J. Roeck, J. R. & Smith, P. A New Class of Polymers: Starburst-Dendritic Macromolecules. *Polym. J.*

- 17, 117–132 (1985).
58. Khurana, K. & Twyman, L. J. Exploring a new methodology for drug delivery using non covalent chemistry. (University of Sheffield, 2015).
  59. Chandrudu, S., Simerska, P. & Toth, I. Chemical Methods for Peptide and Protein Production. *Molecules* **18**, 4373–4388 (2013).
  60. Sheehan, J. C. & Hess, G. P. A New Method of Forming Peptide Bonds. *J. Am. Chem. Soc.* **77**, 1067–1068 (1955).
  61. Pande, S. & Crooks, R. M. Analysis of poly(amidoamine) dendrimer structure by UV-Vis spectroscopy. *Langmuir* **27**, 9609–9613 (2011).
  62. Kesharwani, P., Jain, K. & Jain, N. K. Dendrimer as nanocarrier for drug delivery. *Prog. Polym. Sci.* **39**, 268–307 (2014).
  63. Copeland, R. A. A Practical Introduction to Structure, Mechanism, and Data Analysis. in *Analytical Biochemistry* **291**, 278 (Wiley-Blackwell, 2001).
  64. Berg, J., John, M., Tymoczko, L. & Stryer, L. *Biochemistry*. (W.H. Freeman and Company, 2007).
  65. Paul F. Cook, W. W. C. *Enzyme Kinetics and Mechanism*. (Garland Science, 2007).
  66. Garrett, R. H. & Charles M. Grisham. *Biochemistry. Brooks Cole, a division of Cengage Learning . Inc* (2013).
  67. Chiba, F. & Twyman, L. J. Effect of Terminal-Group Functionality on the Ability of Dendrimers to Bind Proteins. *Bioconjug. Chem.* **28**, 2046–2050 (2017).
  68. Wenck, K., Koch, S., Renner, C., Sun, W. & Schrader, T. A noncovalent switch for lysozyme. *J. Am. Chem. Soc.* **129**, 16015–16019 (2007).
  69. Wang, M. & Twyman, L. J. Investigating the Inhibition of Protein-Protein Interactions by PAMAM Dendrimers. (University of Sheffield, 2014).
  70. Morgan, M. T., Nakanishi, Y., Kroll, D. J., Griset, A. P., Carnahan, M. a., Wathier, M., Oberlies, N. H., Manikumar, G., Wani, M. C. & Grinstaff, M. W. Dendrimer-encapsulated camptothecins: Increased solubility, cellular uptake, and cellular retention affords enhanced anticancer activity in vitro. *Cancer Res.* **66**, 11913–11921 (2006).
  71. Yavuz, B., Pehlivan, S. B. & Unlu, N. Dendrimeric systems and their applications in ocular drug delivery. *ScientificWorldJournal.* **2013**, 732340 (2013).
  72. Yung-Chi, C. & Prusoff, W. H. Relationship between the inhibition constant (KI) and the concentration of inhibitor which causes 50 per cent inhibition (I50) of an enzymatic reaction. *Biochem. Pharmacol.* **22**, 3099–3108 (1973).

73. Woody, R. W. & Dunker, A. K. *Aromatic and Cystine Side-Chain Circular Dichroism in Proteins*. (Springer, Boston, MA, 1996).
74. Chiba, F., Mann, G. & Twyman, L. J. Investigating possible changes in protein structure during dendrimer-protein binding. *Org Biomol Chem* **8**, 5056–5058 (2010).
75. Battistuzzi, G., Loschi, L., Borsari, M. & Sola, M. Effects of nonspecific ion-protein interactions on the redox chemistry of cytochrome c. *J. Biol. Inorg. Chem.* **4**, 601–607 (1999).
76. Allhorn, M. & Klapyta, A. Redox properties of the lipocalin a 1 -microglobulin : Reduction of cytochrome c , hemoglobin , and free iron. *Free Radic. Biol. Med.* **38**, 557–567 (2005).
77. Yamaguchi, Y., Kato, N., Azuma, H., Nagasaki, T. & Ohkanda, J. Protein recognition of hetero-/homoleptic ruthenium(II) tris(bipyridine)s for  $\alpha$ -chymotrypsin and cytochrome c. *Bioorg. Med. Chem. Lett.* **22**, 2354–2358 (2012).
78. Yang, D., Shin, J., Choi, M. & De, C. L. Cytochrome c assembly on fullerene nanohybrid metal oxide ultrathin films. *RSC Adv.* **6**, 19173–19181 (2016).
79. Braun, M., Atalick, S., Guldi, D. M., Lanig, H., Brettreich, M., Burghardt, S., Hatzimarinaki, M., Ravanelli, E., Prato, M., Eldik, R. Van & Hirsch, A. Electrostatic Complexation and Photoinduced Electron Transfer between Zn-Cytochrome c and Polymeric Fullerene Dendrimers. *Chem. Eur. J* **9**, 3867–3875 (2003).
80. Chigu, N. L. & Hirosue, S. Cytochrome P450 monooxygenases involved in anthracene metabolism by the white-rot basidiomycete *Phanerochaete chrysosporium*. *Appl. Microbiol Biotechnol* **87**, 1907–1916 (2010).
81. Clark-ferris, K. K. & Fisher, J. Topographical mimicry of the enzyme binding domain of cytochrome c. *J. Am. Chem. Soc.* **107**, 5007–5008 (1985).
82. Aya, T. & Hamilton, A. D. Tetrabiphenylporphyrin-based receptors for protein surfaces show sub-nanomolar affinity and enhance unfolding. *Bioorganic Med. Chem. Lett.* **13**, 2651–2654 (2003).
83. Hamuro, Y., Calama, M. C., Park, H. S. & Hamilton, A. D. A Calixarene with Four Peptide Loops: An Antibody Mimic for Recognition of Protein Surfaces. *Angew. Chemie Int. Ed.* **36**, 2680–2683 (1997).
84. Park, H. S., Lin, Q. & Hamilton, A. D. Protein Surface Recognition by Synthetic Receptors: A Route to Novel Submicromolar Inhibitors for  $\alpha$ -Chymotrypsin. *J Am Chem Soc* **121**, 8–13 (1999).
85. Douglas, R. & John, C. Mitochondria and apoptosis. *Science.* **281**, 1309–1312 (1998).
86. Martos, V., Castreño, P., Valero, J. & de Mendoza, J. Binding to protein surfaces by

- supramolecular multivalent scaffolds. *Curr. Opin. Chem. Biol.* **12**, 698–706 (2008).
87. Zhou, H., Baldini, L., Hong, J., Wilson, A. J. & Hamilton, A. D. Pattern Recognition of Proteins Based on an Array of Functionalized Porphyrins. *J Am Chem Soc* **128**, 2421–2425 (2006).
  88. Crowley, P. B., Ganji, P. & Ibrahim, H. Protein Surface Recognition : Structural Characterisation of Cytochrome c – Porphyrin Complexes. *ChemBioChem* **9**, 1029–1033 (2008).
  89. Jain, R. K. & Hamilton, A. D. Designing Protein Denaturants : Synthetic Agents Induce Cytochrome c Unfolding at Low Concentrations and Stoichiometries. *Angew. Chem. Int. Ed. Engl* **41**, 641–643 (2002).
  90. Parr, G. R. & Robert F. Pasternack. The Interaction of Some Water-Soluble Porphyrins and Metalloporphyrins with Human Serum Albumin. *Bioinorg. Chem.* **7**, 277–282 (1977).
  91. Robert F. Pasternack, Gillies, S. & Julia P. Stromsted. Substitution reactions of a water-soluble metalloporphyrin with azide and 1,1,3,3-tetramethyl-2-thiourea. *Bioinorg. Chem.* **8**, 33–44 (1978).
  92. Paul, D., Miyake, H., Shinoda, S. & Tsukube, H. Proteo-Dendrimers Designed for Complementary Recognition of Cytochrome c : Dendrimer Architecture toward Nanoscale Protein Complexation. *Chem. Eur. J* **12**, 1328–1338 (2006).
  93. Adler, A. D.; Longo, F. R.; Finarelli, J. D.; Goldmacher, J.; Assour, J.; Korsakoff, L. J. Condensation of Pyrrole with Benzaldehyde Under Adler Conditions; Tetraphenylporphyrins. *Org. Chem* **32**, 476–476 (1967).

## **CHAPTER 5**

***An orthogonal supramolecular approach towards protein binding and protein sensing using dendrimers as scaffolds for the non-covalent assembly of binding and sensing groups.***

## 5.0 Abstract

Developing macro-ligands that can interact with the very large binding surfaces of proteins, is a useful strategy for inhibiting unwanted or disease related protein-protein complexes. Although covalently functionalized macromolecules have shown significant promise in this area, they are often difficult to synthesize and functionalize, particularly with respect to controlling the relative position and 3D geometries of binding and targeting groups. In this paper we report a new paradigm towards these aims, through a modularized, non-covalent self-assembly of binding and sensing units within and around an inert dendrimer scaffold. Although embedded within the dendrimer, the binding units are mobile and free to move. As such, when a target protein is added to the solution, the binding units readjust their position to maximize any (cooperative) interactions with the protein's binding surface. This dynamic process is controlled by the protein, as it guides and controls the formation of its own optimized macromolecular ligand. We describe the synthesis of the component parts, along with the assembly process. When binding and "sensor units" are combined and included in the assembly program, binding could also be detected and quantified. Binding and control experiments using unfunctionalized and non-covalently functionalized dendrimers are reported. Although no binding could be detected using the dendrimer, sensing or binding were used alone, very strong binding was observed when all components were used and allowed to self-assemble (the dendrimer, tyrosine functionalized chains and a sensing porphyrin). The resulting complex bound cytochrome-c with a  $K_d$  of 32 nM, as determined using fluorescence titration techniques.

## 5.1 Introduction and Aim

The complexes formed when proteins interact with proteins or other biological macromolecules, play essential roles in all biological processes.<sup>1</sup> Unwanted or uncontrolled interactions, as well as conditions leading to protein mutations, often result in disease.<sup>2</sup> These include neurodegenerative diseases such as Alzheimer's and Huntington's disease.<sup>3</sup> Protein-protein interactions are also involved in viral and bacterial infections. For example, binding between proteins on the surface of bacteria and cells can facilitate internalization (of the bacteria) within the host cell.<sup>4</sup> Using a similar mechanism, it has been demonstrated that viral proteins can bind to host proteins, resulting in internalization and infection.<sup>5</sup> As such, understanding how to modulate or inhibit protein-protein interactions is an emerging concept in drug design.

Proteins recognize each other through complementary functionalities positioned at precise points on large interacting surfaces that can range from 500 Å<sup>2</sup> to 5000 Å<sup>2</sup>; the key component of which is known as the "hot spot" or interfacial area.<sup>6</sup> Therefore one challenge in designing inhibitors is the construction of architectures that are large enough to interact with most, or all, of the interfacial area of a protein.<sup>7</sup> As well as size, an array of non-covalent interactions are also important with respect to an inhibitor's selectivity, including charge/charge, hydrophobic, aromatic/ $\pi$ - $\pi$  interactions and hydrogen bonding.<sup>8</sup> Studies into protein-protein interactions have identified specific amino acids that consistently contribute more than 2 kcal/mol to the binding energy, whilst appearing at the interfacial surface with a frequency greater than 10%.<sup>9</sup>

These amino acids are capable of making multiple interactions and include; tryptophan 21%, arginine 14% and tyrosine 13%. As such, multi/polyvalency, functionality, charge and size are key design determinants with respect to obtaining selective ligands for protein binding. Given these requirements it is not surprising that macromolecular ligands show great promise with regards to protein binding. Examples include calixarene and porphyrin scaffolds,<sup>10,11</sup> nanomaterials,<sup>12</sup> and linear polymers.<sup>13,14</sup>

We have studied the use of dendrimers and functionalized dendrimers as protein binding ligands.<sup>15,16</sup> These macromolecules can be constructed in specific sizes and are capable of binding to a range of protein binding interfacial areas/hot-spots. Our preliminary studies involved a series of negatively charged carboxylate dendrimers designed to interact with proteins possessing positively charged interfacial areas of various sizes. The results revealed that selective binding could be achieved by matching the dendrimer's size/maximum addressable area, with the protein's interfacial or binding area.<sup>15</sup> We then investigated the importance of terminal group functionality on binding affinity using dendrimers functionalized with tyrosine. Binding experiments indicated that the tyrosine dendrimer binds chymotrypsin with an affinity around 30% stronger than an unfunctionalized dendrimer of similar size and charge.<sup>17</sup> These results were extended further, using a porphyrin cored dendrimer whose fluorescence was quenched when bound to cytochrome-c.<sup>18</sup> Overall, these experiments demonstrated the importance of size and functionality when designing macromolecular ligands for selective protein binding. Although these results were successful and demonstrated a clear proof of principle, covalent chemistry is time consuming with respect to incorporation of

specific terminal groups and core functionality. In addition, errors in design or synthesis could not be corrected easily, requiring a new macromolecular/dendrimer ligand to be synthesized. Furthermore, although adding a *single/specific* functional group many times to the surface of the dendrimer is relatively easy (polyvalency), it is extremely difficult to position such moieties in respect to each other with geometric precision. It is even more difficult to add a number of *different* functional groups (multivalency) with control regarding their relative position to each other: Yet, any therapeutically useful macromolecule will require such precision in its design. Towards this aim, we developed a non-covalent methodology for the assembly of targeting and sensing units within and around a dendrimer scaffold. Control over the relative position of targeting groups can be achieved using a target protein as a template, directing formation of an optimized macromolecular protein ligand through various reversible cooperative interactions. In this paper we describe this new methodology and show how non-covalent combinatorial chemistry can be used to simultaneously functionalize a dendrimer with targeting and sensing groups. Through this approach, a dendrimer that cannot intrinsically bind or interact with a protein, can be used as a scaffold to support various binding and sensing components within and around their structure.

## 5.2 Results and Discussion

### 5.2.1 Design and synthesis of materials.

The new approach uses non-covalent chemistry to assemble an optimized macromolecular ligand around a protein template. The design and methodology is shown schematically in Figure 1. The dendrimer, its binding units and a sensing component are added to water, where they can assemble into the random complex **1**. When a protein is added, the randomly distributed binding units are free to move within the dendrimer and maximize any cooperative protein-binding interactions. Binding can then be detected and quantified via perturbation of an encapsulated sensing group's photophysical properties.

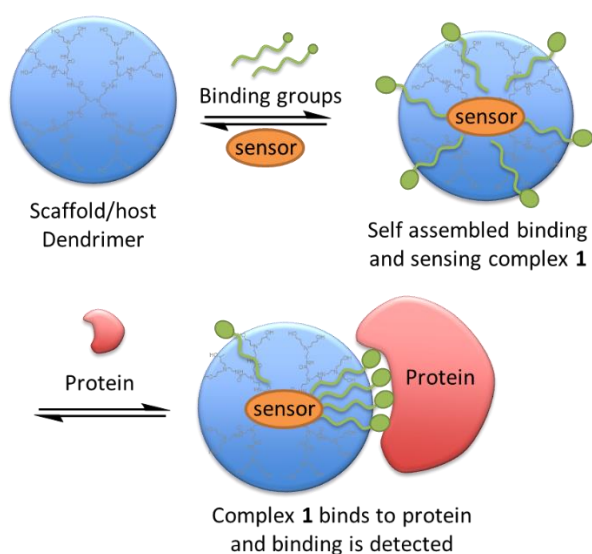


**Figure 1:** Schematic showing the proposed self-assembled protein binding complex **1** and its binding to a target protein. A neutral/non-binding dendrimer acts as a scaffold to support and encapsulate the binding and sensing units. The use of non-covalent chemistry allows the targeting groups to move and maximize their binding efficiency in the presence of a target protein.

This design concept requires three separate components as shown in Figure 2. With respect to the dendrimer, it must be water-soluble, to ensure that the protein and the assembled ligand are in the same aqueous phase. In addition, the dendrimer's terminal groups must be neutral and inert. This is vitally important, as the dendrimer must not react, bind or interact in any way with the protein's binding surface (in the absence of any encapsulated functionality). Additionally, the dendrimer needs to be large enough to address the full size of the target protein's binding/interfacial area, whilst also ensuring that incorporation of the binding/sensing units are not prevented or limited by a dense shell or dense packed structure.<sup>19,20</sup> For this work we selected cytochrome-c as the target protein. The structure of this protein is well known, having a binding interface (hot-spot) around 1100 Å<sup>2</sup> in size.<sup>21</sup> As such, the neutral G3.5 PAMAM dendrimer **2**, with 32 terminal OH groups<sup>22</sup> and a maximum addressable area around 1200 Å<sup>2</sup> was selected as the scaffold unit.<sup>23,15</sup>

The second component, is the targeting or binding units that will be encapsulated/incorporated within the dendrimer's interior. A cooperative combination of hydrophobic, electrostatic and H-bonding interactions were chosen to drive encapsulation. To achieve this, a series of hydrophobic oligomeric amide chains, terminated with an amino acid (the binding functionality) were selected. For this proof of principle work, tyrosine terminated chains **22** and **26**, with 2 or 3 hydrogen bonding groups were selected as the binding/recognition motif and valine terminated chains **24** and **28** selected as controls. These amino acids are known respectively to contribute significantly well, or extremely poorly, to protein-protein interactions.<sup>9</sup> The oligomeric amide chains were synthesized from propyl amine and the stepwise addition of two β-alanine repeat units. The protected amino acids were then added,

giving the final amide linked linear chains, LC-Tyr **22/26** and LC-Val **24/28**, after a simple deprotection step, Figure 53.

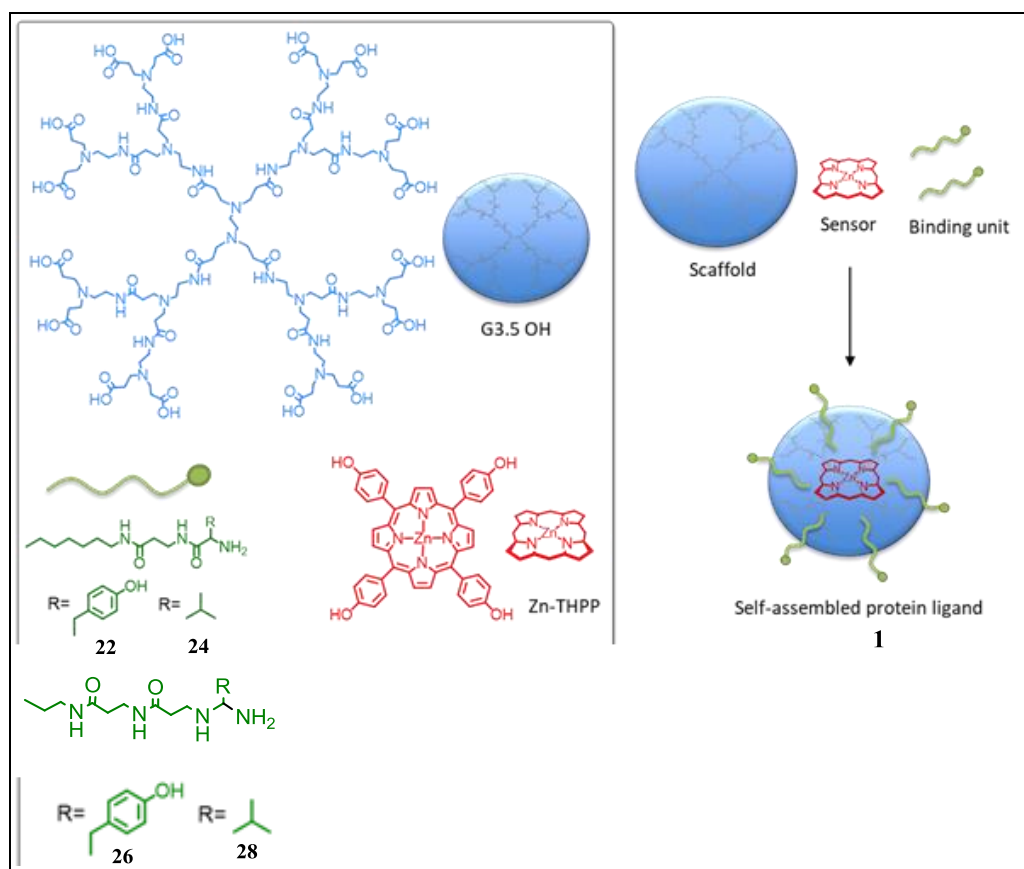


**Figure 53:** The three components involved in formation of the self-assembled macromolecular protein ligand **1**.

The final component of the self-assembled system **1** is simple porphyrin that can be used as the sensing/detection unit. As well as possessing a well-characterized binding area and a size compatible with the scaffold dendrimer **10**, cytochrome-c is a porphyrin containing protein that emits a strong fluorescence signal that can be perturbed by a bound quencher. This property can be exploited to detect and quantify binding using a hydrophobic quencher encapsulated

within the interior of the dendrimer. It is essential that this quencher does not bind to the protein independently and is retained within the dendrimer. As such, zinc-tetra-4-hydroxyphenyl porphyrin **29** (Zn-THPP) was selected as the internal quencher. Zn-THPP **29** is hydrophobic and although it is almost insoluble in water,<sup>24</sup> it can be encapsulated within the dendrimer using simple hydrophobic interactions.<sup>25</sup> In addition, porphyrin **29** has a central metal that can coordinate to the dendrimer's internal amines. Porphyrin **29** also has four phenolic OH groups that can hydrogen bond to the dendrimers amides. In addition, the OH groups are acidic enough to be deprotonated by the internal amines, resulting in additional electrostatic interactions.<sup>25</sup> As such, there are a number of cooperative interactions that will help ensure porphyrin **29** stays encapsulated within the scaffold dendrimer **10**. Zn-THPP **29** was obtained easily in three steps, starting from 4-methoxybenzaldehyde and pyrrole.

### **5.2.3 Encapsulation and self-assembly of protein binding units.**

Encapsulation of the linear chains and the sensor unit within the G 3.5-OH dendrimer **10**, was achieved using a procedure similar to that used to solubilize and encapsulate hydrophobic drugs within water soluble PAMAM dendrimers.<sup>25</sup> For the linear chains, 10 equivalents of **22/26** or **24/28** were added to methanolic solutions of dendrimer **10**. The methanol was removed and a known volume of buffer (0.01M PBS, pH 7.4) was added, to give a final dendrimer concentration of  $1 \times 10^{-6}$  M. The solution was then filtered to remove any undissolved material. Beer Lambert analysis confirmed that all 10 linear chains had been encapsulated, giving a final concentration of  $1 \times 10^{-5}$  M for 3HBLC-Tyr **26** and 3HBLC-Val **28**. This is higher than the solubility of either linear chain without the dendrimer ( $0.51 \times 10^{-5}$  M for 3HBLC-Tyr **26** and

$0.58 \times 10^{-5}$  M LC-Val **4**). Furthermore, a 5 nanometre bathochromic shift was observed in  $\lambda_{\max}$  when either LC-Tyr **22/26** or LC-Val **24/28** were encapsulated within the dendrimer as shown in Figure 54 and in Figure 55, respectively.

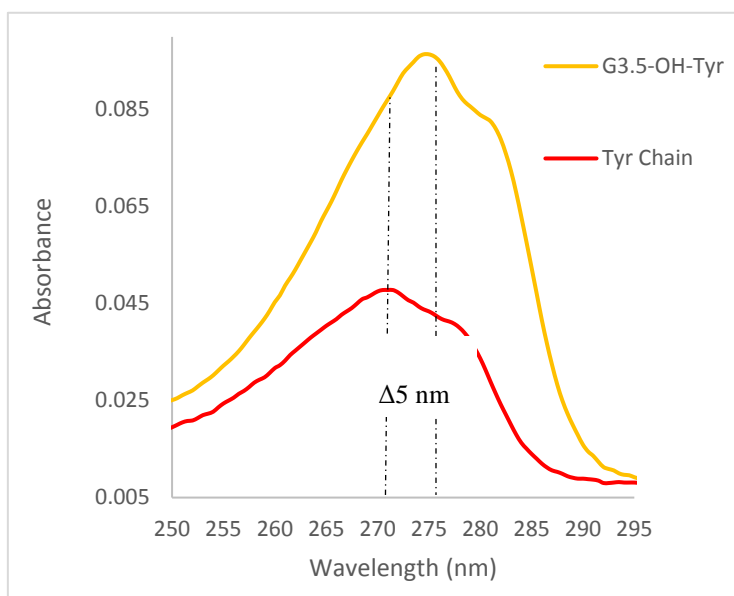


Figure 54: UV spectra (buffer-pH 7.4) of the free and encapsulated 3HBLC-Tyr **26** chain

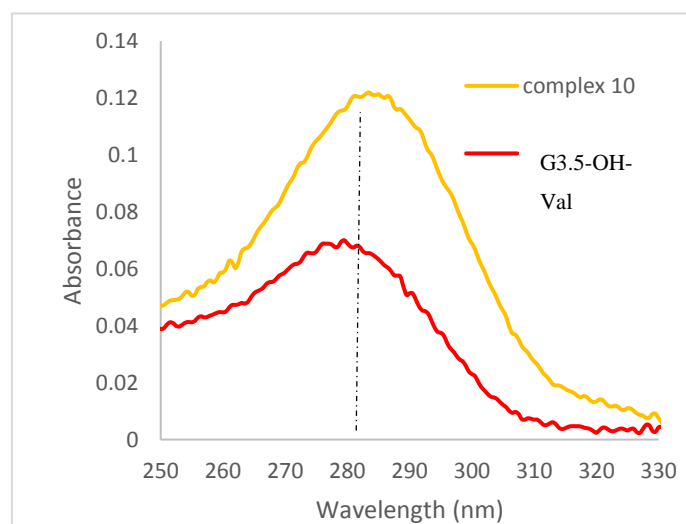
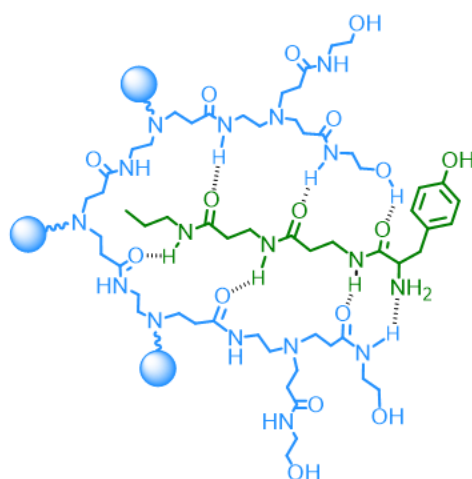


Figure 55: UV spectra (buffer-pH 7.4) of the free and encapsulated 3HBLC-Val **28** chain

This shift is consistent with a change in environment, as the water solvating the linear chains is replaced by the dendrimer's interior groups. For the 3-H bonded systems, the solubility and spectroscopic data confirmed that all 10 linear chains were encapsulated within the dendrimer. For the 2-H bonded system, spectroscopic data revealed that between 5 and 6 chains had been encapsulated. Again, encapsulation was demonstrated and confirmed by shifts in  $\lambda_{\text{max}}$ . It is assumed that the driving force for complexation was a cooperative process involving hydrophobic and H-bonding interactions, Figure 56. The methodology is similar to that used by Meijer to construct dendrimer complexes that could aggregate on dilution.<sup>26</sup>



**Figure 56:** Schematic showing a segment of the G3.5-OH dendrimer **10** and possible H bonding motif to the linear chain, 3HBLC-Tyr **26**.

A similar procedure was used to encapsulate the porphyrin-signalling unit Zn-THPP **5**. In this case, one equivalent of Zn-THPP **29** was added with respect to dendrimer. Concentration was determined by UV,<sup>27</sup> which confirmed a 1:1 stoichiometry for the Zn-THPP/dendrimer complex. UV analysis of the complex also indicated a change in the porphyrin's Soret band,

which shifted from 412 nm to 425 nm. This shift is a characteristic of complexation (between Zn and the dendrimer's internal nitrogens) and confirms encapsulation within the dendrimer. Having established and quantified encapsulation of the various components, the next step involved a series of binding experiments to test whether or not the self-assembled complex could bind to cytochrome-c and be detected.

#### **5.2.4 Protein interaction and quantification of binding affinities for the 2-H bonding system.**

Protein binding experiments were attempted using the 2-H bonding system. Titrations using the same methods described above, did not show any changes in intensity for the porphyrin emission peak when the dendrimer/LC complex was added. As such, the 2-H bonding systems do not appear to bind.

#### **5.2.5 Protein interaction and quantification of binding affinities for the 3-H bonding system.**

Binding experiments were carried out on the 3-H bonding system at pH 7.4 by titrating solutions of cytochrome-c into a solution of the dendrimer complex **1** assembled from all three components in a 1:1:10 ratio for dendrimer **10**, Zn-THPP **29**, and linear chain **26** or **28** respectively ( $1 \times 10^{-6}$  M for dendrimer and Zn-THPP and  $1 \times 10^{-5}$  M for linear chain). Detection and quantification of binding was observed by following changes in the intensity of the Zn-THPP **29** emission band at 610 nm, which is quenched if cytochrome-c binds.<sup>15</sup> Our initial experiments involved the 3HBLC-Tyr **26** dendrimer complex **1**. As increasing amounts of

cytochrome-c were added, a significant reduction in the emission peak at 610 nm was observed, indicating protein binding.

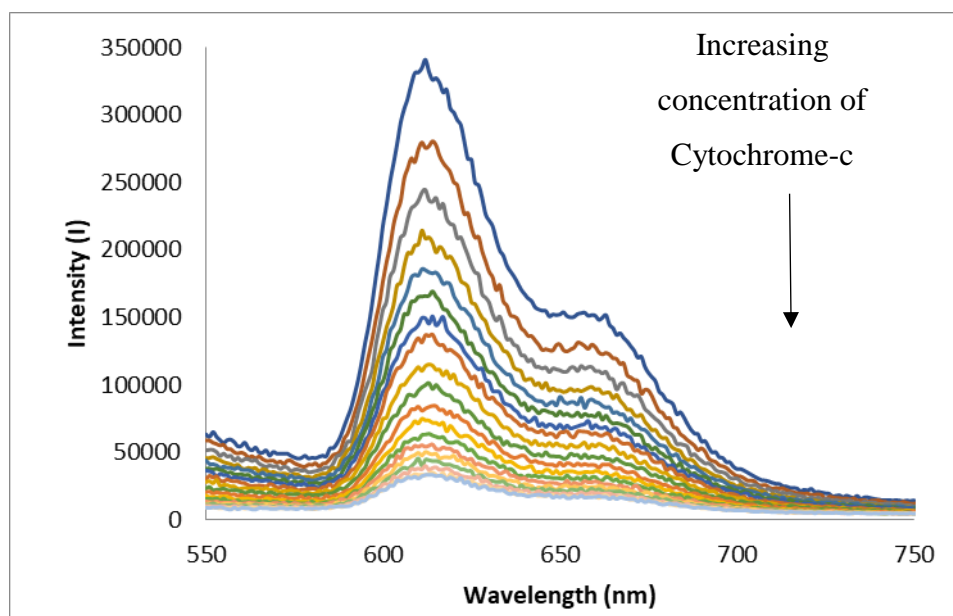


**Figure 57:** Emission spectra reduced after addition of each aliquot of a 1.0  $\mu\text{M}$  Cyt-c to a solution of the G3.5-OH complex **1** (1.0  $\mu\text{M}$  in dendrimer **10** and ZnTHPP **5**, and 10.0  $\mu\text{M}$  in 3HBLC-Tyr **26**).

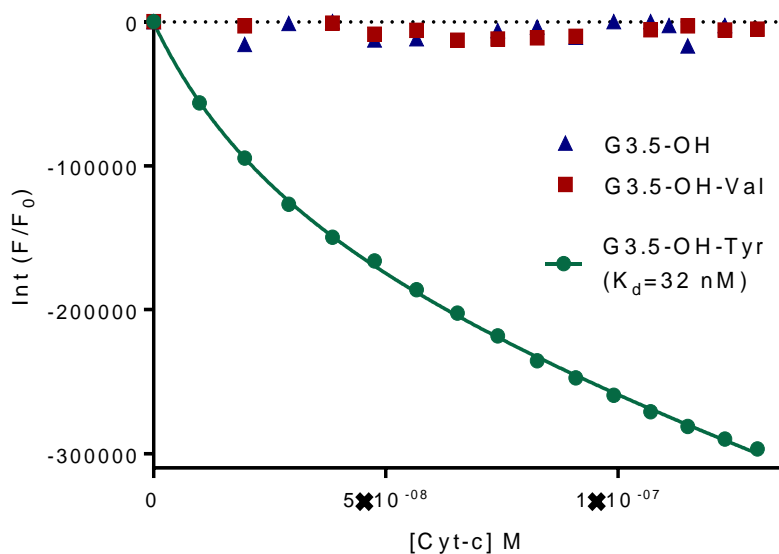


**Figure 58:** Titration plots showing changes of intensity for the Zn-THPP **29** peak at 615 nm when cytochrome-c was added (excitation at 410 nm).

The change in intensity vs cytochrome-c concentration was plotted and the data fitted to a 1:1 binding model (Graphpad) and a dissociation constant ( $K_d$ ) of 32 nM was obtained, (Figure 58).

Despite the fact that our self-assembled system does not possess any negative charges, that could interact with cytochrome-c's positive rich surface (and strengthen the overall interaction), binding was comparable to data reported for other surface binding ligands and cytochrome-c. For example, Hamilton reported  $K_d$  values between 120 and 20 nM for various porphyrins possessing up to 8 terminal negative charges.<sup>28</sup> Similarly, Wilson observed dissociation constants ranging from 23 to 2 nM for a series of metal ligands, again possessing a number of terminal negative charges.<sup>29</sup> Therefore, as our system does not possess any negative charges, binding must come from other features that combine cooperatively to give the high binding affinity observed. These include  $\pi$ - $\pi$  stacking, hydrogen bonding and

hydrophobic interactions from the tyrosine linear chain, as well as the possibility of additional hydrogen bonds from the dendrimer.

The experiments were then repeated using a dendrimer complex containing the linear chain functionalized with valine (3HBLC-Val **28**), an amino acid not normally associated with protein-protein binding.<sup>9</sup> On this occasion, the intensity of the porphyrin fluorescence did not change as cytochrome-c was titrated into the dendrimer complex, indicating that binding did not take place, Figure 58. The concentration of cytochrome-c was increased, but again no reduction in porphyrin intensity was observed. As valine is *not* favoured with respect to surface protein binding, this result was expected. However, the result represented a useful control that confirms the orientation of the amino acid chains within the dendrimer. Specifically, that the tyrosine head groups point out from the dendrimer when binding to the protein surface, as shown schematically in Figure 59(a). If this were not the case and the tyrosine and valine head groups were buried within the dendrimer, then both linear chains (LC-Tyr and LC-Val) would present the same functionality at the dendrimer surface, as shown schematically in Figure 5 (b). This would result in an identical dissociation constant being determined for 3HBLC-Tyr **26** and 3HBLC-Val **28**, which was *not* the case.

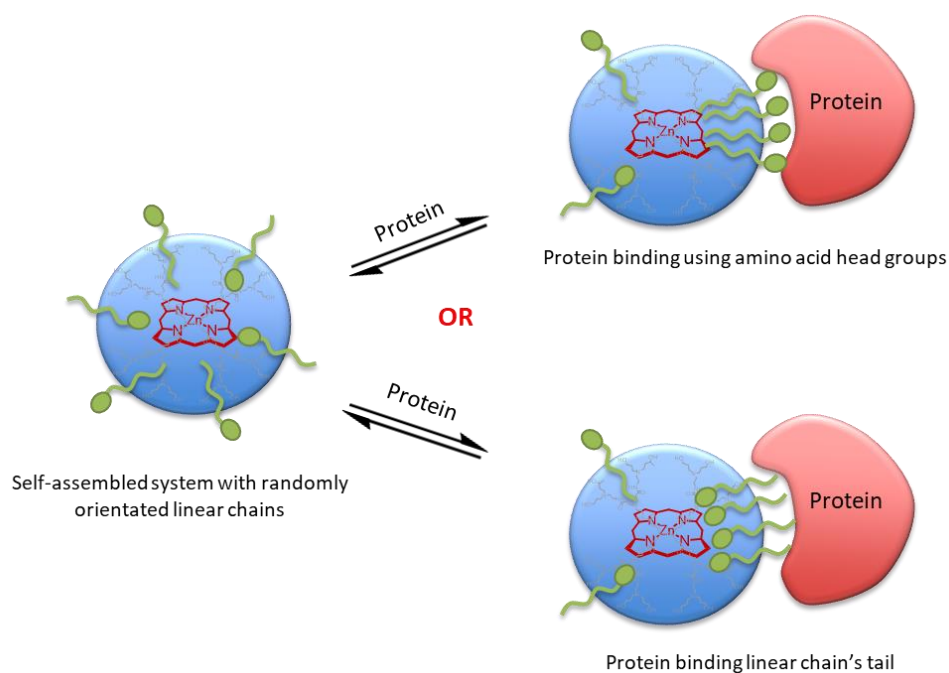


**Figure 59:** There are two extreme binding orientations possible for the linear chains. (a) All of the head groups pointing out enabling interaction with the protein surface. If this occurs, then binding will be different for different head groups (observed). (b) An alternative orientation with the tails pointing out, which then bind to the protein surface. If this occurs, then binding would be identical for different head groups (not observed).

## 5.2.6 Control experiments

A series of additional controls were carried out to confirm that binding was taking place via the self-assembled process shown in Figure 60. These included the addition of cytochrome-c to a solution of a dendrimer-porphyrin complex (no linear chains), which showed no change in the porphyrin emission intensity, and therefore no binding, Figure 60(a). A control using just Zn-THPP **29** was difficult, due to its lack of solubility. However, a saturated solution showed a very weak emission that was not quenched when cytochrome-c was added, confirming that the porphyrin did not bind independently to the protein, Figure 60 (b). A final control using the tyrosine or valine linear chain (3HBLC-Tyr **26** or 3HBLC-Val **28**) dissolved in the saturated

Zn-THPP **29** solution, did not show any evidence of quenching or bonding when cytochrome-c was added, Figure 60 (c).

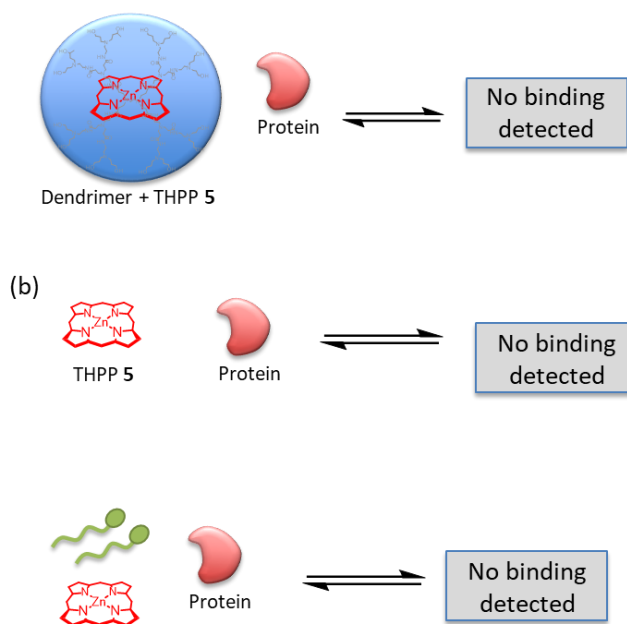


**Figure 60:** Control experiments indicated that binding was not detected when the experiments were carried out without the linear chains (a), or without dendrimer, (b) and (c).

### 5.3 Conclusions

In conclusion, we have demonstrated a macro supramolecular methodology that has the potential to generate new ligands that can bind selectively or specifically to the large interfacial binding areas found on the surface of target proteins. Although covalently functionalized macromolecules showed promise in this area, it can be difficult to functionalize their surfaces and impossible to control their relative position with respect to any 3 dimensional geometric requirements (of the functional groups).

To overcome these problems, we developed a supramolecular methodology for the construction of macromolecular protein ligands that can bind *and* detect proteins. The methodology involved a dendrimer scaffold that could support a targeting/binding group, as well as a sensing groups via encapsulation. Encapsulation was achieved through a combination of hydrophobic, electrostatic and hydrogen bond interactions. Specifically, linear amide chains terminated with tyrosine and valine (amino acids known respectively to contribute significantly or poorly to protein-protein binding affinities). Self-assembled complexes were constructed using a 10:1 ratio of the linear chains and dendrimer. Encapsulation resulted in an increase in the linear chain's aqueous solubility and complexation was confirmed through UV, which indicated a 5 nm bathochromic shift in the linear chains  $\lambda_{\max}$ .

Complexes containing the targeting groups and a sensing unit were obtained by adding a hydrophobic, insoluble porphyrin (1 equivalent with respect to dendrimer). UV analysis indicated that the porphyrin was soluble and that encapsulation was successful. Protein binding was subsequently assessed using cytochrome-c as a test protein, which was titrated into solutions of the porphyrin/dendrimer complexes, containing either valine or tyrosine. Two

linear chain systems were analysed, specifically linear chains with 2 or 3 H bonding groups. No binding was observed for the 2-H bonding system, but better results were obtained for the 3-H bonding. This is due to the stronger overall binding possible for the system with more H-bonding interactions.

Although the valine complex did not show any binding for the 3-bonding system, the tyrosine complex bound the protein with a very strong affinity, giving an binding constant of  $3.13 \times 10^8 \text{ M}^{-1}$  ( $K_d = 32 \text{ nM}$ ). Control experiments using a dendrimer/porphyrin complex without linear chains showed no evidence of binding. Similar results were obtained for controls involving, the (dilute) porphyrin, the linear chains or solutions of the porphyrin and linear chains. The methodology described is essentially modular in approach, which means that the same scaffold can be used to bind and sense a number of different proteins and only the binding and/or sensing components need to be changed. Alternatively, the same binding and/or sensing units can be used with a variety of dendrimers of differing size and/or sensing units. Therefore, this method will allow libraries of dendrimer scaffolds, binding groups and sensing units to be prepared, which can then be combined in an almost infinite array to target many different types of protein. As well developing methods to fix or trap the linear chains within the dendrimer, future experiments will also involve combining a number of different targeting groups and studying a variety of additional proteins.

## 5.4 Experimental

**Materials.** All reagents and solvents were obtained from commercial sources (primarily Sigma- Aldrich) and were used without further purification. Dry solvents were obtained from the University of Sheffield Chemistry Department Grubbs solvent dispensing system. All glassware was cleaned and dried in an oven overnight (100 °C) before use.

**UV Spectrophotometry.** Absorbance was recorded on an Analytic Jena AG Specord s600 uv/vis spectrometer and analyzed using WinASPECT. **Infra-red spectroscopy.** IR spectra were recorded using a Perkin-Elmer UATR Infrared spectrometer. Spectra were analyzed with Spectrum100 software and positions of peaks are stated as wave numbers ( $\text{cm}^{-1}$ ). **Fluorescence spectroscopy** Emission was recorded on a Perkin Elmer Fluoromax-4 Spectrofluorometer at 25 °C, Spectra were analyzed with FluorEssence V3software. **NMR Spectroscopy.** All NMR samples were prepared using deuterated solvents supplied by Sigma Aldrich.  $^1\text{H}$  NMR and  $^{13}\text{C}$  NMR spectra were recorded using a Bruker AV1400 MHz machine. Chemical shifts are quoted using ppm, coupling constants are quoted in Hertz referenced to residual solvent signals. The NMR spectra were analyzed using Topspin 3.0 NMR software. **Mass Spectrometry.** For dendrimers, a Bruker reflex III MALDI-ToF mass spectrometer was used. For all other samples, a Waters LCT Premier XE spectrometer, and Electrospray Ionization (ES) was used. High Resolution Agilent 6530 Accurate-Mass Q-TQF LC/MS was used.

## 5.4.1 Synthesis of PAMAM dendrimer

### G0.5 PAMAM dendrimer 1

Instead of the full generation dendrimer, a mixture of ethylenediamine (EDA; 10 mL, 0.15 mol), methyl acrylate (57 mL, 0.63 mol) and methanol (50 mL) was stirred for 24 h according to the standard protocol for the synthesis of the half-generation dendrimer (G0.5 PAMAM). The mixture was then washed as described above to obtain the desired product in the form of a yellow oil (64.0 g, 106 % residual solvent). The product was characterised as follows:

FTIR ( $\nu_{\max}/\text{cm}^{-1}$ ): 2952, 2826, 1730, 1170 ;  $^1\text{H}$  NMR (400 MHz, MeOD): 2.48 (8H, *t*, J 7.0), 2.54 (4H, *s*), 2.78 (8H, *t*, J 7.0), 3.68 (12H, *s*);  $^{13}\text{C}$  NMR (400 MHz, MeOD): 32.0, 49.5, 51.6, 50.7, 173.3; MS (ES), Calculated for  $\text{C}_{18}\text{H}_{32}\text{N}_2\text{O}_8 = 405$  ( $\text{MH}^+$ ) found 405

### G1.0 PAMAM dendrimer 2

A mixture of the G0.5 PAMAM dendrimer (53.0 g, 0.13 mol), EDA (175 mL, 2.6 mol) and methanol (230 mL) was stirred for 4 days according to the standard protocol for the synthesis of the full generation dendrimer. The mixture was then washed as described above to obtain the desired product in the form of a sticky, viscous, dark amber oil (70.9 g, 106% residual solvent). The product was characterised as follows:

FTIR ( $\nu_{\max}/\text{cm}^{-1}$ ): 3276, 2926, 2816, 1635, 1547, 1029  $\text{cm}^{-1}$ ;  $^1\text{H}$  NMR (400 MHz, MeOD): 2.39 (8H, *t*, J 7.0), 2.56 (4H, *s*), 2.73 (8H, *t*, J 6.0), 2.78 (8H, *t*, J 7.0), 3.27 (8H, *t*, J 6.0), 3.37 (4H, *s*);  $^{13}\text{C}$  NMR (400 MHz, MeOD): 33.3, 41.6, 49.9, 51.0 MS (ES), Calculated for  $\text{C}_{22}\text{H}_{48}\text{N}_{10}\text{O}_4 = 516$  ( $\text{MH}^+$ ) found 516

### G1.5 PAMAM dendrimer 3

A mixture of the G1.0 PAMAM dendrimer (38.5 g, 0.07 mol), methyl acrylate (107 mL, 1.18 mol) and methanol (350 mL) was stirred for 48 h according to the standard protocol for the synthesis of the half-generation dendrimer. The mixture was then washed as described above to obtain the desired product in the form of a brown oil (74.4 g, 88%). The product was characterised as follows:

FTIR ( $\nu_{\max}/\text{cm}^{-1}$ ): 3300, 2951, 2826, 1731, 1643, 1534, 1034;  $^1\text{H}$  NMR (400 MHz, MeOD): 2.41 (8H, t, J 7.0), 2.48 (16H, t, J 7.0), 2.57 (8H, t, J 6.5), 2.63 (4H, s), 2.80 (24H, m), 3.27 (8H, t, J 6.5), 3.37 (4H, s), 3.69 (24H, s);  $^{13}\text{C}$  NMR (400 MHz, MeOD): 50.8, 52.3, 50.9, 49.8, 37.1, 33.2, 173.3; MS (ES), Calculated for  $\text{C}_{54}\text{H}_{96}\text{N}_{10}\text{O}_{20} = 1205$  ( $\text{MH}^+$ ) found 1206

#### **G2.0 PAMAM dendrimer 4**

A mixture of the G1.5 PAMAM dendrimer (63.7 g, 0.053 mol), EDA (283 mL, 4.23 mol) and methanol (250 mL) was stirred for 7 days according to the standard protocol for the synthesis of the full-generation dendrimer. The mixture was then washed to obtain the desired product in the form of a viscous, sticky, dark amber oil (86.7 g, 114% residual solvent). The product was characterised as follows: FTIR ( $\nu_{\max}/\text{cm}^{-1}$ ): 2916, 2811, 1635, 1530, 1030;  $^1\text{H}$  NMR (400 MHz, MeOD): 2.39 (24H, t, J 6.5), 2.60 (12H, m), 2.75 (16H, t, J 6.5), 2.82 (24H, tr, J 7.0), 3.27 (24H, t, J 6.5), 3.37 (12H, s);  $^{13}\text{C}$  NMR (400 MHz, MeOD): 52.1, 49.8, 41.6, 40.7, 37.3, 33.4, 33.2, 173.8, 173.4; MS (ES), Calculated for  $\text{C}_{62}\text{H}_{128}\text{N}_{26}\text{O}_{12} = 1429$  ( $\text{MH}^+$ ) found 1430

#### **G2.5 PAMAM dendrimer 5.**

A mixture of the G2.0 PAMAM dendrimer (52.0g, 0.036 mol), methyl acrylate (105 mL, 1.16 mol) and methanol (350 mL) was stirred for 72 h according to the standard protocol for the synthesis of the half-generation dendrimer. The mixture was then washed to give the desired product in the form of a viscous, brown oil (87.3 g, 86 %). The product was characterised as follows: FTIR ( $\nu_{\max}/\text{cm}^{-1}$ ): 3292, 2818, 1731, 1643, 1534;  $^1\text{H}$  NMR (400 MHz, MeOD): 2.40 (24H, J 7.0), 2.49 (32H, t, J 7.0), 2.61 (28H, m), 2.82 (56H, m), 3.28 (24H, t, J 6.5), 3.37 (12H, s), 3.69 (48H, s);  $^{13}\text{C}$  NMR (400 MHz, MeOD): 50.8, 52.4, 52.1, 49.7, 48.5, 37.3, 37.1, 33.4, 33.2, 32.2, 173.3; Calculated for  $\text{C}_{126}\text{H}_{224}\text{N}_{26}\text{O}_{44} = 2807$  ( $\text{MH}^+$ ) found 2808

#### **G3.0 PAMAM dendrimer 6**

A mixture of the G2.5 PAMAM dendrimer (44.1 g, 0.0157 mol), EDA (2.51 mol, 168 mL) and methanol (200 mL) was stirred for 6 days according to the standard protocol for the synthesis of the full-generation dendrimer. The mixture was then washed to give the desired

product in the form of a sticky, viscous, dark amber oil (51.3 g, 100%). The product was characterised as follows: FTIR ( $\nu_{\max}/\text{cm}^{-1}$ ): 3275, 3070, 2929, 2819, 1634, 1544, 1031;  $^1\text{H}$  NMR (400 MHz, MeOD): 2.39 (56H, t, J 6.5), 2.60 (28H, m), 2.74 (24H, t, J 6.5), 2.81 (56H, t, J 6.5), 3.27 (56H, t, J 6.5), 3.37 (28H, s);  $^{13}\text{C}$  NMR (400 MHz, MeOD): 52.1, 49.7, 41.7, 40.7, 37.2, 33.4, 173.7, 173.3; Calculated for  $\text{C}_{142}\text{H}_{288}\text{N}_{58}\text{O}_{28}$  3256 ( $\text{MH}^+$ ) found 3257

## 5.5 Synthesis of Functionalised PAMAM

### PAMAM G3.5-OH dendrimer

A PAMAM G3.5 dendrimer (11.08g, 1.84 mmol) with 32 terminal methyl ester groups was dissolved in 8 mL of anhydrous DMSO containing potassium carbonate (9.00 g, 66 mmol). Ethanolamine (4.42 g, 72 mmol) was added and the mixture stirred and heated at 50 °C for 72 hours. The crude product was filtered under reduced pressure to remove the solid residues and the solution transferred to a large conical flask. Acetone (600 mL) was added and the crude product formed a thick oil/paste at the bottom of the flask. The acetone was decanted off carefully and enough distilled water added to dissolve the product (5 mL). The product was precipitated using the minimum amount of acetone and allowed to settle. The initial solid product proved to be hygroscopic and quickly became a paste when left. The acetone was decanted off and the precipitation procedure repeated once more. The product was dissolved in methanol and transferred to a round bottomed flask, where the solvents were removed under vacuum to give the final PAMAM-G3.5 OH dendrimer as a pale yellow/cream paste in 90%. FTIR ( $\nu_{\max}/\text{cm}^{-1}$ ), 3265, 3072, 2918, 2826, 1640, 1549;  $^1\text{H}$  NMR (400 MHz,  $\text{D}_2\text{O}$ ), 3.56 (62H, t, J 7.0), 3.25 (120H, m), 2.75 (120H, m), 2.55 (60H, t, J 7.0), 2.36 (120H, m);  $^{13}\text{C}$  NMR (100 MHz,  $\text{D}_2\text{O}$ ), 175.1, 174.5, 61.5, 60.0, 52.0, 49.0, 44.0, 42.0, 37.0, 33.0; MS (ES), Calculated for  $\text{C}_{302}\text{H}_{576}\text{N}_{90}\text{O}_{92}$  [ $\text{MH}^+$ ]: 6941, found 6491.

### 5.5.1 Synthesis of two hydrogen bonding linear chain.

#### Boc- $\beta$ -alanine 12

$\beta$ -alanine (6.06 g, 0.067 mol) was dissolved in 120 mL of 1:2 1M NaOH:THF and acetic anhydride (14.77 g, 0.067 mol) was added to form a cloudy solution. This was stirred at room temperature for 22 h, then concentrated under vacuum prior to the addition of 100 mL each of water and diethyl ether. The solution was then acidified with 4M aqueous HCl (pH 1.7) to obtain a precipitate, followed by the addition of diethyl ether (100 mL) and washing twice with water (100 mL) and twice with brine (175 mL). The organic layer was collected and dried over magnesium sulphate prior to filtration and vacuum concentration to obtain a clear, viscous oil. Finally, this was allowed to stand overnight under ambient air to obtain the white solid (6.46 g, 50 %). The product was characterised as follows

FTIR ( $\nu_{\max}/\text{cm}^{-1}$ ) 3440, 1704;  $^1\text{H}$  NMR (400 MHz,  $\text{CDCl}_3$ ): 3.44 (2H, t, J 6.7), 2.54 (2H, t, J 6.7), and 1.43 (9H, s);  $^{13}\text{C}$  NMR (400 MHz,  $\text{CDCl}_3$ ):  $\delta$  = 34.3, 156.2, 28.2, 28.2, 28.2 175.2, 80.4, and 36.3; MS (ES), Calculated 188 [MH<sup>+</sup>] found 212.1 (MNa<sup>+</sup>) and 188.1 (MH<sup>+</sup>).

#### Boc-protected of amide 13

Heptylamine (1.5 ml, 0.010 mol), triethylamine (0.020 mol, 2.8 ml), 4-Dimethylaminopyridine (DMAP, 1.479 g, 0.012 mol) and 1-ethyl-3-(3-dimethylaminopropyl)carbodiimide (EDC) hydrochloride (2.320 g, 0.012 mol) were added to a solution of Boc-  $\beta$ -alanine (1.91 g, 0.010 mol) in dichloromethane (DCM, 100 mL) to obtain a clear, colourless solution. After stirring for 24 h at room temperature, the solution was washed, dried, and allowed to stand overnight under ambient air to obtain a white powder (0.775 g, 27 %). The product was characterised as follows:

FTIR ( $\nu_{\max}/\text{cm}^{-1}$ ): 3332, 1718, 1680;  $^1\text{H}$  NMR (400 MHz,  $\text{CDCl}_3$ ): 3.44 (2H, t, J 6.0), 3.38 (2H, t, J 7.0), 2.42 (2H, triplet, J 6.5), 1.49 (2H, m), 1.45 (9H, s), 1.32 (8H, m), 0.95 (3H, t, J 7.0), 5.20 (1H, s), 5.70 (1H, s);  $^{13}\text{C}$  NMR (400 MHz,  $\text{CDCl}_3$ ): 39.3, 80.4, 27.2, 37.2, 32.4, 29.0, 28.2, 28.2, 28.2, 156.2, 35.3, 29.41, 22.6, 168.7 and 14.0; (LC-MS): calculated for  $\text{C}_{15}\text{H}_{30}\text{N}_2\text{O}_3$  286, found 309.3 [MNa<sup>+</sup>].

### Deprotected Amide chain 14

Trifluoroacetic acid (TFA; 5 mL, 0.066 mol) was added to a solution of **13** (0.645 g, 0.0023 mol) in DCM (6.4 mL) and stirred for 23 h to obtain a clear, yellow solution. The TFA and solvent were then removed to give a viscous orange oil (1.027, 240 % residual solvent). The product was characterised as follows:

FTIR ( $\nu_{\max}/\text{cm}^{-1}$ ): 3332 1689 ;  $^1\text{H}$  NMR (400 MHz,  $\text{CDCl}_3$ ): 3.18 (2H, t, J 7.4), 2.83 (2H, t, J 6.6), 2.24 (2H, t, J 6.6), 1.69 (2H, m), 1.30 (8H, m), 0.90 (3H, t, J 7.0);  $^{13}\text{C}$  NMR (400 MHz,  $\text{CDCl}_3$ ): 14.0, 168.7, 32.4, 34.7, 40.1, 29.0, 27.2, 39.3, 29.4 and 22.6; (LS-MS): calculated for  $\text{C}_{10}\text{H}_{22}\text{N}_2\text{O}$  186, found 187 [ $\text{MH}^+$ ]

### Boc-tyrosine linear chain 21

From the deprotected of amide **14** (1.0 g, 4.98 mmol), Boc-tyrosine-OH (1.4 g, 4.98 mmol), EDC hydrochloride (0.78 g, 4.0 mmol), DMAP (1.21 g, 9.96 mmol) and triethylamine (1.52 g, 0.015 mol). The crude product (a pale-yellow solid) was purified by silica chromatography using a DCM/1% MeOH eluent to obtain the desired product in the form of a white powder (1.5 g, 71%). The product was characterised as follows:

FTIR ( $\nu_{\max}/\text{cm}^{-1}$ ), 3305, 2968, 2950, 2878, 1688, 1645, 1502,  $^1\text{H}$  NMR (400 MHz,  $\text{CDCl}_3$ ): 7.12 (2H, m, J 8.0), 6.71 (2H, m, J 8.0), 4.72 (1H, t, J 6.5), 3.65 (2H, q, J 7.5), 3.36 (2H, m), 3.26 (2H, m), 2.48 (2H, t, J 6.5), 1.56 (3H, t, J 7), 1.45 (9H, s), 1.28 (8H, m), 0.90 (3H, triplet, J 7.0);  $^{13}\text{C}$  NMR (400 MHz,  $\text{CDCl}_3$ ): 172.7, 168.7, 157.8, 155.3, 130.4, 130.4, 128.9, 115.7, 115.7, 80.4, 55.8, 39.3, 38.4, 36.4, 35.2, 32.4, 29.4, 29.0, 28.2, 28.2, 28.2, 27.2, 22.6 and 14.0. (LS-MS): calculated for  $\text{C}_{24}\text{H}_{39}\text{N}_3\text{O}_5$  450, found 449 [ $\text{MH}^+$ ]

### Deprotected tyrosine 2HB-LC-Tyr 22

The deprotected amide **22** from the Boc-protected tyrosine **21** (1.0 g, 2.15 mmol) with TFA (10 mL) and DCM (20 mL) to give the desired product in the form of a white powder (510 mg, 65%). The product was characterised as follows:

$\nu_{\max}/\text{cm}^{-1}$  (FTIR) 3066, 2904, 1643, 1287, 1231,  $^1\text{H}$  NMR (400 MHz,  $\text{CDCl}_3$ ): 7.12 (2H, m, J 8.0), 6.71 (2H, m, J 8.0), 4.72 (1H, t, J 6.5), 3.65 (2H, q, J 7.5), 3.36 (2H, m), 3.26 (2H, m),  $\delta =$

2.48 (2H, t, J 6.5), 1.28 (8H, m), 0.90 (3H, t, J 7.0);  $^{13}\text{C}$  NMR (400 MHz,  $\text{CDCl}_3$ ): 130.4, 130.4, 54.3, 39.3, 37.0, 29.0, 157.8, 115.7, 115.7, 126.17, 36.4, 14.0, 171.2, 35.2, 29.4, 27.2, 22.6, 168.7, 32.4 (LS-MS): calculated for  $\text{C}_{19}\text{H}_{31}\text{N}_3\text{O}_3$  349, found 350  $[\text{MH}^+]$

### **Boc-valine chain 2HB-LC-Val 23**

From the deprotected of amide **14** (1.0 g, 4.98 mmol), DMAP (1.21 g, 9.96 mmol), Boc-Valine-OH (1.1 g, 4.98 mmol), EDC hydrochloride (0.78 g, 4.0 mmol,) and triethylamine (1.52 g, 0.015 mol) were added and left for 24 hours. The product was characterised as follows:

FTIR ( $\nu_{\text{max}}/\text{cm}^{-1}$ ), 2944, 1633, 1565, 1333, 1166, 1131;  $^1\text{H}$  NMR (400 MHz,  $\text{CDCl}_3$ ): 4.42 (1H, d, J 7.0), 3.18 (2H, t, J 7.0), 2.83 (2H, t, J 7.0), 2.24 (2H, t, J 7.0), 2.08 (1H, sept, J = 7.0), 1.56 (2H, t, J 7.0), 1.45 (9H, s), 1.30 (8H, m), 0.90 (6H, d, J 7.0) and 0.90 (3H, t, J 7.0);  $^{13}\text{C}$  NMR (400 MHz,  $\text{CDCl}_3$ ): 171.3, 168.7, 155.5, 80.4, 57.4, 39.3, 36.4, 35.2, 32.4, 31.4, 29.4, 29.0, 28.2, 28.21027, 28.2, 27.2, 22.6, 18.6, 18.6, 14.0 (LS-MS): calculated for  $\text{C}_{20}\text{H}_{39}\text{N}_3\text{O}_4$  386, found 387  $[\text{MH}^+]$

### **Deprotected valine 2HB-LC-Val 24**

Boc-protected valine **23** (1.0 g, 2.50 mmol), TFA (10 mL) and DCM (20 mL). The desired product was obtained in the form of a white powder (435 mg, 58%) and was characterised as follows:

FTIR ( $\nu_{\text{max}}/\text{cm}^{-1}$ ), 2988, 1650, 1562, 1284, 1130,  $^1\text{H}$  NMR (400 MHz,  $\text{CDCl}_3$ ): 4.42 (1H, d, J 7.0), 3.18 (2H, t, J 7.0), 2.83 (2H, t, J 7.0), 2.24 (2H, t, J 7.0), 2.08 (1H, sept, J 7.0), 1.56 (2H, t, J 7.0), 1.30 (8H, m), 0.90 (6H, d, J = 7.0), 0.90 (3H, triplet, J 7.0);  $^{13}\text{C}$  NMR (400 MHz,  $\text{CDCl}_3$ ): 170.6, 168.7, 58.3, 39.3, 36.4, 35.2, 32.4, 30.2, 29.4, 29.0, 27.2, 22.6, 17.9, 17.9, 14.0. (LS-MS): calculated for  $\text{C}_{15}\text{H}_{31}\text{N}_3\text{O}_2$  285, found 286  $[\text{MH}^+]$

## 5.5.2 Synthesis of three hydrogen bonding

### Boc-protected amide chain **17**

n-propylamine **15** (1.0 g, 0.0169 mol), Boc- $\beta$ -alanine **16** (3.41 g, 0.018 mol) and DMAP (4.40 g, 0.036 mol) were dissolved in DCM (100 mL). EDC.HCl (3.45 g, 0.018 mol) and triethylamine (5.17 g, 0.0507 mol) were added and the mixture stirred under nitrogen for 24 hours. The solution was transferred to a separating funnel and the crude product washed with brine solution (3 $\times$ 100 mL) and the aqueous layers extracted with DCM. The organic layers were collected and dried with Mg<sub>2</sub>SO<sub>4</sub>. The solvent was concentrated under reduced pressure and dried under a high vacuum to give the Boc protected chain **17** (3.97 g, 96 %) as a white powder. FTIR ( $\nu_{\max}/\text{cm}^{-1}$ ), 3335, 2968, 1682, 1645, 1528; <sup>1</sup>H NMR (400 MHz; CDCl<sub>3</sub>) 5.85 (1H, *s*), 5.25 (1H, *s*), 3.45 (2H, *q*, J= 7.0), 3.25 (2H, *q*, J 7.0), 2.45 (2H, *t*, J 7.0), 1.55 (2H, *m*), 1.45 (9H, *s*), 0.95 (3H, *t*, J 7.0); <sup>13</sup>C NMR (100 MHz; CDCl<sub>3</sub>); 172.5, 155.8, 80.5, 41.5, 37.0, 36.5, 29.0, 23.0; MS (ES), Calculated for C<sub>11</sub>H<sub>22</sub>N<sub>2</sub>O<sub>3</sub> [MH<sup>+</sup>]: 231, found 231.

### Deprotected amide chain **18**

Boc protected chain **17** (3.0 g, 0.013 mol) was dissolved in DCM (25 mL) and TFA (25 mL) was added. The solution was stirred under nitrogen for 24 hours, before being transferred to a separating funnel and washed with water (5 $\times$ 25 mL). The organic layer was collected, dried (MgSO<sub>4</sub>) and then removed using a rotary evaporator. The final product was dried under a high vacuum to yield amide chain **18** (1.4 g, 82 %) as a yellow oil, which was used directly in the next step. FTIR ( $\nu_{\max}/\text{cm}^{-1}$ ), 2978, 1645, 1558; <sup>1</sup>H NMR (400 MHz; D<sub>2</sub>O) 3.10 (2H, *t*, J 7.0), 2.98 (2H, *t*, J 7.0), 2.51 (2H, *t*, J 7.0), 1.36 (2H, *m*), 0.75 (3H, *t*, J 7.0); <sup>13</sup>C NMR (100 MHz; D<sub>2</sub>O) 171.5, 43.0, 41.5, 36.0, 32.0, 21.5; MS (ES), Calculated for C<sub>6</sub>H<sub>14</sub>N<sub>2</sub>O [M<sup>+</sup>]: 130, found 130.

### Boc-protected di-amide chain 19

The title compound was synthesized using the method described above for the Boc-protected amide chain **19**, using the following; EDC.HCl (3.83 g, 0.020 mol), Boc- $\beta$ -alanine **16** (3.85 g, 0.020 mol), deprotected amide chain **18** (2.65 g, 0.020 mmol), DMAP (4.89 g, 0.04 mol), and triethylamine (6.11 g, 0.06 mol). After work up and purification the Boc-protected diamide chain **19** was obtained as a white solid (4.7 g, 78 %). FTIR ( $\nu_{\max}/\text{cm}^{-1}$ ), 3306, 2965, 2935, 2875, 1689, 1635, 1538;  $^1\text{H}$  NMR (400 MHz;  $\text{CDCl}_3$ ) 6.83 (1H, *s*), 6.28 (1H, *s*), 5.32 (1H, *s*, NH), 5.18 (1H, *s*, NH), 3.55 (2H, *q*, J 7.0), 3.37 (4H, *m*), 3.24 (2H, *q*, J 7.0), 2.55 (2H, *m*), 2.43 (4H, *m*), 1.55 (2H, *m*), 1.42 (9H, *s*), 0.95 (3H, *t*);  $^{13}\text{C}$  NMR (100 MHz;  $\text{CDCl}_3$ ) 175.6, 156.0, 79.5, 37.2, 37.9, 42.5, 36.1, 39.8, 23.1, 28.4, 12.0; HRMS (ES), Calculated for  $\text{C}_{14}\text{H}_{27}\text{N}_3\text{O}_4$  [MH<sup>+</sup>]: 302.2074, found 302.2072.

### Deprotected di-amide chain 20

Boc-protected di-amide chain **19** (4.5 g, 0.016 mol) was dissolved in DCM (25 mL) and TFA (25 mL) added and the mixture was allowed to react for 24 hours under nitrogen. The DCM was removed by a rotary evaporator to give the crude product as a thick brown oil. Water (100 mL) was added and then removed by decantation. This washing step was repeated a further two times, before drying the product under a high vacuum. The crude product was dissolved in DCM (100 mL), and washed twice with diluted HCL (2 mL of 2M HCl diluted with 100 mL of water). The organic layer was dried with  $\text{Mg}_2\text{SO}_4$  and the solvent removed on a rotary evaporator. The product was then left to dry under a high vacuum. The crude product was obtained as a brown oil in a 93% yield and was used directly in the next step. FTIR ( $\nu_{\max}/\text{cm}^{-1}$ ), 2938, 1645, 1555, 1178 and 1130;  $^1\text{H}$  NMR (400 MHz;  $\text{CDCl}_3$ ), 7.86 (2H, *t*, J 7.0), 7.75 (2H, *s*), 3.26 (2H, *dd*, J 13.0, 7.0), 3.18 (4H, *s*), 2.96 (6H, *m*), 2.54 (2H, *t*, J 7.0), 2.45 (4H, *m*), 1.38 (2H, *m*), 0.90 (3H, *t*, J 7.0);  $^{13}\text{C}$  NMR (100 MHz;  $\text{CDCl}_3$ ) 172.5, 170.5, 170.0, 40.5, 36.0, 35.5, 35.0, 33.0, 32.0, 23.0, 12.0; HRMS (ES), Calculated for  $\text{C}_9\text{H}_{19}\text{N}_3\text{O}_2$  [MH<sup>+</sup>]: 202.1550, found 202.1557

### **Boc-protected tyrosine chain 25**

The title compound was synthesized using the method described above for the Boc-protected amide chain **25**, using the following; deprotected di-amide chain **20** (1.0 g, 4.98 mmol), Boc-Tyrosine-OH (1.4 g, 4.98 mmol), DMAP (1.21 g, 9.96 mmol), triethylamine (1.52 g, 0.015 mol) and EDC.HCl (0.78 g, 4.0 mmol). The crude product was obtained as a pale yellow solid and was purified using silica chromatography with DCM (MeOH 1%) as eluent. The Boc product chain **25** was obtained as a white powder (1.5 g, 71%): UV (MeOH)  $\lambda_{\max}$  (nm) 273, 225. FTIR ( $\nu_{\max}/\text{cm}^{-1}$ ), 3305, 2968, 2935, 2878, 1688, 1639, 1536, 1168;  $^1\text{H}$  NMR (400 MHz; MeOD) 7.04 (2H, *d*, J 8.5, *m*), 6.72 (2H, *d*, J 8.5), 4.18 (1H, *t*, J 7.0), 3.42 (4H, *m*), 3.15 (2H, *t*, J 7.0), 2.98 (1H, *dd*, J 14.0, 7.0), 2.75 (1H, *dd*, J 14.0, 7.0), 2.38 (2H, *t*, J 7.0), 2.31 (2H, *q*, J 7.0), 1.55 (2H, *m*), 1.38 (9H, *s*), 0.95 (3H, *t*, J 7.0);  $^{13}\text{C}$  NMR (100 MHz; MeOD) 174.5, 173.5, 132, 128.5, 115.5, 49.0, 41.0, 36.0, 35.0, 23.0, 28.5; MS (ES) Calculated for  $\text{C}_{23}\text{H}_{36}\text{N}_4\text{O}_6$  [M+]: 464, found 464

### **Tyrosine linear chain - 3HB-LC-Tyr 26**

The title compound was synthesized using the method described above for the deprotected amide chain **26**, using the following; Boc-protected tyrosine chain **25** (1.0 g, 2.15 mmol), DCM (20 mL) and TFA (10 mL). 3HB LC-Tyr **26** was obtained as a white powder (510 mg, 65%). UV (MeOH)  $\lambda_{\max}$  (nm) 272, 225. FTIR ( $\nu_{\max}/\text{cm}^{-1}$ ) 3288, 3086, 2936, 1634, 1536, 1512, 1185, 1138;  $^1\text{H}$  NMR (400 MHz; MeOD) 7.08 (2H, *d*, J 8.5), 6.78 (2H, *d*, J 8.5), 3.96 (1H, *t*, J 7.0), 3.42 (4H, *m*), 3.15 (2H, *t*, J 7.0), 3.05 (1H, *dd*, J 14.0, 7.0), 2.95 (1H, *dd*, J 14.0, 7.0), 2.40 (2H, *t*, J 7.0), 2.35 (2H, *q*, J 7.0), 1.55 (2H, *m*), 0.92 (3H, *t*, J 7.0);  $^{13}\text{C}$  NMR (100 MHz; MeOD) 173.5, 173.5, 171.0 (C=O), 133.0, 126.0, 117.0 (ArC), 60.0, 43.0, 38.0, 37.5, 37.5, 36.8, 36.5, 24.0, 12.0, HRMS (ES), Calculated for  $\text{C}_9\text{H}_{19}\text{N}_3\text{O}_2$  [MH+]: 365.2183, found 365.2189

### **Boc-protected valine chain 27**

The title compound was synthesized and purified using the method described above for the Boc-protected amide chain **27**, using the following; deprotected diamide chain **20** (1.0 g, 4.98

mmol), Boc-Valine-OH (1.1 g, 4.98 mmol), DMAP (1.21 g, 9.96 mmol), triethylamine (1.52 g, 0.015 mol) and EDC.HCl (0.78 g, 4.0 mmol). UV (MeOH)  $\lambda_{\max}$  (nm) 278, 227; FTIR ( $\nu_{\max}/\text{cm}^{-1}$ ), 2932 (N-H stretch), 1640 (C=O, stretch), 1552 (N-H, bend), 1324, 1170 and 1131 (C-N);  $^1\text{H}$  NMR (400 MHz; MeOD), 4.55 (1H, *d*, J 5.5, CH), 3.45 (4H, *m*,  $\text{CH}_2\text{CH}_2\text{NH}_2$ ), 3.10 (2H, *t*, J 7.0,  $\text{CH}_2\text{CH}_2$ ), 2.66 (1H, *sept*, CH( $\text{CH}_3$ )<sub>2</sub>), 2.40 (2H, *t*, J 7.0,  $\text{CH}_2\text{NH}$ ), 2.35 (2H, *q* J 7.0,  $\text{CH}_2\text{CH}_2$ ), 1.58 (2H, *m*,  $\text{CH}_3\text{CH}_2\text{CH}_2$ ), 1.44 (9H, *s*, 3x  $\text{CH}_3$ ), 1-0.98 (6H, *d*,  $\text{CH}(\text{CH}_3)_2$ ), 0.95 (3H, *t*, J 7.5,  $\text{CH}_2\text{CH}_3$ );  $^{13}\text{C}$  NMR (100 MHz; MeOD) 173.0, 172.0, 160.5 (C=O), 80.0 (C), 64.0, 41.0, 37.0, 34.5, 32.0, 29.0 ( $\text{CH}_3$ ), 19.5 ( $\text{CH}_3$ ), 12.0 ( $\text{CH}_3$ ); 72% yield; MS (ES), Calculated for  $\text{C}_{19}\text{H}_{36}\text{N}_4\text{O}_5$  [ $\text{M}^+$ ]: 400, found 400.

### Valine linear chain – 3HB-LC-Val 28

The title compound was synthesized using the method described above for the deprotected amide chain **28**, using the following; Boc-protected valine chain **27** (1.0 g, 2.50 mmol), DCM (20 mL) and TFA (10 mL). 3HBLC-Val **28** was obtained as a white powder (435 mg, 58%). UV (MeOH)  $\lambda_{\max}$  (nm) 278, 227; FTIR ( $\nu_{\max}/\text{cm}^{-1}$ ), 2940, 1657, 1566, 1280, 1130;  $^1\text{H}$  NMR (400 MHz; MeOD), 5.28 (1H, *s*, NH), 3.55 (1H, *d*, J 5.5, CH), 3.45 (4H, *m*,  $\text{CH}_2\text{CH}_2\text{NH}_2$ ), 3.10 (2H, *t*, J 7.0,  $\text{CH}_2\text{CH}_2$ ), 2.40 (2H, *t*, J 7.0,  $\text{CH}_2\text{NH}$ ), 2.35 (2H, *q* J 7.0,  $\text{CH}_2\text{CH}_2$ ), 2.26 (1H, *sept*, CH( $\text{CH}_3$ )<sub>2</sub>), 1.58 (2H, *m*,  $\text{CH}_3\text{CH}_2\text{CH}_2$ ), 1-0.98 (6H, *d*,  $\text{CH}(\text{CH}_3)_2$ ), 0.91 (3H, *t*, J 7.5,  $\text{CH}_2\text{CH}_3$ );  $^{13}\text{C}$  NMR (100 MHz; MeOD) 172.5, 170 (C=O), 41.0, 38.0, 35.0, 32.0, 29.0 ( $\text{CH}_2$ ), 18.5 ( $\text{CH}_3$ ), 13.0 ( $\text{CH}_3$ ); 55% yield; HRMS (ES), Calculated for  $\text{C}_{14}\text{H}_{28}\text{N}_4\text{O}_3$  [ $\text{MH}^+$ ]: 301.2234, found 301.2240.

### Tetrahydroxyphenylporphyrin – THPP

Freshly distilled pyrrole (12.51 g, 180 mmol) and 4-hydroxybenzaldehyde (30.0 g, 120 mmol) were refluxed in propionic acid (500 mL) for 24 hours. The mixture was allowed to cool to room temperature and left for 2 hours at  $-5^\circ\text{C}$ . The crude product precipitated and was collected by filtration. The solid was washed with propionic acid and then recrystallized from

ethanol. The product was collected and dried to give purple crystals. Yield (2.0 g, 2.5%). UV (MeOH)  $\lambda_{\text{max}}$  (nm) 418, 520, 560, 595, 655; FTIR ( $\nu_{\text{max}}/\text{cm}^{-1}$ ) 3248, 2924, 1609, 1463, 1378, 1172, 964, 798;  $^1\text{H}$  NMR (400 MHz; DMSO) 9.97 (s, 4H), 8.84 (s, 8H), 7.96 (d, J 8.50, 8H), 7.18 (d, J 8.50, 8H), -2.92 (s, 2H);  $^{13}\text{C}$  NMR (100 MHz;  $\text{CDCl}_3$ ) 134.5, 127.6, 126.5, 120.4, 11.8; MS (ES), Calculated for  $\text{C}_{44}\text{H}_{30}\text{N}_4\text{O}_4$  [ $\text{MH}^+$ ] 679 ( $\text{MH}^+$ ), Found 679.

### **Zinc tetrahydroxyphenylporphyrin – Zn-THPP 29**

THPP (2.0 g, 2.0 mmol) and an excess of zinc acetate-dihydrate (2.0g) were refluxed in 100 mL of DCM for 10 minutes. The solution was filtered and evaporated and the crude product recrystallized from DCM/hexane to give Zn-THPP **29** as purple crystals in a yield of 87%. UV (MeOH)  $\lambda_{\text{max}}$  (nm) 425.5, 595, 660; FTIR ( $\nu_{\text{max}}/\text{cm}^{-1}$ ) 2923, 3245, 2924, 1609, 1465;  $^1\text{H}$  NMR (400 MHz; DMSO) 9.97 (s, 4H), 8.84 (s, 8H), 7.96 (d, J 8.50), 7.18 (d, 8H, J 8.50);  $^{13}\text{C}$  NMR (100 MHz;  $\text{CDCl}_3$ ) 134.5, 127.6, 126.5, 120.4, 11.8; MS (ES), Calculated for  $\text{C}_{44}\text{H}_{28}\text{N}_4\text{O}_4\text{Zn}$  [ $\text{MH}^+$ ] 743 ( $\text{MH}^+$ ), Found 743.

### **Protein binding titration**

A stock solution of the macromolecular ligand was prepared by adding dendrimer, linear chain and Zn-THPP to methanol. The methanol was removed and phosphate buffer (pH 7.4, 0.01M) was added to the resulting paste to give a solution that was 1.0  $\mu\text{M}$  in dendrimer and Zn-THPP and 10  $\mu\text{M}$  in linear chain. For control experiments the same procedure was used, but one or more components were removed. To ensure the titration was performed under constant concentration of Zn-THPP, the stock solution was also used as the solvent to make a 1.0  $\mu\text{M}$  Cytochrome-c solution.

1.5 mL of the stock solution was added to a quartz cuvette and placed into a fluorimeter. Aliquots of the cytochrome-c solution were then added and the intensity of the emission peak at 610 nm (excitation at 410 nm) monitored after each addition. The data was plotted with respect to the concentration of cytochrome-c and curve fitting analysis used to fit the experimental data to a 1:1 binding model (Graphpad prism 7.0).

## 5.6 References

1. Chothia, C. and Janin, J. Principles of protein-protein recognition. *Nature* **256**, 705–708. (1975).
2. Ryan, D. P. and Matthews, J. M. Protein-protein interactions in human disease. *Curr. Opin. Struct. Biol.* **15**, 441–446 (2005).
3. Shen, K. Gamerdinger, M. Chan, R., Gense, K. Martin, E. M. Sachs, N., Knight, P. D. Schlömer, R. Calabrese, A. N. LStewart, K. L. Leiendecker, L. Baghel, A. Radford, S. E. Frydman, J. and Deuerling. E. Dual role of ribosome-binding domain of NAC as a potent suppressor of protein aggregation and aging-related proteinopathies. *Molecular Cell* **74**, 1–13 (2019).
4. You, J., Croyle, J. L. Nishimura, A. Ozato, K. and Howley. P. M. Interaction of the bovine papillomavirus E2 protein with Brd4 tethers the viral DNA to host mitotic chromosomes. *Cell*. **117**, 349-360 (2004).
5. Schwarz-Linek, U. Werner, J. M. Pickford, A. R. Gurusiddappa, S., Kim, J. H. Pilka, E. S. Briggs, J. A. Gough, T. S. Hook, M. Campbell, I. D. and Potts, J. R. Pathogenic bacteria attach to human fibronectin through a tandem beta-zipper. *Nature*. **423**,177-181 (2003).
6. Jones, S. and Thornton, J. M. Principles of protein-protein interactions. *Proc. Natl. Acad. Sci.* **93**, 13–20 (1996).
7. Yin, H. and Hamilton, A. D. Strategies for targeting protein-protein interactions with synthetic agents. *Angew. Chemie - Int. Ed.* **44**, 4130–4163 (2005).
8. Talavera D, Robertson D. L. Lovell, S. C. Characterization of Protein-Protein Interaction Interfaces from a Single Species. *PLoS ONE*. **6(6)**, e21053 (2011).
9. Bogan, A. Thorn, K. S. Anatomy of hot spots in protein interfaces. *J. Mol. Biol.* **280**, 1–9 (1998).
10. Park, H. Lin, Q. and Hamilton, A D.. Modulation of protein–protein interactions by synthetic receptors: Design of molecules that disrupt serine protease–proteinaceous inhibitor interaction. *Proc. Natl. Acad. Sci.* **99**, 5105–5109 (2002).
11. Baldini, L. Wilson, A. J. Hong, J. and Hamilton, A. D. Pattern-based detection of different proteins using an array of fluorescent protein surface receptors. *J. Am. Chem. Soc.* **126**, 5656–5657 (2004).
12. De, M. Chou, S. S. and Dravid, V. P. Graphene oxide as an enzyme inhibitor: Modulation of activity of  $\alpha$ -chymotrypsin. *J. Am. Chem. Soc.* **133**, 17524–17527 (2011).

13. Wei, Q. Becherer, T. Angioletti-Uberti, S. Dzubiella, J. Wischke, C. Neffe, A. T. Lendlein, A. Ballauff, M. and Haag, R. Protein interactions with polymer coatings and biomaterials. *Angew. Chemie. Int. Ed.* **53**, 8004–8031 (2014).
14. Welsch, N. Dzubiella, J. Graebert, A. and Ballauff, M. Protein binding to soft polymeric layers: A quantitative study by fluorescence spectroscopy. *Soft Matter.* **8**, 12043–12052 (2012).
15. Chiba, F. Hu, T. C. and Twyman, L. J. and Wagstaff, M. Dendrimers as size selective inhibitors to protein-protein binding. *Chem, Commun.* 4351–4353 (2008).
16. Chiba, F. Mann, G. and Twyman, L. J. Investigating possible changes in protein structure during dendrimer-protein binding. *Org. Biomol. Chem.* **8**, 5056–5058 (2010).
17. Chiba, F. and Twyman, L. J. Effect of terminal-group functionality on the ability of dendrimers to bind proteins. *Bioconjug. Chem.* **28**, 2046–2050 (2017).
18. Hu, T. Synthesis of dendrimers for protein binding. PhD Thesis, *University of Sheffield, Sheffield, UK.* (2007).
19. Borris, D. and Rubinstein. M. A self-consistent mean field model of a starburst dendrimer: dense core vs dense shell. *Macromolecules.* **29(22)**, 7251–7260 (1996).
20. Ellis, A. and Twyman L. J. Probing dense packed limits of a hyperbranched polymer through ligand binding and size selective catalysis. *Macromolecules.* **46(17)**, 7055–7074 (2013).
21. Recio, J. F. Totrov, M. Skorodumov, C. and Abagyan, R. Optimal docking area: A new method for predicting protein–protein interaction sites. *Proteins, Struct. Funct. Bioinformat.* **58**, 134–143 (2005).
22. Tomalia, D. A. Baker, H. Dewald, J. Hall, M. Kallos, G. Martin, S. Roeck, J. Ryder, J. and Smith. P. A. A new class of polymers: Starburst-dendritic macromolecules. *Polym J.* **17**, 117–132 (1985).
23. The maximum addressable area of a dendrimer is the maximum theoretical size of a surface that can interact with a dendrimer, and can be estimated from its diameter. See reference 15 above.
24. When a completely hydrophobic porphyrin was used, almost no encapsulation was observed. However, if the porphyrin has some solubility, it can be encapsulated with control to achieve the required 1:1 stoichiometry. The key requirement is that the porphyrin cannot, and does not interact with the protein on its own (tested through the control experiments described).

25. Twyman, L. J. Beezer, A. E. Esfand, R. Hardy, M.J. and Mitchell, J. C. The synthesis of water soluble dendrimers, and their application as possible drug delivery systems. *Tett. Lett.* **40(9)**, 1743-1746 (1999).
26. Hermans, T. M. Broeren, M. A. C. Gomopoulos, N. van der Schoot, P. van Genderen, M. H. P. Sommerdijk, N. A. J. M. Fytas, G. and Meijer, E. W. Self-assembly of soft nanoparticles with tuneable patchiness. *Nature Nanotech.* **4**, 721-726 (2009).
27. Jain, R. K. and Hamilton, A.D. Protein surface recognition by synthetic receptors based on a tetraphenylporphyrin scaffold. *Org. Lett.* **2(12)**, 1721–1723 (2000).
28. Muldoon, J. Ashcroft, A. E. and Wilson, A. J. Selective protein- surface sensing using ruthenium(ii) tris(bipyridine) complexes. *Chem. Eur. J.* **16**, 100-103 (2010).